UNIVERSIDAD NACIONAL DE COLOMBIA

Frequency Selective Surfaces to Camouflage Directive Antennas

Laura Maria Pulido Mancera

Universidad Nacional de Colombia
Physics Department
Bogotá, Colombia
2014

UNIVERSIDAD NACIONAL DE COLOMBIA

Masters Thesis

Frequency Selective Surfaces to Camouflage Directive Antennas

Author
Laura Maria Pulido Mancera
lmpulidom@unal.edu.co

Supervisor
Prof. Juan Domingo Baena Doello
jdbaenad@unal.edu.co

Co-Supervisor
Prof. Javier Leonardo Araque Quijano
jlaraqueq@unal.edu.co

A thesis submitted in fulfilment of the requirements for the degree of Masters in Physics

Physics Department

May 2014

"Any sufficiently advanced technology is indistinguishable from magic".

Arthur C. Clarke.
Science fiction Author

Dedicated to my family that always encouraged me to do what I love the most.

Abstract

This master's thesis is focused on the improvement in the design of Frequency Selective Surfaces (FSSs) and metasurfaces in order to develop different applications: short waveguide filters, antenna camouflaging and sensors. Thus, we start with the general study of FSSs and some basic definitions as the radar cross section and the quality factor. Besides, a brief description of the computational analysis of FSS is presented. Then, we focus on the mathematical description of the scattering parameters, obtained when an electromagnetic wave impinges upon a two-dimensional periodic array, the FSS, made of electrically small resonators ,metasurfaces; useful for any angle of incidence. This approach yields some useful constraints between the scattering parameters as well as their paths in the complex plane, which form a mathematical treatment that has not been previously described in the literature. In the second part, we study the properties of the small resonators used for the metasurface design, and the models used to predict the resonance of thin metasurfaces. Subsequently, we analyse the geometric parameters that increase the quality factor of a metasurface by means of two new proposed models to predict the resonant frequency. The novelty is that these models do not require full-wave numerical simulations, so its design is considerably facilitated. In fact, these results are summarized in a convenient computer program that computes the resonance frequency of SRR based resonators and their complementaries in terms of the geometrical parameters only. Furthermore, we explore three different applications verified at an experimental level: A short waveguide filter of high quality factor fabricated and used to verify the proposed models as well as to analyse the resonators of better performance. Besides, a device to measure the permittivity of liquids, based on a microstrip line technology. It was characterized using liquids whose permittivity was known. Then, it was used to estimate the permittivity of a solution of silver nanoparticles. Finally, a small metasurface that behaves as a spatial filter served to improve the manufacturing processes to be made in the future, and to propose the design of a filtenna: Filter + Antenna. The results obtained from this last proposal are helpful for antenna camouflaging.

Acknowledgements

Thanks to my family because they are my driven force in this process of becoming a Physicist. With the wheels of love, patience, comprehension and wisdom that they have given to me, I have faced several challenges in the race of life.

Thanks to my friends because I they have been the best professors that I have ever met and a great support. Not only about physics, but about becoming a professional and an integral person, giving passion to every decision we take.

Thanks to my advisor, Prof. Baena, for his patience and clear mind. For renewing my interest in physics: Our ability to understand our everyday phenomena, and to create something new with that understanding. It is very interesting to realize how it is possible to develop new and ideas, even when current life has so many difficulties or distractions.

Thanks to the Universidad Nacional de Colombia, where my heart belongs since I was a little girl. To the group of Applied Physics, to Juan Pablo and Julian for their enormous patience, to the group of Electromagnetic Compatibility an Telecommunications, in particular, thanks to my co-advisor Prof. Javier Araque for his clarity and kindness, and to the engineers Oscar and Germán for their support with the experimental work.

Thanks to the Universidad de los Andes, where I got a very interesting perspective about engineering and the challenges of the modern world. I am very glad with my course of nanotechnology with Prof. Alba Ávila which is not only brilliant but a very motivating person.

Thanks to the Institute of Photonics Sciences, ICFO for allowing me to have the best research experience outside Colombia. In particular thanks to Davide Janner for his support and encouragement with the challenges that a PhD. student is expected to pursue. Thanks to Selva Vía, for her technical support with the anechoic chamber.

The list of the people that have been important along this masters is infinitely long, so thanks to all, for making these two so enjoyable.

Contents

List of Figures

List of Tables

Chapter 1

Introduction and Basic Concepts

The use of high frequency electromagnetic signals has increased since the mid-20th century [1]. The concept of "microwaves" is not attached to a margin of frequencies but it is used to identify the signals whose generation, propagation and processing uses a set of specific techniques that are not used in electronics at low frequencies or optics. Thus, the microwaves may vary within the frequency range of [300 MHz - 300 GHz] [2]. Some of the most notable applications of microwaves and radio frequency include radio communications, industrial applications like heating processes, medical applications for cancer treatment and scientific applications as accelerators of particles.

One of the primary applications is the radar systems, that basically consists of a transmitter's signal that illuminates the body to detect, and a receiver that detects the reflected signal from the illuminated body. Originally designed for military applications, the radars currently can be used for navigation, cartography, traffic control of airports, etc. From the point of view of the EM scattering of bodies, a big effort has been done in order to better control of the electromagnetic wave transmission and scattering, and one of the fundamental devices for this purpose is the Frequency Selective Surface (FSS).

Since the advent of FSSs in the late 1960s, there has been a great effort to study them from the theoretical, computational and practical viewpoint. In the last two decades, the major applications of FSSs are high performance antenna radomes and reflector antennas. The complexity in the design of existing FSSs, their required size, and the sensitivity to the angle of incidence; limit their functionality, showing the demand for improving their filtering properties. In this research, we are focused in the design of FSSs with low dependence respect to the incidence angle of the signal, the ability to operate in close proximity to a radiation source and the improvement of the quality factor.

In order to "camouflage" an antenna, it is necessary to reduce its radar cross section (RCS) for any angle of incidence without changing the emission pattern of the antenna itself. So the question is: *how to design a FSS that covers an antenna (as a radome) that is "invisible" at the centre frequency of the antenna (at any angle of incidence) but at the same time reduces its RCS in such a way that it is not easy to target?*

To solve this question, metamaterial based FSSs, so called **metasurfaces**, have attracted the attention of physicists and engineers because these satisfy the characteristics stated above such as its filtering response is independent of the angle of incidence and polarization state. Thus, becoming suitable candidates for antenna camouflaging [3]. In addition, the metasurfaces properly perform even at a close distance of about a tenth of the wavelength to an antenna [4]. The localized characteristic implies it can take up a small area in comparison to the wavelength and still maintain their frequency-selective properties. The key factor of the metasurfaces is the unit cell that composes the entire surface, whose origin comes from the field of metamaterials: materials with exotic electromagnetic properties.

At the year 2000, it was recovered the idea of Veselago on the left-handed media thanks to the pioneering work J. Pendry, David Smith and his collaborators [5], who showed an artificial left-handed material through the combination of regular metal cylinders, providing negative permittivity, and **Split Ring Resonators (SRRs)** [6], providing the negative permeability. Some of the most interesting properties of these metamaterials is the possibility to manufacture "perfect lens" and "invisibility cloaks". The former one, capable of producing an image that is perfect copy of the source, overcoming the diffraction limit [7]. The latter, able to isolate an object from the surrounding electromagnetic waves in a region of space. Because of its exotic properties, it was assigned the term of metamaterial structures and, for 2D structures, metasurfaces.

Like a FSS, the metasurface is made as a periodic array of metallic strips packaged close together and placed on a substrate. Similarly, the complementary metasurface is made as a metallic layer with a periodic array of slits etched on it. Some of the advantages these structures is that these suppress the grating lobes when a incident wave is filtered through it, because its resonance frequency corresponds to a wavelength much bigger than the separation between the objects that compose the metasurface. Therefore, the metasurface can be considered as uniform medium able to filter at fixed frequency and it can be modelled with equivalent circuits that predict the resonance frequency without full-wave numerical simulations [8][9], such that the design process is improved. It is very important to remark that the modelling of thin complementary metasurfaces uses equivalent circuit models and the **Babinet's Principle** that relates the scattered fields of any thin screen with the scattered fields of its complementary [10].

When the thickness of the screen is not negligible, Babinet's principle is no longer valid, and different responses from metasurfaces and their complementary are expected. However, it has not been found a model for thick metasurfaces (neither its complementaries), which may be more accurate to compare with experiments. It is very important to analyze how thick surfaces respond to an incident wave because the thickness is not negligible at an experimental level. Besides, it has been previously demonstrated that thick FSSs possess better quality factor than the thin ones, so the same response is expected for the metasurfaces. Indeed, to predict the response of thick FSSs, the transmission line theory has been used [11].

Physicists usually try to explain how nature works, whereas engineers try to apply this knowledge to the design of new devices and systems, useful for certain applications [12]. Metasurfaces are placed at an intermediate position between science and engineering, and in this work, we will develop two different models to predict the resonance frequency of thick metasurfaces made of SRRs, its complementary (C-SRRs) and similar geometries of small electric size. Furthermore, based on the possibility of designing devices and systems with new properties or functionalities, the last part of this work is focused in some of the applications that can be developed by using the initial geometry for metasurfaces, the SRRs and C-SRRs, obtaining improvements in the applications in comparison with the common techniques. The three applications described and studied are: a short waveguide filter, and spatial filter and a permittivity sensor.

The applications presented in this work were fabricated and studied in collaboration with different institutions: Universidad Nacional de Colombia, Universidad de los Andes, Tec-Laser, The Institute of Photonic Sciences (ICFO) and the Centre of Technology and Telecomunications of Catalunya (CTTC).

Universidad Nacional de Colombia Fabrication of a small metasurface by using Printed Circuit Board technology (PCB). Indeed, this fabrication process was part of the Colciencias's Project "Frequency Selective Surfaces to Camouflage Antennas" and the first metasurface was fabricated for the purpouses of this work.

Universidad de los Andes Fabrication of a defected ground microstrip line by using PCB and a drilling machine at the laboratory of Electrical and Electronic Engineering.

Tec-Laser Fabrication of a short waveguide filter for rectangular waveguides. The prototypes were manufactured using a laser drilling machine and a water drilling machine.

ICFO and CTTC Workshop on the experimental techniques to perform measurements inside an anechoic chamber and laboratory facilities to test the filtering response of a metasurface.

1.1 Frequency Selective Surfaces and Metasurfaces

This section is dedicated to the basics of FSSs and the initial concepts to be used throughout this work. We start with the passband and stopband response posed in terms of the *Scattering Parameters* and a brief description of the computational analysis of FSSs. Then, the basics of metasurfaces are described, showing the improvements of these structures in comparison with the FSSs: isotropic filtering response and small electrical size.

A two-dimensional periodic array of patch or aperture metallic elements is called a frequency selective surface because of the filtering property suggested by this structure [13]. In the last years, fascinating applications of the FSSs and sophisticated analytical techniques have emerged like the multiband FSS in reflector antennas and radome design. *Radomes* are structures made to protect the antenna from the enviroment. A FSS can be adapted to a radome to act as a band pass filter that is used to reduce the Radar Cross Section (RCS) of an antenna system outside its frequency band of operation.

The FSS may have low-pass or high-pass frequency response, depending upon the array element type and the work frequency. The configuration of each element (either patch or aperture within an array of periodic cells), as well as the spacing, will contribute to the form of the scattered fields-transmitted or reflected. Basically, upon contact with a plane-wave, the elements of the periodic surface resonate at frequencies where the effective length of the elements is a multiple of the resonance length, $\lambda/2$. Corresponding to the wavefront of the wave, these elements have a certain phase delay, as a result, the scattered radiations of individual elements add up coherently. For instance, a planar array of strip dipoles produces a frequency response consisting of multiple notches at frequencies where the length of the dipoles is a multiple $\lambda/2$. A similar effect can explain the operation of other elements as the square loop element, that can be imagined as two dipoles that are connected to one another at each end [14][15]. Indeed, the resonance wavelength is directly related with the size of the resonator element of the FSS, its ratio is known as the *electrical size*.

Figure 1.1 shows some of the most common shapes for FSSs: circular, rectangular-dipole, ring, cross dipole, Jerusalem Cross, etc. When a strip dipole element is illuminated by any RF source and its length is a multiple of $\lambda/2$, it will resonate and scatter the

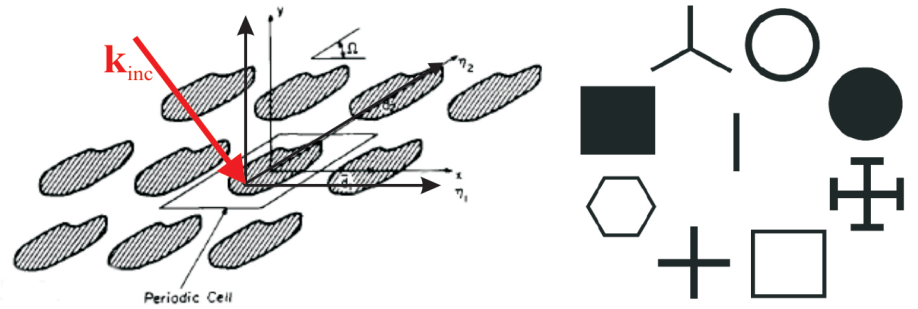

(a) (b)

FIGURE 1.1: (a) A FSS, photography from [13].(b) Common element shapes for FSS design [5].

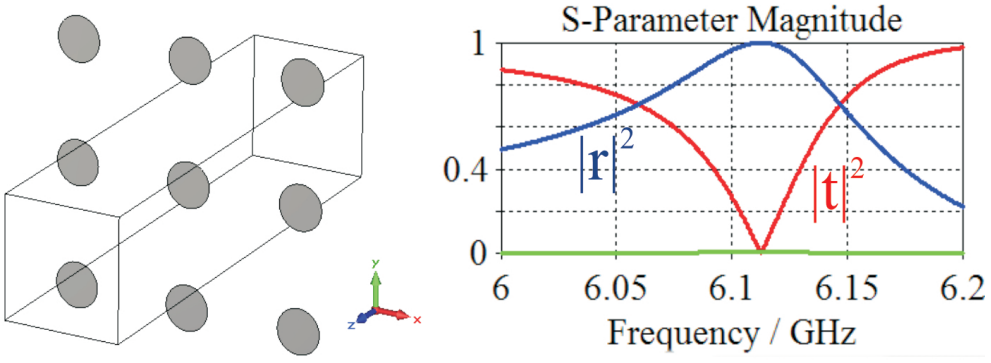

(a) (b)

FIGURE 1.2: Resonant response of a FSS made of circular patches of radius r =9mm. (a) Numerical simulations (b) Scattering parameters. The FSS acts as a bandstop filter.

energy. If many strip dipoles are arranged periodically, the reradiated energy from all the elements will be coherent towards the direction as if a reflection is occurring. For instance, in a circle of average radius equal to r =9mm, the resonance wavelength is $\lambda =$ 56.54 mm and the resonance frequency corresponds to f =5.5 GHz. When the element size is quite different from the resonant dimensions, the incident wave will travel through a FSS screen as if the screen were essentially transparent, as shown in figure 1.2.

A FSS can be categorized as thick- or thin-screen FSS, depending on the thickness of the resonator object. The term thin-screen FSS usually refers to a screen with printed-circuit-type elements, this means, patch or aperture elements less than 0.001λ thick, with λ the resonance wavelength. In general, the thin-screen is lightweight, low volume, and can be inexpensively fabricated with conventional printed circuit technology. Instead, thick FSSs are heavy and require precise and expensive machining. The applications of FSSs include antenna camouflaging by means of FSS based radomes, dichroic subreflectors and spatial filters among other applications [13]. Figure 1.3 shows these devices; the radome (a) and a sketch of the operation of a dichroic subreflector.

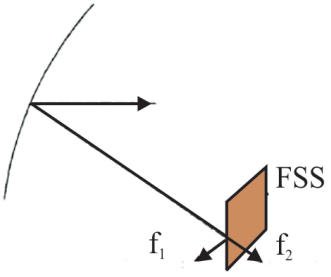

(a) (b)

FIGURE 1.3: Applications of FSS. (a) Radomes at the Cryptologic Operations Center, Misawa, Japan. (b) Dichroic subreflectors. Images from [5].

Spatial Filters The effect of the incident wave through an aperture-element FSS at different angles of incidence allow us to use it as a spatial filter. The spatial filter has applications in sidelobe supression and beam forming.

Dichroic Subreflectors In a dual-reflector antenna system, a FSS can be used as a subreflector. Different frequency feeds are optimized independently and placed at the real and virtual focus of the subreflector. Thus, a single structure is required for multifrequency operation, reducing the overall mass, volume, and most importantly the fabrication cost.

Radome Design FSS radomes with aperture-type element can be tuned to provide bandpass characteristics. At the operating band of the antenna the signal passes through the radome with minimum reflection [16], whereas out-of-band the signal is reflected. In practice, bandpass spatial covers of this type are used in certain applications, for example, in the fabrication of an aircraft [3]. Radome have two modes of operation, in the transparent mode the signal passes through the radome and is collected by the antenna whereas in the reflecting mode, the radome behaves like a metallic surface which reflects the signal in the specular direction. The advantage of this method is that it can be shaped a particular radome in order to reach the lowest levels of RCS. This can be done by designing the shape of the radome so that the direction of the strong reflection (specular) in reflecting mode is out of the sight of the transmitter of the signal, i.e. it is not directed toward the incoming signal.

1.2 Radar Cross Section and Quality Factor

The Radar Cross Section (RCS) is the measure of a target's ability to reflect radar signals in the direction of the radar receiver. Thus it is the measure of the ratio of

backscatter density in the direction of the radar from the target, to the power density intercepted by it[16]. Since the power is distributed on the shape of a sphere, a small part of it can be received back by the radar. The RCS of a target can be viewed as a comparison between the strength of the reflected signal from a target, and the reflected signal from a perfectly smooth sphere of cross sectional area of 1 m, as shown in figure 2.4.

RCS's conceptual definition includes the fact that not all of the radiated energy falls on the target. The RCS is the product of three factors: projected cross section, *reflectivity* that corresponds to the percent of power reradiated from the target; and *directivity*, the ratio between the power scattered back in the radar's direction and the power that would have been backscattered uniformly in all directions (i.e. isotropically).

If an directive antenna is covered with a FSS that respond as a bandpass at the work frequency of the antenna itself, (which means that the FSS is invisible to the antenna at a single frequency or a small frequency range), the RCS is reduced because the radome scatters in all the directions, decreasing the percentage of reflected energy in the direction of the radar. However, it is important that the FSS does not change the the radiation pattern of the antenna at the working frequency. If the size of the elements that compose the FSS is comparable with the wavelength, grating lobes generated by interference may appear such that the signal is modified. In order to reduce this interference, the size of the elements must be smaller than the wavelength. Actually, smaller elements enable closer packaging which turns out in a better stability at the resonance frequency.

In addition to the RCS reduction for antenna camouflaging, it is important the **Quality Factor** Q. This is a dimensionless parameter that describes how under-damped an oscillator or resonator is, or equivalently, that characterizes a resonator's bandwidth relative to its center frequency [10]. Higher Q indicates a lower rate of energy loss relative to the stored energy of the resonator; the oscillations die out more slowly. Q calculated as $Q = f_0/\Delta f_0$ and is measured from a curve presenting a maximum frequency of the scattering parameters (transmission for bandpass filters and reflection for stopband filters). For FSSs, the highest Q means better filtering response, as shown in figure 2.4.

1.3 Method of Moments and Floquet's Theorem

The computational analysis of FSSs can be found in [13, 14, 17]. This is related to the calculation of the scattering from arbitrary bodies, especially large bodies in comparison to the wavelength. The most common numerical approach to the calculation of the characteristics of a FSS is the periodical *Method of Moments* [9, 18].

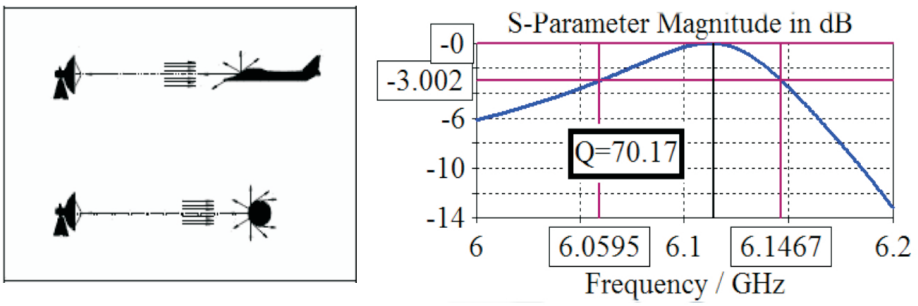

FIGURE 1.4: (a) Definition of the RCS, a far-field parameter, which is used to characterize the scattering properties of a radar target. (b) Q-factor, $Q = f/\Delta f$ with Δf is corresponds to the bandwidth when the power is reduced to its half i.e. -3dB for the S-parameter that presents a maximum.

The method of moments (MoM) is a numerical computational method of solving the differential Maxwell's equations formulated as integral equations. Basically, this method replaces the structure of interest (the scatterer object) for a mesh over the object's surface with a uniform electric current $\mathbf{J}$. The effective currents produce the scattered fields in the space and, making use of the boundary conditions for the electric and magnetic fields, the currents are related with the incident field.

Now, let us consider an infinite 2D periodic surface in the $xy-$plane of cell size a. If any function $E(x, y)$ represents an incident electric field on the surface reacting with the periodic surface, the geometric periodicity forces the field to be periodic, such that $E(x + na, y + na, z) = C^n E(x, y, z)$ with $C = e^{-jka}$ a complex constant. This relation means that the fields in the adjacent periods differ only by a constant complex multiplier. Thus, we can sum all these contributions as Fourier series

$$\mathbf{E}(x, y, z) = \sum_{m=-\infty}^{\infty} \mathbf{E}_m(z) e^{-j(k + \frac{2\pi m x}{a} + \frac{2\pi n y}{a})}. \tag{1.1}$$

The members of this series are called *Floquet modes* [19]. From the computational approach, the response of the FSS is calculated by using the method of moments for the calculation of the electromagnetic fields of a single unit cell, then, these fields correspond to the Floquet modes $\mathbf{E}_m$ and the full solution is given by equation 1.1. The software **CST-Microwave Studio** performs this type of numerical simulations, as shown in figure 1.5(a) [20]. Initially, the geometrical parameters of the structure and the materials are defined, then, the boundary conditions corresponding to the floquet modes are specified. By means of the MoM, we performed simulations with the *Frequency Domain Solver*, once the meshing properties are specified, as shown in figure 1.5(b). This method is general for any geometry or structure, and can be used for both FSSs and metasurfaces. As the wavelength approaches the period, higher-order Floquet modes must be

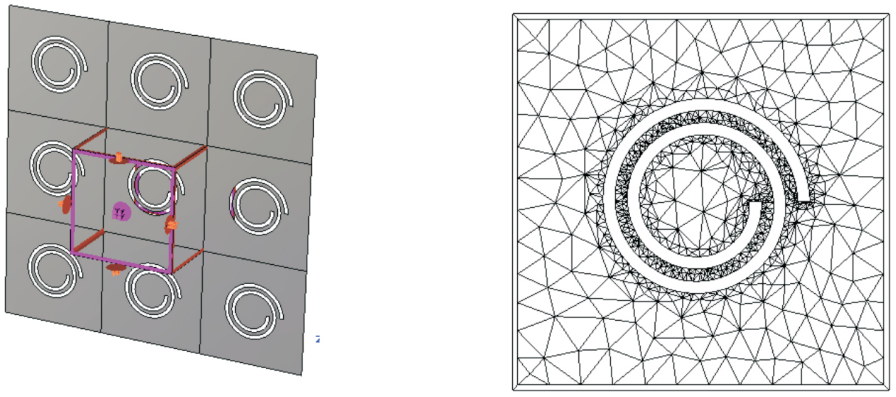

(a) (b)

FIGURE 1.5: CST-Microwave Studio Software to analyze Frequency Selective Surfaces. (a) Periodic boundary conditions. (b) Mesh over the unit cell to perform the method of moments [RWG].

considered. At certain frequencies, the structure blocks the propagation of EM waves through the material. The frequency bands where this occurs are referred to as stop-bands. At other frequencies, the periodic structure allows energy to propagate through the structure: these frequency bands are referred to as pass bands.

1.4 Metasurfaces

In traditional designs, the frequency-selective properties result from mutual interactions of the unit cells. Therefore, to observe the filtering response, a large number of unit cells must be present. Consequently, the overall size of the surface is electrically large. For some applications where a low sensitivity with respect to the angle of incidence of the exciting wave is required, or in cases where a uniform wavefront is difficult to establish, the screen size needs to be small. To address this problem, a new class of FSSs called miniaturized-element frequency-selective surfaces have been developed, whose origin comes from the field of *metamaterials*. Metamaterials are typically engineered by arranging a set of small scatterers or apertures in a regular array throughout a region of space, thus obtaining some desirable bulk electromagnetic behavior. So, this type of FSSs are called **Metasurfaces** [5, 7, 21, 22].

Metasurfaces have a wide range of potential applications in electromagnetics (ranging from low microwave to optical frequencies), including controllable "smart" surfaces, miniaturized cavity resonators, novel wave-guiding structures, angular-independent surfaces, absorbers, biomedical devices and terahertz switches, to name only a few [23]. The main difference between a metasurface and a FSS is the size of its scatterers in comparison to the wavelength at resonance, giving them different responses.

If the wavelength is much larger than the period of the structure, these scatterers could have induced or permanent dipole moments, as is the case for atoms or molecules for classical materials [21]. Alternatively, these scatterers can be generic in shape and placed in a host matrix to obtain a man-made composite material designed to achieve some specified behavior. In this case, effective medium properties are calculated as the permittivity ϵ_r and the permeability μ_r. But when the wavelength becomes comparable to or smaller than the period of the structure, the fields no longer "see" the composite as an effective medium. In this case, a more complicated field behavior exists, and full-wave techniques for analyzing the electromagnetic response are needed. The classical analytical approach for this is the Floquet mode expansion previously described, in which the fields are expanded into an infinite sum of plane waves propagating in various directions.

In the case of metasurfaces, in addition to the effective medium properties that can be calculated, it is possible to approximate the induced currents on the surface as uniform, in order to create equivalent circuit models based in the geometry of the resonators used.

Chapter 2

Electromagnetism of FSS

When an EM plane wave passes through any metallic screen, induced currents are formed on the surface, that reradiate to both sides from it. This response depends of the geometry and dimensions of the scatterers etched on the screen, the polarization state of the incident wave, the materials used, and the frequency. In this chapter, we provide the theoretical background to analyze the electromagnetic phenomena behind FSSs under normal incidence, by means of the transmission and reflection coefficients. As an important remark, this chapter will provide some interesting features on these coefficients in the complex plane, that has not been found in the literature. [2, 12, 19, 24].

2.1 Plane Wave Reflection and Transmission at Media Interface

Electric and magnetic phenomena are described by *Maxwell Equations*. For harmonic time dependence, $e^{-i\omega t}$ of the electric field $\mathbf{E}$, magnetic flux density $\mathbf{B}$, magnetic field strength $\mathbf{H}$, and displacement field $\mathbf{D}$, these equations are

$$\begin{aligned} \nabla \cdot \mathbf{D} &= \rho & \nabla \cdot \mathbf{B} &= 0 \\ \nabla \times \mathbf{E} &= i\omega \mathbf{B} - \mathbf{M} & \nabla \times \mathbf{E} &= -i\omega \mathbf{D} + \mathbf{J} \end{aligned} \tag{2.1}$$

with $\mathbf{J}$ the electric current density and $\mathbf{M}$ the fictitious magnetic current density. This is a fictitious source in the sense that it is only a mathematical convenience: the real source of a magnetic current could be any type of magnetic dipole, as opposed to the flow of an actual magnetic charge. Thus, the electric charge density ρ is the ultimate source of electromagnetic field [2].

When electromagnetic fields exist in material media, the field vectors are related to each other by the *Constitutive Relations*:

$$\begin{aligned} \mathbf{D}(\mathbf{r},\omega,\mathbf{E},\mathbf{H}) &= \epsilon(\mathbf{r},\omega,\mathbf{E},\mathbf{H})\cdot\mathbf{E}(\mathbf{r},\omega) \\ \mathbf{B}(\mathbf{r},\omega,\mathbf{E},\mathbf{H}) &= \mu(\mathbf{r},\omega,\mathbf{E},\mathbf{H})\cdot\mathbf{H}(\mathbf{r},\omega). \end{aligned} \tag{2.2}$$

where ϵ (μ) corresponds to the electric permittivity (magnetic permeability) of the material, which possesses an scalar value when the material is isotropic. When this value is independent of the electric field (magnetic field), the material is known as linear and it is proportional to the *electric susceptibility* (magnetic susceptibility). In addition, Maxwell's Equations require known boundary values for a unique and complete solution. As a general description, these boundary conditions are

$$\begin{aligned} \hat{n}\cdot(\mathbf{D_2}-\mathbf{D_1}) &= \rho_\mathbf{s} \\ \hat{n}\cdot(\mathbf{B_2}-\mathbf{B_1}) &= 0 \\ \hat{n}\times(\mathbf{E_2}-\mathbf{E_1}) &= -\mathbf{M_s} \\ \hat{n}\times(\mathbf{H_2}-\mathbf{H_1}) &= \mathbf{J_s}. \end{aligned} \tag{2.3}$$

2.2 Surface Equivalence Principle

By means of the uniqueness theorem [25], two sources producing the same field within a region of the space are said to be equivalent. If we are interested in the EM fields in a certain region of the space, it is not necessary to know the actual sources but the *equivalent sources* will serve as well.

As shown in figure 2.1, both the incident field and the sources inside a region S, produce the fields $\mathbf{E},\mathbf{H}$ inside and outside S. We can setup an equivalent problem external to S as follows: Let the original field $\mathbf{E},\mathbf{H}$ exist external to S, and the null field internal to S with free space everywhere. To support this field there must exist surface currents $\mathbf{J_i},\mathbf{M_i}$ on S according to the boundary conditions 2.3. These currents are therefore:

$$\begin{aligned} \mathbf{J_i} &= \mathbf{n}\times\mathbf{H} \\ \mathbf{M_i} &= -\mathbf{n}\times\mathbf{E} \end{aligned} \tag{2.4}$$

where $\mathbf{n}$ is the outwards normal vector to the surface S and $\mathbf{E},\mathbf{H}$ are the original fields over S. Since the currents act in unbounded free space, it is possible to find the field from them, by using the equations (c.g.s. unit system):

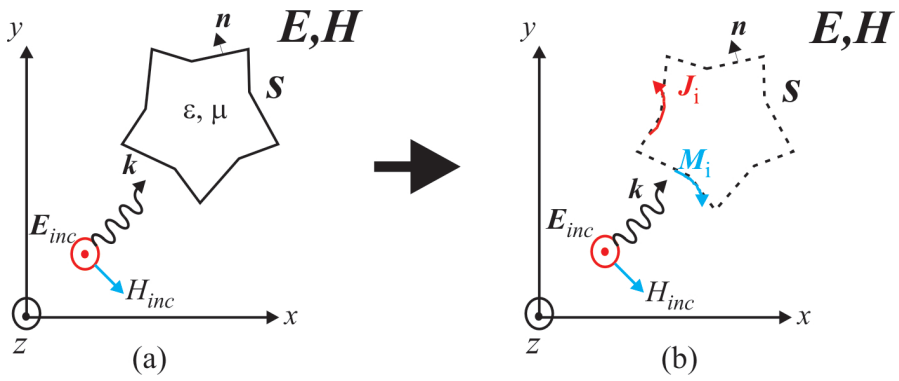

FIGURE 2.1: Surface Equivalence Principle

$$\begin{aligned}\mathbf{E} &= -\nabla \times \mathbf{F} + \frac{\nabla\nabla\cdot\mathbf{A}+k^2\mathbf{A}}{i\omega\epsilon_0} \\ \mathbf{H} &= \nabla \times \mathbf{A} + \frac{\nabla\nabla\cdot\mathbf{F}+k^2\mathbf{F}}{i\omega\mu_0}\end{aligned} \tag{2.5}$$

where $\mathbf{A}, \mathbf{F}$ correspond to the electric and magnetic potential vectors respectively

$$\begin{aligned}\mathbf{A}(\mathbf{r}) &= \frac{1}{4\pi}\int\int\int \frac{\mathbf{J}(\mathbf{r}')e^{ik|\mathbf{r}-\mathbf{r}'|}}{|\mathbf{r}-\mathbf{r}'|}dr' \\ \mathbf{F}(\mathbf{r}) &= \frac{1}{4\pi}\int\int\int \frac{\mathbf{M}(\mathbf{r}')e^{ik|\mathbf{r}-\mathbf{r}'|}}{|\mathbf{r}-\mathbf{r}'|}dr'\end{aligned} \tag{2.6}$$

which are derived from the wave equation. When these potential vectors are replaced in equation 2.5, we obtain the so-called *Integro-differential equations: EFIE and MFIE*, which are the key basis of the computational Method of Moments [9, 18] mentioned in Chapter 1. From the uniqueness theorem, we know that the calculated field will be the originally postulated field. The final result of this procedure is a formula for $\mathbf{E}, \mathbf{H}$ everywhere external to S in terms of the tangential components of $\mathbf{E}, \mathbf{H}$ on S [25].

2.3 Image Theory

Now, problems for which the field in a given region of space is determined from a knowledge of the field over the boundary of the region, are called *boundary-value problem*. If we consider the boundary-value problems for which the boundary is made of Perfect Electric Conductor, PEC or Perfect Magnetic Conductor, PMC, where the tangential components of $\mathbf{E}$ ($\mathbf{H}$) vanish, we can use a procedure known as *Image theory*. By noting that the conducting surfaces have a constant potential, these can be placed at the equipotential lines in any field distribution without altering the fields. For instance, two point charges with opposite sign separated a distance $2d$ form an equipotential plane at a distance of d between them. Thus, in this plane, any surface (PEC) can be placed without any change in the electric field distribution. Oppositely, the field

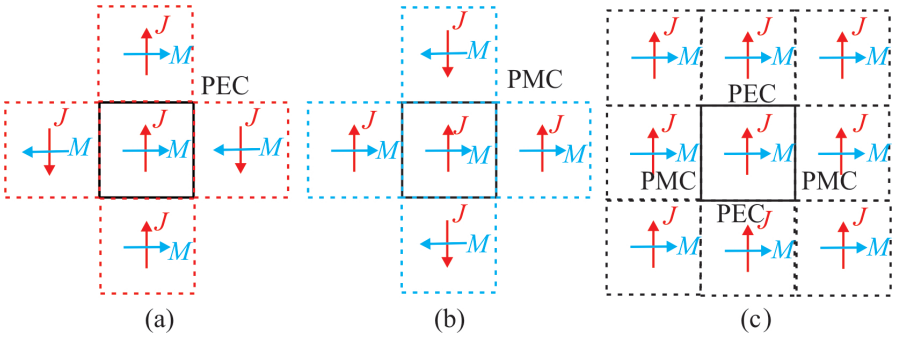

FIGURE 2.2: Image theory for electric and magnetic dipole moments placed in a square cavity with PEC and PMC walls. a) PEC walls, b) PMC walls, c) proper combination to have equal images on each side, thus, *Periodic Boundary Conditions*

distribution formed by a charge separated d to a planar PEC surface is equivalent to create the "image charge" (opposite charge) spaced the same distance below the original conducting surface [26]. In general, the electric and magnetic density currents $\mathbf{J}, \mathbf{M}$ have its equivalent images in front of electric and magnetic walls. Properly placed, it can be seen that the configuration of a rectangle with two PEC and two PMC walls produces periodic identical images of the currents placed inside the rectangle, as shown in Fig 2.2.

2.4 Transmission Matrix

When any electromagnetic wave impinges on a 2D structure, it can be reflected, transmitted or absorbed. The *Transmission Matrix* is a practical form to mathematically describe this phenomena. In general, under any angle of incidence and polarization state, the dimension of this matrix is 4×4 in order to consider both tangential components to the structure. As shown in Figure 2.3, the fields $\mathbf{E}$ and $\mathbf{H}$ have the superscript "+" if the propagation vector goes to the surface and "−" when it goes out from the surface. The transmission matrix $\mathbf{T}$ relates the electric fields at both sides of the surface and these are propagated in any direction (+ or − z) as follows:

$$\begin{pmatrix} E_{1x}^{+} \\ E_{1y}^{+} \\ E_{1x}^{-} \\ E_{1y}^{-} \end{pmatrix} = \mathbf{T} \cdot \begin{pmatrix} E_{2x}^{+} \\ E_{2y}^{+} \\ E_{2x}^{-} \\ E_{2y}^{-} \end{pmatrix} \implies \begin{pmatrix} \mathbf{E}_{1,\mathrm{t}}^{+} \\ \mathbf{E}_{1,\mathrm{t}}^{-} \end{pmatrix} = \begin{pmatrix} \mathbf{T}_{\mathrm{a}} & \mathbf{T}_{\mathrm{b}} \\ \mathbf{T}_{\mathrm{c}} & \mathbf{T}_{\mathrm{d}} \end{pmatrix} \cdot \begin{pmatrix} \mathbf{E}_{2,\mathrm{t}}^{+} \\ \mathbf{E}_{2,\mathrm{t}}^{-} \end{pmatrix} \tag{2.7}$$

The matricial form of the transmission and reflection coefficients $(\mathbf{t})(\mathbf{r})$, when the incident wave $\mathbf{E}_1^+$ comes from side 1 (see figure 2.3), are determined as:

$$\mathbf{E}_{2,\mathrm{t}}^{+} = \mathbf{t} \cdot \mathbf{E}_{1,\mathrm{t}}^{+},$$

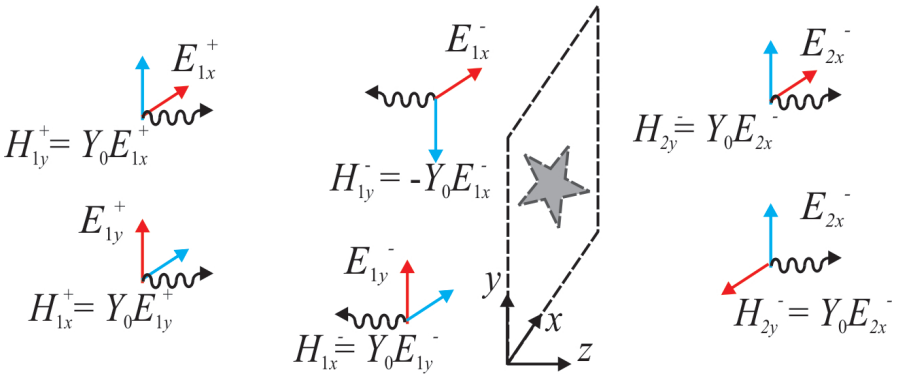

FIGURE 2.3: Electromagnetic Waves impinging on a surface from both sides.

$$\mathbf{E}^-_{1,\mathrm{t}} = \mathbf{r} \cdot \mathbf{E}^+_{1,\mathrm{t}},$$

when $\mathbf{E}^-_2 = 0$. On the other hand, when the incident wave comes from the side 2, $\mathbf{E}^-_2$, the coefficients $\mathbf{t}'$ and $\mathbf{r}'$ satisfy:

$$\mathbf{E}^-_{1,\mathrm{t}} = \mathbf{t}' \cdot \mathbf{E}^-_{2,\mathrm{t}},$$

$$\mathbf{E}^+_{2,\mathrm{t}} = \mathbf{r}' \cdot \mathbf{E}^-_{2,\mathrm{t}},$$

when $\mathbf{E}^+_1 = 0$. Thus, all the components x and y of the transmission and reflection coefficients are given by:

$$t_{xx} = \underset{\substack{E^+_{1y}=0\\ \mathbf{E}^-_2=0}}{\left.\frac{E^+_{2x}}{E^+_{1x}}\right|}, \quad t_{xy} = \underset{\substack{E^+_{1x}=0\\ \mathbf{E}^-_2=0}}{\left.\frac{E^+_{2x}}{E^+_{1y}}\right|}, \quad t_{yx} = \underset{\substack{E^+_{1y}=0\\ \mathbf{E}^-_2=0}}{\left.\frac{E^+_{2y}}{E^+_{1x}}\right|}, \quad t_{yy} = \underset{\substack{E^+_{1x}=0\\ \mathbf{E}^-_2=0}}{\left.\frac{E^+_{2y}}{E^+_{1y}}\right|} \tag{2.8a}$$

$$r_{xx} = \underset{\substack{E^+_{1y}=0\\ \mathbf{E}^-_2=0}}{\left.\frac{E^-_{1x}}{E^+_{1x}}\right|}, \quad r_{xy} = \underset{\substack{E^+_{1x}=0\\ \mathbf{E}^-_2=0}}{\left.\frac{E^-_{1x}}{E^+_{1y}}\right|}, \quad r_{yx} = \underset{\substack{E^+_{1y}=0\\ \mathbf{E}^-_2=0}}{\left.\frac{E^-_{1y}}{E^+_{1x}}\right|}, \quad r_{yy} = \underset{\substack{E^+_{1x}=0\\ \mathbf{E}^-_2=0}}{\left.\frac{E^-_{1y}}{E^+_{1y}}\right|} \tag{2.8b}$$

$$t'_{xx} = \underset{\substack{E^-_{2y}=0\\ \mathbf{E}^+_1=0}}{\left.\frac{E^-_{1x}}{E^-_{2x}}\right|}, \quad t'_{xy} = \underset{\substack{E^-_{2x}=0\\ \mathbf{E}^+_1=0}}{\left.\frac{E^-_{1x}}{E^-_{2y}}\right|}, \quad t'_{yx} = \underset{\substack{E^-_{2y}=0\\ \mathbf{E}^+_1=0}}{\left.\frac{E^-_{1y}}{E^-_{2x}}\right|}, \quad t'_{yy} = \underset{\substack{E^-_{2x}=0\\ \mathbf{E}^+_1=0}}{\left.\frac{E^-_{1y}}{E^-_{2y}}\right|} \tag{2.8c}$$

$$r'_{xx} = \underset{\substack{E^-_{2y}=0\\ \mathbf{E}^+_1=0}}{\left.\frac{E^+_{2x}}{E^-_{2x}}\right|}, \quad r'_{xy} = \underset{\substack{E^-_{2x}=0\\ \mathbf{E}^+_1=0}}{\left.\frac{E^+_{2x}}{E^-_{2y}}\right|}, \quad r'_{yx} = \underset{\substack{E^-_{2y}=0\\ \mathbf{E}^+_1=0}}{\left.\frac{E^+_{2y}}{E^-_{2x}}\right|}, \quad r'_{yy} = \underset{\substack{E^-_{2x}=0\\ \mathbf{E}^+_1=0}}{\left.\frac{E^+_{2y}}{E^-_{2y}}\right|} \tag{2.8d}$$

and the transmission matrix is presented in terms of the transmission and reflection coefficients as:

$$\mathbf{T} = \begin{pmatrix} \mathbf{t}^{-1} & -\mathbf{t}^{-1} \cdot \mathbf{r}' \\ \mathbf{r} \cdot \mathbf{t}^{-1} & \mathbf{t}' - \mathbf{r} \cdot \mathbf{t}^{-1} \cdot \mathbf{r}' \end{pmatrix} \tag{2.9}$$

In general, a transmission matrix can be associated to an element that reflects and transmits the incident wave on side 1 in a determined form at side 2. Thus, a cascade array of elements can be mathematically represented as a cascade multiplication of transmission matrices. When the incident wave is given in terms of voltage and current (*Transmission Line Theory* [2]) the Transmission Matrix is equivalent to the ABCD Matrix. The ABCD matrix of the cascade connection of the two networks is equal to the product of the ABCD matrices representing the individual two-ports. Note that the order of multiplication of the matrix must be the same as the order in which the networks are arranged, since matrix multiplication is not, in general, commutative. The transmission matrix is useful when our interest is the total field in a region when passes through different objects.

2.5 Scattering Matrix

A representation more in accord with direct measurements and with the ideas of incident, reflected, and transmitted waves, is given by the *Scattering Matrix*. This matrix provides a complete description of the structure that transmits, reflects and absorbs as seen on both sides. The scattering matrix relates the incident waves incident on the structure itself (no matter its incoming side) to those reflected from the structure, the outgoing waves. For some components and circuits, the scattering parameters can be calculated using network analysis techniques. [2, 16]. Otherwise, the scattering parameters can be measured directly with a Vector Network Analyzer. Once the scattering parameters of the network are known, conversion to other matricial description can be performed, if needed.

The scattering matrix, connects the incoming and outgoing waves from the structure by the linear relation $\left[E_{x1}^{-}, E_{y1}^{-}, E_{x2}^{-}, E_{y2}^{-}\right] = \mathbf{S}\left[E_{x1}^{+}, E_{y1}^{+}, E_{x2}^{+}, E_{y2}^{+}\right]$ with

$$\mathbf{S} = \left(\begin{array}{cc|cc} r_{xx} & r_{xy} & t_{xx} & t_{xy} \\ r_{yx} & r_{yy} & t_{yx} & t_{yy} \\ - & - & - & - \\ t_{xx} & t_{xy} & r_{xx} & r_{xy} \\ t_{yx} & t_{yy} & r_{yx} & r_{yy} \end{array}\right)$$

With r_{xx} for instance, the reflection coefficient along the x axis due to an incident electric field along the x axis too. Likewise, the cross polarization effects,r_{xy} the reflection on the x axis produced by an incident wave polarized along the y axis. Rewriting $r_x \equiv r_{xx}$ and $r_y \equiv r_{yy}$ the *direct* reflection coefficients, $t_x \equiv t_{xx}$ and $t_y \equiv t_{yy}$ the *direct* transmission coefficients, and $c \equiv r_{xy} = r_{yx} = t_{xy} = t_{yx}$; it is worth to note that, due to the reflection symmetry along the $z-$axis, the coefficients for one direction of propagation equal those of the opposite direction. From the reciprocity theorem $r_{xy} = r_{yx}$ and $t_{xy} = t_{yx}$, besides, from the continuity of the electric field on the screen ($z = 0$) we have $r_{yx} = t_{yx}, r_{xy} = t_{xy}$ and

$$1 + r_{xx} = t_{xx}. \tag{2.10}$$

Thus, the $\mathbf{S}$ matrix can be rewritten as

$$\mathbf{S} = \begin{pmatrix} r_x & c & 1+r_x & c \\ c & r_y & c & 1+r_y \\ 1+r_x & c & r_x & c \\ c & 1+r_y & c & r_y \end{pmatrix} = \begin{pmatrix} \mathbf{R} & \mathbf{R} \\ \mathbf{R} & \mathbf{R} \end{pmatrix} + \begin{pmatrix} \mathbf{0} & \mathbf{1} \\ \mathbf{1} & \mathbf{0} \end{pmatrix}, \tag{2.11}$$

with $\mathbf{R}$ the 2×2 reflection matrix and $\mathbf{1}$ the identity matrix. It is well known that for reciprocal [25] and lossless structures $\mathbf{S} \cdot \mathbf{S}^* = \mathbf{1}$. Imposing this property onto 2.11 we rapidly get the relation

$$\left[\begin{pmatrix} \mathbf{R} & \mathbf{R} \\ \mathbf{R} & \mathbf{R} \end{pmatrix} + \begin{pmatrix} \mathbf{0} & \mathbf{1} \\ \mathbf{1} & \mathbf{0} \end{pmatrix}\right] \cdot \left[\begin{pmatrix} \mathbf{R} & \mathbf{R} \\ \mathbf{R} & \mathbf{R} \end{pmatrix} + \begin{pmatrix} \mathbf{0} & \mathbf{1} \\ \mathbf{1} & \mathbf{0} \end{pmatrix}\right]^* = \begin{pmatrix} \mathbf{1} & \mathbf{0} \\ \mathbf{0} & \mathbf{1} \end{pmatrix}$$

such that each component satisfies $\mathbf{R} \cdot \mathbf{R}^* + Re[\mathbf{R}] = 0$, or more precisely

$$\begin{pmatrix} |r_x|^2 + |c|^2 + r_{xr} & r_x c^* + r_y^* c + c_r \\ r_y c^* + r_x^* c + c_r & |r_y|^2 + |c|^2 + r_{yr} \end{pmatrix} = \begin{pmatrix} 0 & 0 \\ 0 & 0 \end{pmatrix}. \tag{2.12}$$

On the other hand, boundary conditions for tangential components of the magnetic field can be written as: $H_{2x} - H_{1x} = J_y$ and $H_{2y} - H_{1y} = -J_x$, where J_x and J_y are components of the macroscopic surface electric current on the structure. Now, if we assume that the pattern of currents on the resonator is not depending on frequency neither on the incident electric wave polarization, (for frequencies close to the resonance) it is possible to introduce the hypothesis

$$J_y = kJ_x. \tag{2.13}$$

This condition is particularly valid when the pattern of currents is determined by the geometry of the resonator. Applying this hypothesis 2.13 and properly traducing magnetic

fields into electric fields, we can achieve the relation

$$-E_{2y}^{-} + E_{1y}^{+} - E_{1y}^{-} = -k(E_{2x}^{-} - E_{1x}^{+} + E_{1x}^{-}). \tag{2.14}$$

Assuming either $x-$ or $y-$polarized normal incident waves and normalizing by the incident field, we get

$$r_x = c/k \quad r_y = kc \quad r_x r_y = c^2. \tag{2.15}$$

Considering this new relation 2.15 between the direct reflection coefficients and the cross coefficients into the first term of equation 2.12, which in fact is associated to energy conservation, we can show that all the coefficients r_x, t_x, and c describe circumference paths on the complex plane as

$$\left(r_{xr} + \frac{1}{2(1+|k|^2)}\right)^2 + r_{xi}^2 = \left(\frac{1}{2(1+|k|^2)}\right)^2 \tag{2.16}$$

$$\left(t_{xr} - 1 + \frac{1}{2\,(1+|k|^2)}\right)^2 + t_{xi}^2 = \left(\frac{1}{2(1+|k|^2)}\right)^2 \tag{2.17}$$

$$\left(c_r + \frac{k_r}{2\,(1+|k|^2)}\right)^2 + \left(c_i + \frac{k_i}{2\,(1+|k|^2)}\right)^2 = \left(\frac{|k|^2}{4(1+|k|^2)}\right). \tag{2.18}$$

These equations remain valid for r_x and r_y. Basically, while the reflection moves along a circumference within a frequency range of a single resonance, the transmission moves along the same circumference but displaced by the unity. A smaller trajectory is followed by the cross coefficients, which lie on the same side of the reflection loci. The second term of equation 2.12 allows us to demonstrate that k is complex but $\left(\frac{r_x - r_y}{c}\right)$ is real: as $r_x c^* + r_y^* c + c_r = r_x^* c + r_y c^* + c_r^* = 0$, thus

$$\frac{r_x - r_y}{c} = \frac{r_x^* - r_y^*}{c^*} \tag{2.19}$$

The description stated above for the scattering parameters on the complex plane has been found only at [24] but no relations between the direct reflection coefficients and the cross polarization terms has been previously found in literature.

2.6 Babinet's Principle

For thin and lossless plates, the Babinet's principle [10] must hold. This principle states that the total field transmitted by a metallic screen with an arbitrary aperture,

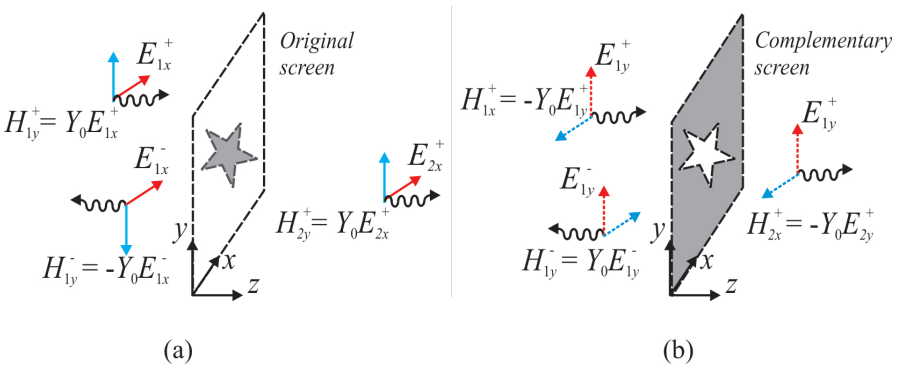

FIGURE 2.4: Babinet's Principle: definition of the original and complementary problem.a) Original problem b) complementary problem.

added to the total field transmitted by its complementary screen, illuminated by the complementary incident wave, as shown in figure 2.4(a) and (b), gives the incident wave over this last structure. For the incident fields on any screen, $\mathbf{E}_0$ and $\mathbf{B}_0$, and the incident fields of its complementary $\mathbf{E^c}_0$,$\mathbf{B^c}_0$, the following relation must hold:

$$\begin{aligned} \mathbf{E}_0^c &= c\mathbf{B}_0 \\ \mathbf{B}_0^c &= \tfrac{-1}{c}\mathbf{E}_0, \end{aligned} \tag{2.20}$$

which can be seen as a 90 grades rotation between the incident wave of the original and the complementary problem. The total field is the sum of the incident and the scattered field and the Babinet's principle relates these fields by

$$c\mathbf{B} + \mathbf{E}_c = c\mathbf{B^0}. \tag{2.21}$$

In order to express the Babinet's principle in terms of the electric field only with the proper signs of each component, we get

$$\begin{gathered} E_x - cB_{cx} = E_x^0 \quad \longrightarrow \quad E_x + E_{cy} = E_x^0 \\ t_{xx}E_x^0 + t_{xy}E_y^0 - t_{yx}^c E_y^0 + t_{yy}^c E_x^0 = E_x^0 \end{gathered} \tag{2.22}$$

.

We can divide the equation 2.22 into two separated problems: under $x-$polarization incidence ($E_x^0 \neq 0$, $E_y^0 = 0$), or $y-$polarization incidence ($E_x^0 = 0$, $E_y^0 \neq 0$) which yields the simplified equations

$$\begin{aligned} t_x + t_y^c &= 1 \\ t_{xy} - t_{yx}^c &= 0 \end{aligned} \tag{2.23}$$

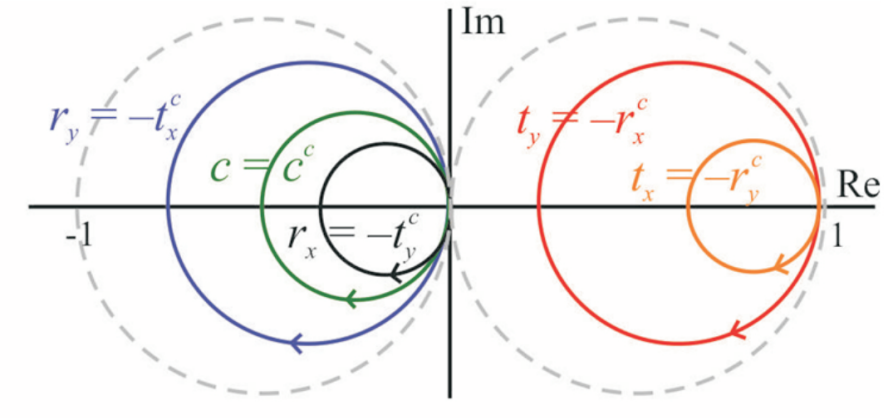

FIGURE 2.5: Theoretical sketch of reflection coefficients r_x and r_y, transmission coefficients t_x and t_y, the cross terms c and its relations with the coefficients of the complementary problem (superscript ^{c})

Babinet's principle can be expressed in terms of the reflection coefficients as

$$\begin{aligned} r_x + r_y^c &= -1 \\ c - c^c &= 0 \end{aligned} \tag{2.24}$$

For the complementary problem, the circumferences 2.16, 2.17 and 2.18 are equal and, by means of the Babinet's principle these are related with the original screen by

$$\begin{aligned} t_x + t_y^c &= 1 \\ t_y + t_x^c &= 1 \end{aligned} \tag{2.25}$$

By using equations 2.24 and 2.23, $t^c = -r$ and $r^c = -t$, see Figure 2.5. In practice, these results must be considered as a first approximation. For realistic structures, the most important deviations from the above results come from losses in the screens and substrate effects. Special attention is required on the hypothesis 2.13. This equation is properly working for resonators were the current is forced to lie on specific metal paths. For complementary resonators, the electric current is, in some way, more free to flow on bigger metal regions, so that the hypothesis is no longer true. A way to fix this problem would be to change the hypothesis to another similar relation with effective surface magnetic currents on the slots. Alternatively, we can also use the Babinet's principle along with boundary conditions, in order to obtain the relations shown in figure 2.5.

2.7 Numerical Validation

To check the theory stated above, a set of numerical simulations is carried out by using *CST Microwave Studio*. Figure 2.6 shows the scattering parameters for two surfaces

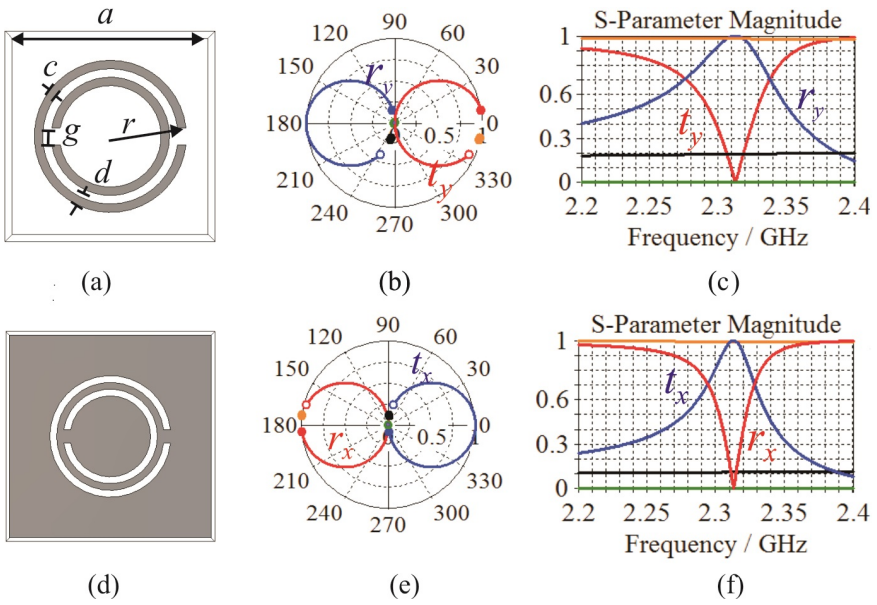

FIGURE 2.6: Scattering parameters for metasurfaces presenting mirror symmetry. a) SRR, b) C-SRR.

presenting mirror symmetry [27–29]. One made of SRRs, that satisfy the small electric size and thin metal strips needed to use the hypothesis of $J_y = kJ_x$ and another one made of C-SRRs, both made of PEC. The geometrical parameters (a), were set as $a =$ 15 mm, $r = 9$ mm, and $c = d =$1mm, $g =$2mm. The reflection and transmission coefficients of the **S** matrix are depicted on the complex plane for the SRR (b) and the CSRR (e), where the relations that the Babinet's principle yields $r_x^c = -t_y$ (red), $r_y^c = -t_x$ (orange), $t_x^c = -r_y$ (blue) and $t_y^c = -r_x$ (black) are verified and no cross polarization effects are observed. Considering its resonant response, these coefficients vary in frequency presenting a dip or peak according to the surface and the $S-$parameter under study, as shown in figure 2.6(c) and (f).

In the case of unsymmetrical geometries, like spirals, a metallic strip forming an *Achimedes' Spiral* was designed as well as its complementary with the same geometrical parameters of the SRR. The spirals designed had two loops, so named *Archimedes Spiral Resonator 2* (ASR2) and its complementary (C-ASR2), as shown in Figure 2.7(a, d) respectively. In the $S-$parameters plotted in the complex plane (c) and (e) it is possible to observe the circle associated to 2.18, the circumference associated to the cross polarization effects, moreover $c = c^c$ is satisfied.

2.8 Resonator Design

For experimental verification, it is necessary to add the *Absorbency* $|a|^2$ to the energy conservation, such that $|r|^2+|t|^2+|a|^2 = 1$. The effect of this term on the circumferences

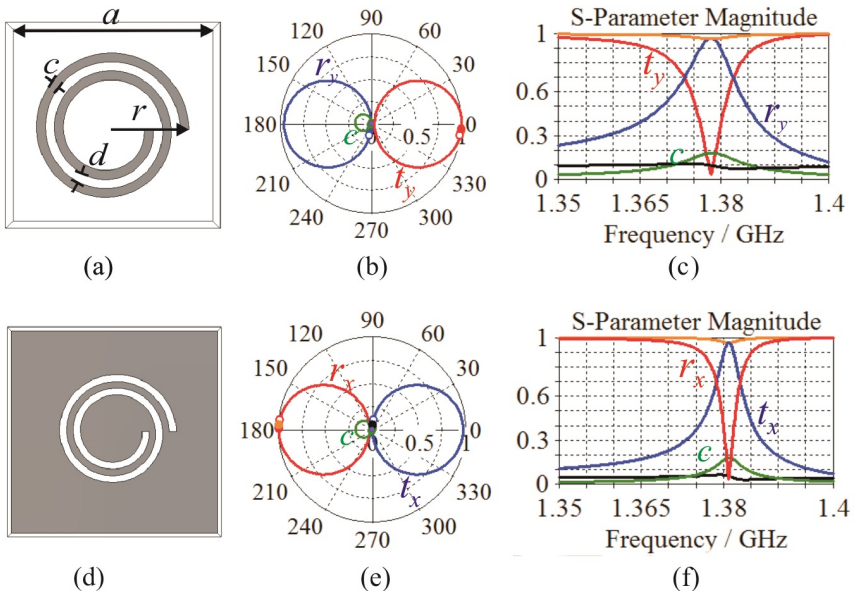

FIGURE 2.7: Scattering parameters for asymmetrical metasurfaces. a) ASR2, b) C-ASR2.

described by the reflection and transmission coefficients is a change of its radius by subtracting the term $\frac{|a|^2}{2(1+|k|^2)}$ on the right side of equations 2.16, 2.17 and 2.18. We performed the same set of numerical simulations for the metasurfaces made of SRR, C-SRR, ASR2 and C-ASR2, but in this case we used a substrate Rogers Ultralam 2000 of relative permittivity $\epsilon_r = 2.5$, thickness h =0.5 mm, and loss tangent of 0.0019. The metallic paths were simulated with copper, as shown in figures 2.8 and 2.9. Under these conditions the resonance frequency between the SRR and C-SRR, is not the same due to the substrate as shown in figure 2.8(e,f).

However, the loci of the transmission and reflection coefficients still as circumferences whose radius is smaller due to the absorption, as shown in figure (c,d). Another interesting fact of these curves, is that the initial and final points of the circumferences do not lie on the real axis as it do under ideal conditions. This fact can be explained by an added phase given by the thickness of the substrate. Besides, the latter case, the cross polarization effects are reduced, thus, more energy is absorbed than radiated in the cross polarization.

In the case of metasurfaces made of ASR2 (C-ASR2), figure 2.9(a) and (b). Indeed, the cross polarization effects are related with the asymmetry of the geometry rather than the materials or the polarization state of the incident wave.

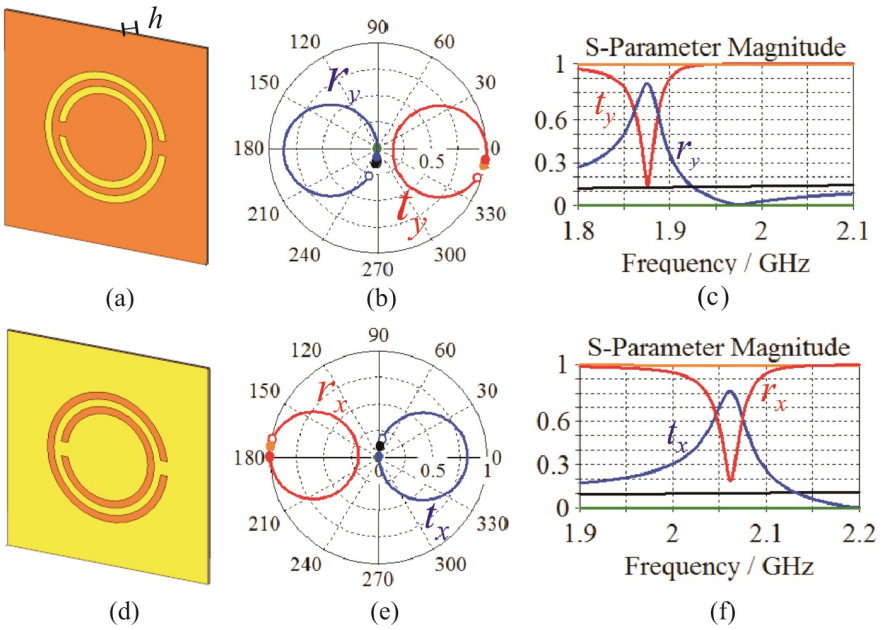

FIGURE 2.8: Scattering parameters for metasurfaces presenting mirror symmetry under realistic conditions. a) SRR, b) C-SRR.

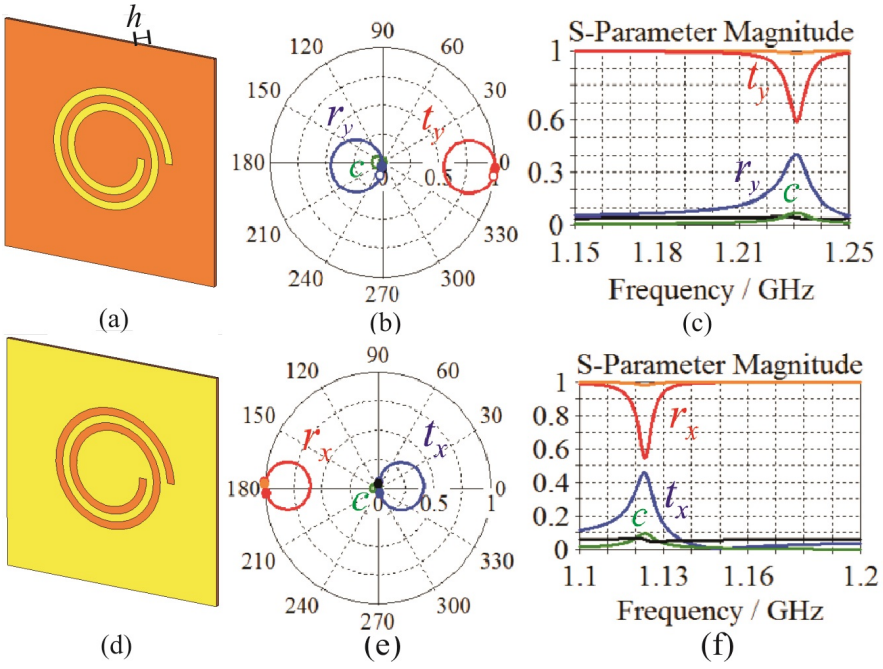

FIGURE 2.9: Scattering parameters for asymmetrical metasurfaces under realistic conditions. a) ASR2, b) C-ASR2.

Chapter 3

Modelling of Metasurfaces

In order to create electromagnetic devices for versatile applications, we need to study complex electromagnetic systems in a experimental, computational and theoretical form. The last one, the reason to develop analytical models. However, analytical modelling requires to separate the most important variables of the system under study, such that our understanding of different EM phenomena is facilitated. In this chapter, we describe the theoretical models previously developed by Marqués, Sorolla, Jelinek, Medina, Baena et. al [8, 30–32] for thin metasurfaces, which are based in LC-circuit models and Babinet's principle.

Then, we analyze the models for thick metasurfaces for SRR and C-SRR based geometries. For the SRR based metasurfaces the model uses equivalent LC-circuit [33], whereas the C-SRR based metasurfaces uses a transmission line model [11]. However, in the range of thickness where Babinet's principle is no longer valid but the thickness itself is small in comparison with the resonant wavelength, no models have been proposed. We will analyze the LC-circuit model for thick SRRs in comparison with a parametric study and its extension to other SRR based geometries. Likewise, for C-SRR based geometries a waveguide model is proposed. The model predicts the resonance frequency of a metasurface avoiding full-wave numerical simulations. Finally, the proposed models are condensed in a user friendly software for the design of metasurfaces.

3.1 Split Ring Resonators

Resonators are key elements in radiofrequency (RF) and microwave engineering. Many passive and active circuits and antennas contain resonant elements in their designs. There are many types of resonators of interest for RF and microwave applications, such as

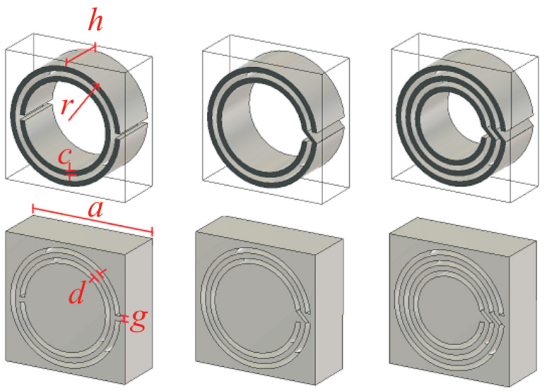

FIGURE 3.1: (a) Resonators to create metasurfaces. First row: the Split Ring Resonator (SRR) and the Spiral Resonators of two and three turns (SR2 and SR3). Second row: complementary unit cell which will be termed as C-SRR, C-SR2, and C-SR3 respectively. The geometric parameters are: $c = d = g$ =1 mm, r = 9 mm, a=15mm, h =3mm. In this throughout this chapter both a and h will vary. Simulations were performed with PEC and aluminium.

cavity resonators, metallic/dielectric resonators, lumped element resonators,transmission line resonators, among others [34].

The SRR (see figure 3.1)(a), originally proposed by Pendry in 1999 [35], has attracted a great interest among physicist and engineers, due to their applications in the synthesis of the so called metamaterials with negative effective permeability [5]. This can be achieved in a certain frequency range sightly above the resonance frequency of the SRR, f_0^{SRR}, and for incident radiation of the appropriate polarization (the polarization that excites the resonator [12]). The success of such artificial media is that around the resonance, SRR's dimensions are small compared to the resonance wavelength. Therefore, an array composed of these small resonators can be considered as an effective medium with effective electromagnetic parameters, which can be deduced from the polarizabilities of these particles when they are illuminated by an external uniform field of the appropriate polarization [36]. Similar geometries have been used for the same purposes like the spirals of two and three turns SR2 and SR3 (see figure 3.1(b,c)) and their usefulness in the design of negative magnetic permeability and left-handed media can be found in [32].

3.2 Thin Metasurfaces

3.2.1 LC-Circuit Model for thin Metasurfaces

The SRR behaves as an LC resonant tank that can be excited by an external magnetic flux and it exhibits a strong diamagnetism above their resonant frequency [12],[8]. It is

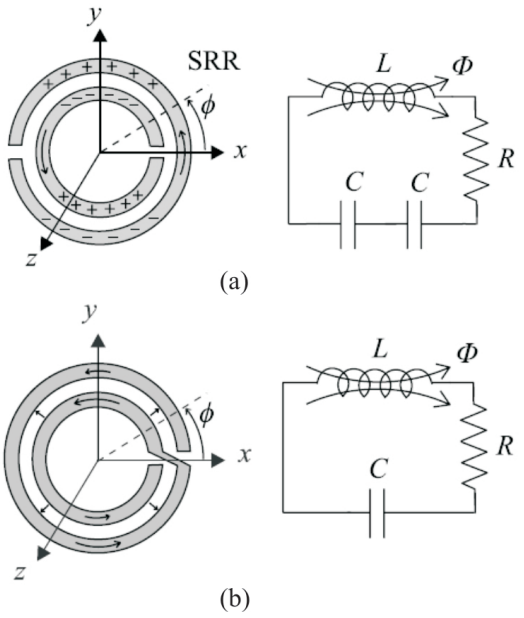

FIGURE 3.2: Equivalent LC-Circuit Models for SRR based resonators and its corresponding equivalent circuit for the determination of the resonance frequency, where C is the capacitance across the slot between the rings and L the inductance of a cylinder of average radius r. (a) SRR (b) SR2. Images from [Metamaterials-Book]

usually excited by an external time-varying magnetic field applied parallel to the particle axis, thus producing a quasi-static resonant effect. The application of an axial, uniform, and time varying magnetic field to the rings induces current loops at resonance. These current loops are closed through the distributed capacitance between concentric rings which can be potentially very high due to the presence of the splits, so that the SRR behaves as an externally driven LC resonator. Figure 3.2 shows the equivalent circuits of the SRR based particles. The capacitance is calculated by means of the capacitance between two coplanar strips [37] and the inductance as the one corresponding to a ring of current of average radius r_0. The inductance and capacitance of this ring can be found in the Appendix of [12]. A quasistatic analysis of this configuration for the spirals SR2 and SR3 leads to the equivalent circuit, and to the current and voltage distributions shown in the figure 3.2, such that the resonance frequency of each resonator satisfies

$$f_0^{SRR} = 2f_0^{SR2} = 2\sqrt{2}f_0^{SR3}. \tag{3.1}$$

Let us consider the behaviour of a plane array of SRRs that scatters an incident plane wave of arbitrary polarization coming from the left side. Induced average surface currents re-radiate electromagnetic fields measured as the transmitted and reflected waves. Such average currents arise from the mean surface polarizations (electric and magnetic) which in turn are related with the polarizabilities of equation 3.2. Cross-polarization effects are present in such a particle, so a magnetic and an electric dipole arise simultaneously as a consequence of the particle excitation. This behaviour is summarized in terms of

the four particle polarizabilities α_{xx}^{ee}, α_{yy}^{ee}, α_{yz}^{em}, α_{zz}^{mm} that in general have the form

$$\alpha = \alpha_0 \left(\frac{\omega_0^2}{\omega^2} - 1 \right)^{-1}. \tag{3.2}$$

The effect of an incident electric field along the $y-$direction induces a magnetic dipole moment m_z and an electric dipole moment p_y in such a way that its resonant response yields a stopband filter, as shown in figure 2.6(c). Now, ff we consider the complementary structure, the C-SRR will be excited by an incident magnetic field along the $y-$direction in such a way that the magnetic dipole moment m_y and the electric dipole moment p_z are induced, as shown in figure 2.6 (f). Due to the resonant response on the polarizabilities, the resonant response is obtained on the surface average currents and therefore on the electromagnetic fields radiated. For infinitely thin metasurfaces made of PEC, the resonance frequency between the SRR and the C-SRR is the same. However, when the thickness is not negligible new models are needed.

3.3 Thick Metasurfaces

This section presents an analytical model to design thick metasurfaces based in SRRs and its related geometries like the spirals SR2 SR3. The objective of this model is to perform parametric studies to facilitate a deeper understanding of the filtering response of the metasurfaces, with a significantly shorter computation time than with the use of electromagnetic simulators.

3.3.1 Parametric Study of SRR based Metasurfaces

In order to get some insights about the filtering response of the metasurface by considering the geometrical parameters only, a set of numerical simulations is performed using a commercial electromagnetic solver *CST-Microwave Studio*. We simulate a metasurface made of the SRR, SR2, SR3 and its complementaries, whose dimensions are shown in figure 3.1. We focus on the two parameters that may increase Q, cell size a and thickness h.

Numerical simulations show that periodic arrays of SRRs present certain bandwidth associated with the neighbourhood interaction. Thus, it is expected that the increment a reduces this interaction and therefore the bandwidth becomes narrower. On the other hand, in the FSS design [13, 14], the increment of the Q-factor can be made by a cascade array of FSS along the $z-$axes taking intro account that each FSS account for a

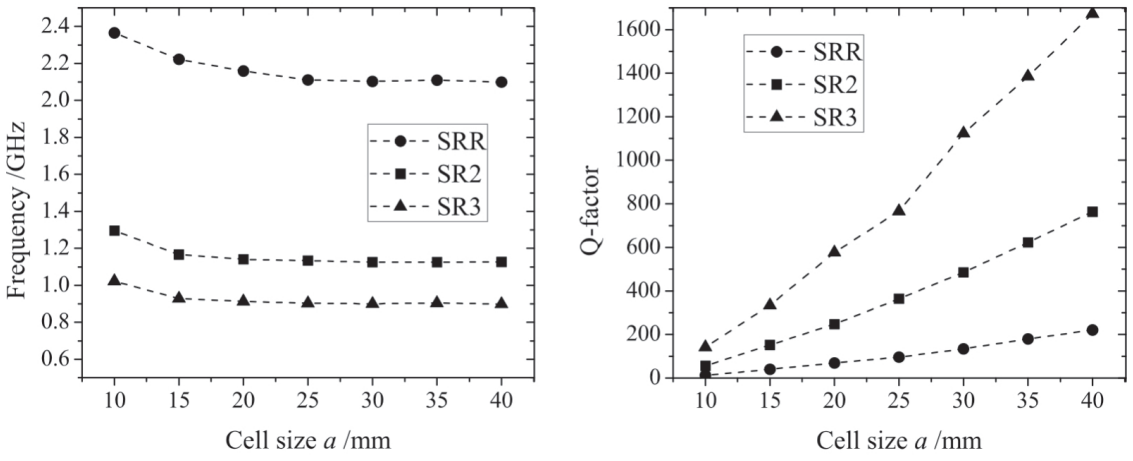

(a) (b)

FIGURE 3.3: Results of the variation of cell size a in unit cells made of PEC. Geometry described in Fig. 3.1 First Row. a) Resonance frequency. b) Quality factor.

transmission matrix and a cascade array is the cascade multiplication of the tranmission matrices, reducing the bandwidth.

3.3.1.1 Variation of cell size

For thin single resonators made of good conductors, the equivalent circuit model yields a single resonance frequency f_0. However, for a periodic structure the cell size plays an important role: as the cell size becomes bigger, the bandwidth is reduced significantly. In the numerical analysis we consider the simplest case of infinitely thin metasurfaces of SRR, SR2, and SR3 made of PEC in order work under the Babinet's Principle conditions (the same resonance frequency for the complementary resonators). As shown in figure 3.3(a), the resonance frequency is approximately constant as a increases because the resonance depends of the geometry of the unit cell only. Besides, it can be seen that the resonance frequency of the SRR simulated tends to 2.1 GHz which is approximately twice the resonance frequency of the SR2, 1.15 GHz. This can be explained by means of the equivalent circuit model described in the previous section, see figure 3.2. Figure 3.3(b) shows that the $Q-$factor increases linearly with a and reaches the highest value for the SR3, the geometry of smallest electric size. Now, the effect of the losses in the material is analyzed. We simulated the same metasurfaces replacing PEC by aluminum and we compared them with the maximum in reflection coefficient curves. As shown in figure 3.4(a), the reflection reaches a maximum close to 1 for all the metasurfaces made of PEC, while it drops significantly for the ones made of aluminum when the cell size increases. This phenomenon is associated with the finite conductivity of lossy aluminium

($\sigma_{cond} = 3.56E+7S/m$) which reduces the maximum in the reflection coefficient due to absorption and dissipation processes.

The resonance frequency f_0, tends to a constant value for all the metasurfaces simulated, see figure 3.4(b). When the cell size increases, the interaction between first neighbors disappears and the resonance depends on a single unit cell. In addition, f_0 is equal between each particle and its complementary which satisfies the Babinet's principle in a good approximation. The difference between the resonance of each particle and its complementary can be associated to the losses induced by material because in this case the Babinet's principle is no longer valid.

Figures 3.4(c) and (d) show Q for the metasurfaces made of PEC and aluminum respectively. In the former case, as the cell size increases the Q also increases linearly. In addition, the complementary metasurface (passband filter) has a higher quality factor compared to the original metasurface (bandstop filter). It is interesting to note that in the latter case, when the FSSs are made of aluminum, a different behavior is obtained: Q tends to a saturation value rather than increase linearly. Besides, the magnitude of Q is reduced up to 10 times approximately. For the practical point of view, it can be concluded that despite a big cell size may increase the Q factor, its maximum at resonance may decrease (according with the geometry used), thus, an equilibrium between both effects must be found. In our simulations, the SRR, SR2 and its complementaries are very good candidates in the metasurface design, whereas the SR3 does not reach a good maximum despite its smallest electrical size.

3.3.1.2 Variation of thickness

The resonance frequency f_0 respect to h is depicted in Fig. 3.5(a). The thickness h and the cell size a vary within the interval 0 to 7 mm and 10 to 40 mm respectively. It is worth to note that, according to the Babinets principle, the resonance frequencies for FSSs made of strips and slots elements coincide when the thickness h tends to zero. Besides, the resonance frequency of FSSs made of original particles (SRR, SR2, and SR3) shifts to lower frequencies while for complementary screens (C-SRR, C-SR2,C-SR3) shifts to higher frequencies. Although this response is not exactly symmetric, it is interesting that the relation between the resonance frequency of the SRR, SR2 and SR3, ($f_0^{SRR} = 2f_0^{SR2} = 2\sqrt{2}f_0^{SR3}$) remains constant at any value of h. Thus, once we get a model that calculates the resonance frequency for thick SRRs, automatically we get the resonance frequency for thick spirals.

Figure 3.5(b) shows Q when the material used is aluminium. As expected, Q increases as the structure is thicker, with the advantage that a single resonance is found instead

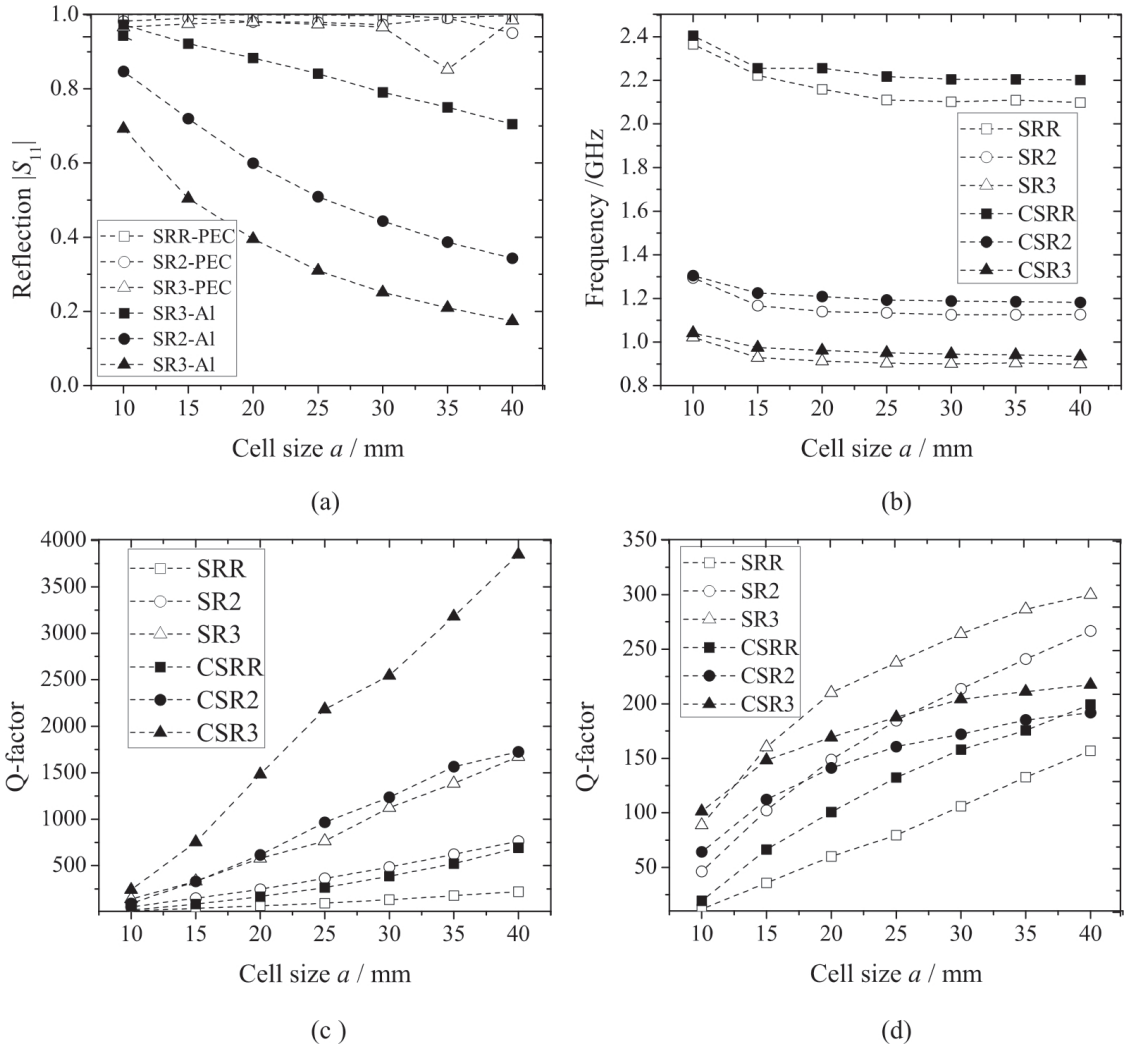

FIGURE 3.4: Results of the variation of cell size a in unit cells made of PEC and aluminium. a) Reflection for SRR,SR2 and SR3 in different materials. b) Resonance frequency for all geometries described in Fig. 3.1. c) Quality factor for all geometries made of PEC. d)Quality factor for all geometries made of aluminium.

of several resonances that appear when a cascade array is made [13, 14]. Although Q is much higher for the spirals in comparison with the SRR, the maximum at resonance is very small (S_{11} for the SRRs and S_{21} for the C-SRRs), as shown in figure 3.5(c). It is worth to note that the response is approximately constant, therefore it only depends on the geometry rather than the material used (simulations with aluminium).

3.3.2 Equivalent Circuit Model for Thick SRR

By using the resulting ideas from previous results, a simple theoretical model that provides circuit parameters and resonance frequency of metallic thick resonators is presented. The topologies under study are SRR and SR2. The main properties of the SRR

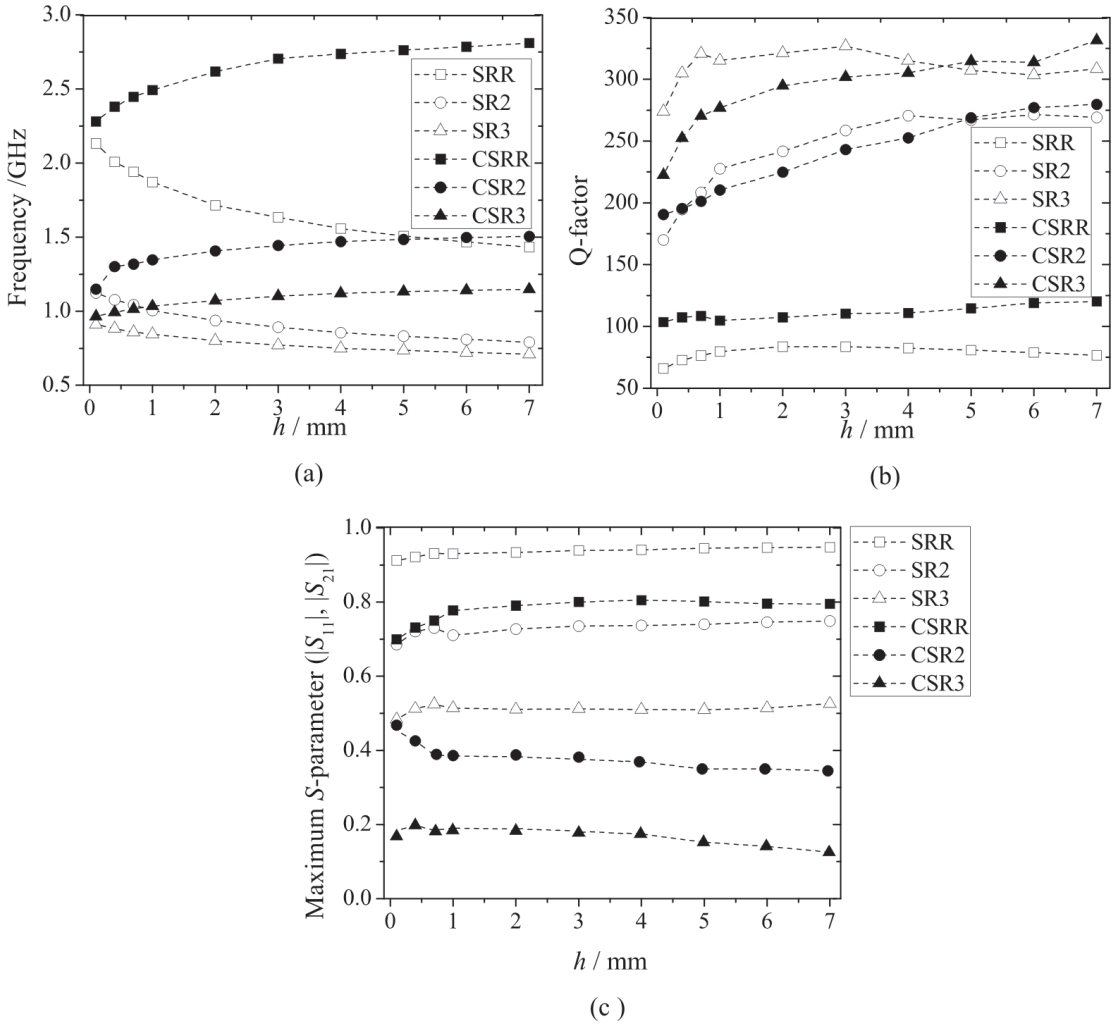

FIGURE 3.5: Results of the variation of thickness h in unit cells made of aluminium. a) Resonance frequency for all geometries described in Fig. 3.1. b)Quality factor for all geometries made of aluminium. c) Maximum of the corresponding S-parameter: $|S_{11}|$ for SRR,SR2 and SR3, $|S_{21}|$ for CSRR, CSR2, and CSR3. Normalized Units.

resonators can be approached by relatively easy LC-circuit models where the circuit parameters may be fully obtained from geometrical dimensions and material properties, as previously shown in figure 3.2. In this section, a generalization of the LC-circuit model for thick resonators is presented considering only one SRR of negligible width c, under the so called *slender ring approximation* [12].

3.3.2.1 Calculation of Inductance L

As the thickness h increases the induced current is spread along the z direction, numerical simulations indicate that its profile the xy-plane approximately remains constant. Simulations also show that near the borders of the metal strips the surface current diverges, so that it could be properly approximated by a Maxwellian distribution, as shown

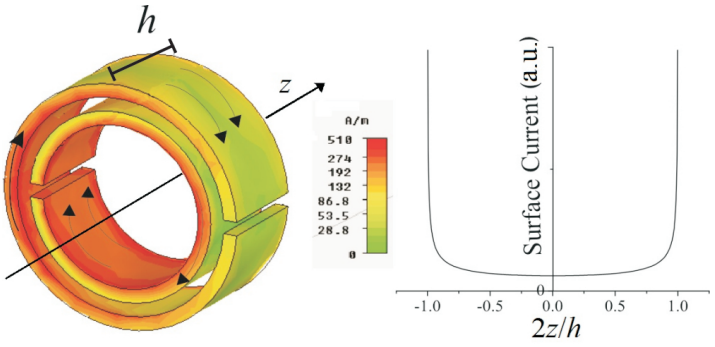

FIGURE 3.6: Maxwellian distribution of the current along the surface of the cylinder vs. thickness h.

in figure 3.6. So, the inductance can be calculated approximating the thick SRR as a thin hollow metal cylinder of average radius r. The inductance of this ideal cylinder is computed by using the variational expression $L = 2U_m/I^2$, where U_m is the magnetic energy. Assuming a Maxwellian distribution of the surface current density along the z direction, we can get the following expression

$$\mathbf{J}(\rho, z) = J_{s\varphi}(z)\delta(\rho - r)\hat{\varphi} = \frac{J_{s0}}{\sqrt{1-(2z/h)^2}}\delta(\rho - r)\hat{\varphi} \tag{3.3}$$

where J_{s0} is the surface current density at $z = 0$. The integration of 3.3 gives the total current

$$I = \int_{-h/2}^{h/2} \frac{J_{s0}dz}{\sqrt{1-(\frac{2z}{h})^2}} = J_{s0}\frac{h\pi}{2} \tag{3.4}$$

On the other hand, the magnetic energy is

$$U_m = \frac{1}{2}\int_V \mathbf{A}\cdot\mathbf{J}dV = \frac{1}{2}(2\pi r J_{s0})\int_{-\infty}^{\infty} \frac{A_\varphi(r,z)dz}{\sqrt{1-(2z/h)^2}} \tag{3.5}$$

where the potential vector $\mathbf{A}$ can be calculated from the Laplace equation in cylindrical coordinates (vector Laplacian operator):

$$\Delta\mathbf{A} = \nabla(\nabla\cdot\mathbf{A}) - \nabla\times(\nabla\times\mathbf{A}) \tag{3.6}$$

The potential vector is $\mathbf{A}(\rho,\phi,z) = A_\phi(\rho,z)\hat{\phi}$, such that its divergence is zero and its rotational is

$$\nabla\times\mathbf{A} = \frac{1}{\rho}\frac{\partial(\rho A_\phi)}{\partial\rho}\hat{z} - \frac{1}{\rho}\frac{\partial(\rho A_\phi)}{\partial z}\hat{\rho}. \tag{3.7}$$

Thus, the total vector Laplacian operator is

$$-\nabla\times(\nabla\times\mathbf{A}) = \frac{1}{\rho^2}\partial_\phi(\partial_\rho(\rho A_\phi))\hat{\rho} - \left[\frac{1}{\rho}\partial_z^2(\rho A_\phi) + \partial_\rho(\frac{1}{\rho}\partial_\rho(\rho A_\phi))\right]\hat{\phi} + \frac{1}{\rho^2}\partial_\phi(\partial_z(\rho A_\phi))\hat{z} = 0 \tag{3.8}$$

The partial derivative ∂_ϕ is zero, such that equation 3.8 is reduced to

$$\frac{1}{\rho}\partial_z^2(\rho A_\phi) + \partial_\rho(\frac{1}{\rho}\partial_\rho(\rho A_\phi)) = 0. \tag{3.9}$$

The general solution for the equation 3.9 can be determined by means of the Fourier transform of A_ϕ

$$A_\phi(\rho, z) = \int_{-\infty}^{\infty} \tilde{A}_\phi(\rho, k_z) e^{-2\pi i k_z z} dz, \tag{3.10}$$

such that eq. 3.9 can be rewritten as

$$-k_z^2 \tilde{A}_\phi(\rho, k_z) + \partial_\rho^2 \tilde{A}_\phi(\rho, k_z) + \frac{\partial \tilde{A}_\phi(\rho, k_z)}{\rho} - \frac{\tilde{A}_\phi(\rho, k_z)}{\rho^2} = 0, \tag{3.11}$$

replacing $x = k_z\rho$, we obtain the characteristic equation for the *Modified Bessel Functions*

$$\frac{\partial^2 \tilde{A}_\varphi}{\partial x^2} + \frac{1}{x}\frac{\partial \tilde{A}_\varphi}{\partial x} - (1 + \frac{1}{x^2})\tilde{A}_\varphi = 0, \tag{3.12}$$

whose solution is given in terms of the functions $I_1(x)$ and $K_1(x)$.

$$\tilde{A}_\phi(x) = \begin{cases} AI_1(x) & x < x_0 \\ BK_1(x) & x > x_0 \end{cases} \tag{3.13}$$

with $x_0 = k_z r$.

Now, in order to get an exact expression for A_ϕ, the boundary conditions of continuity of the potential $A_\phi(r_+, z) = A_\phi(r_-, z)$ and discontinuity of the magnetic field ($\mathbf{B} = \nabla \times \mathbf{A}$) due to a jump in the surface current K can be expressed as

$$\begin{aligned} \hat{n} \times \mathbf{H} = \mathbf{K}, \quad \hat{\rho} \times (\nabla \times \mathbf{A}) = \mu_0 \mathbf{K} \\ \partial_\rho(\rho A_\phi)|_{r^+} - \partial_\rho(\rho A_\phi)|_{r^-} = \mu_0 r \mathbf{K}, \end{aligned} \tag{3.14}$$

where r^+ and r^- correspond to the derivatives evaluated in r from the inner and outer volume of the cylinder. Considering that we transformed A_ϕ to $\tilde{A}_\phi$, it is necessary to calculate the Fourier Transform of the surface current $\mathbf{K}$ as

$$\begin{aligned} \mathbf{K} &= \frac{J_{s0}}{\sqrt{1-(2z/h)}}\hat{\phi} \\ \tilde{\mathbf{K}}_\phi &= \frac{J_{s0}h}{2}\sqrt{\frac{\pi}{2}}J_0(k_z h/2). \end{aligned} \tag{3.15}$$

Thus, the boundary conditions in the Fourier transform are simplified to

$$\begin{aligned} \tilde{A}_\phi(x)|_{x_0^+} &= \tilde{A}_\phi(x)|_{x_0^-} \quad x_0 = k_z r. \\ \partial_x(x\tilde{A}_\phi)|_{x_0^+} - \partial_x(x\tilde{A}_\phi)|_{x_0^-} &= \frac{x_0 \mu_0 \tilde{K}_\phi}{k_z} \end{aligned} \tag{3.16}$$

Equation 3.16 and the properties in the derivatives of the *Modified Bessel Functions* ($\frac{d}{dx}(x^\nu K_\nu(x)) = x^\nu K_{\nu-1}$ and $\frac{d}{dx}(x^\nu I_\nu(x)) = x^\nu I_{\nu-1}$) permits the calculation of the constants A and B of the potential vector 3.13, therefore, the total potential vector as

$$\tilde{A}_\phi = \mu_0 r \tilde{K}_\phi \frac{J_0(x_0 h/2r) I_1(x_0) K_1(x_0)}{x_0[I_1(x_0)K_0(x_0) - I_0(x_0)K_1(x_0)]}. \tag{3.17}$$

By means of the Parseval's Theorem, the integral of the magnetic energy in the z space, is equal to the integral in the Fourier Space of k_z (rewritten in terms of x_0). Thus, equation 3.5 is : (replacing the Fourier Transform of the current equation 3.15)

$$U_m = (2\pi r \mu_0)\frac{J_{s0}^2 h^2 \pi}{4} \int_0^\infty \frac{J_0^2(x_0 h/2r) I_1(x_0) K_1(x_0) dx_0}{x_0[I_1(x_0)K_0(x_0) - I_0(x_0)K_1(x_0)]}. \tag{3.18}$$

Once the magnetic energy and the total induced current is known, the variational expression $L = 2U_m/I^2$ can be used to get

$$L = 2r\mu_0 \int_0^\infty \frac{(J_0(x_0 h/2r))^2 dx_0}{x_0(I_0(x_0)I_1^{-1}(x_0) + K_0(x_0)K_1^{-1}(x_0))} \tag{3.19}$$

3.3.2.2 Calculation of Capacitance C

The capacitance can be calculated by using the well known formula for the capacitance of a long cylindrical capacitor:

$$C_h = \frac{2\pi h \epsilon}{\ln(r/(r-d))}; \tag{3.20}$$

where h is the height or thickness, d distance between the two coaxial cylinders, and ϵ the permittivity filling the space between the cylinders. However, for relatively small h the fringing effect should not be neglected. We assume that the fringing electric field is similar to the field created by two coplanar extremely thin rings with the same shape of the transversal section of the cylindrical capacitor. The fringing capacitance can be approximated by $C_0 = 2\pi r C_{pul}$, where C_{pul} represents the capacitance per unit of length of two parallel coplanar strips [12].

$$\begin{gathered} C_0 = \pi r_0 C_{pul} \quad C_{pul} = \frac{\epsilon}{\pi}\ln\left(2\frac{1+\sqrt{k'}}{1-\sqrt{k'}}\right) \\ k' = \sqrt{1-k^2} \\ k = \frac{d}{2c+d} \end{gathered} \tag{3.21}$$

with w, r_0 and g described in Fig.3.1.

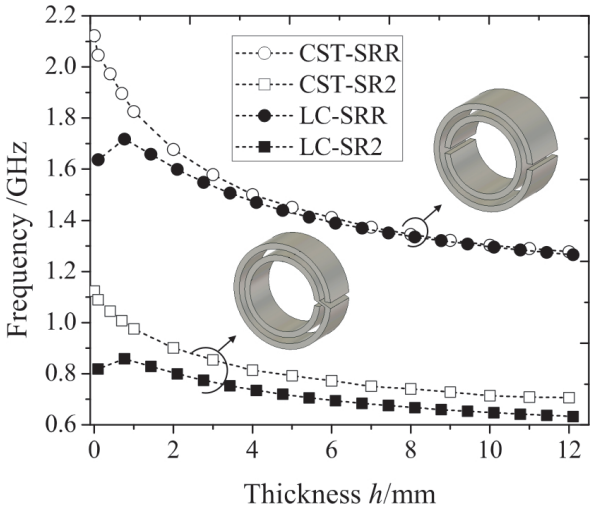

FIGURE 3.7: Resonance frequency vs. thickness h calculated by means of the LC-circuit model and full-wave simulations by using $CST - Microwave\ Studio$.

Considering that the two halves of the SRR are connected in series, the resonance frequency of its equivalent circuit is $\omega_0^{\mathrm{SRR}} = (L(C_h + C_0)/4)^{-1/2}$. Likewise, the capacitance of the thick SR2 must be 4 times bigger, since the two halves are connected in parallel, i.e. $\omega_0^{\mathrm{SR2}} = (L(C_h + C_0))^{-1/2}$. Therefore, the resonance frequency of thick SR2 is half the value for thick SRRs, similar to the case of thin SRRs.

In order to check the validity of the model, we compare the resonance frequency obtained from the previous numerical simulations with the resonances obtained by using equations 3.19 and 3.21 of the model, as shown in figure 3.7. For most part, the agreement between model is good. The disagreement observed for thin particles can be attributed to the fact that the approximation of L for a cylinder of infinitely thin metal is not longer valid, since h start to be comparable to the width of the strips c and the separation between them d and the slender ring's approximation is no longer valid.

3.3.3 Waveguide Model for Thick C-SRR

In this section, an analytical model for the design of metasurfaces based on C-SRRs is presented. Simple expressions are provided for the most important geometrical parameters of the model, yielding an accurate description of the C-SRR resonance frequency. We propose a simple explanation for the first two resonances of thick C-SRR. This explanation simplifies the calculation of the geometrical parameters to design band-pass metasurfaces, avoiding full-wave numerical simulations.

Usually, transmission line models are used to describe the response of thick periodic metallic structures. The problem is simplified to the computation of scattering parameters of a transverse section discontinuity [11]. The incoming electromagnetic plane wave,

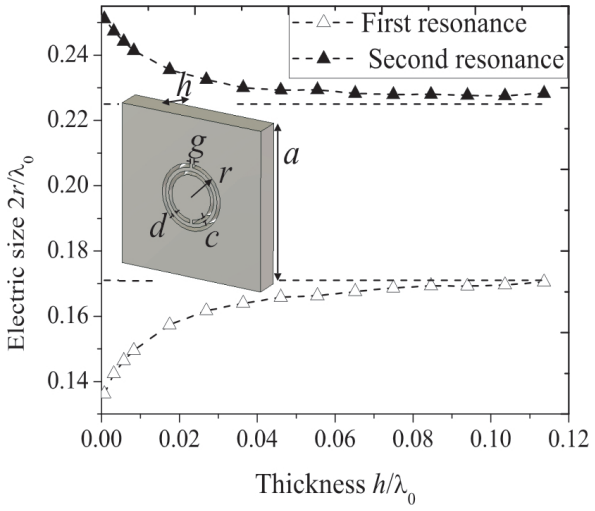

FIGURE 3.8: Electric size vs. Thickness h normalized by resonance wavelength. The normalization shows that the CSRR converges to the cut-off frequency when the thickness increases. The geometrical parameters used in this simulation are a =43mm, r =9mm, $c = d = g$ =1mm. h vary within the range of 0-12mm.

described as a wave travelling along a transmission line equivalent to free space, must match the admittance in the surface of the FSS to be propagated along rectangular slits, considered as a transmission line too. The S-parameters depend on the equivalent admittances of the incident wave, the surface and the slits. The admittance matching occurs only at certain frequencies, such that the S parameters presents different peaks and dips.

Now, let us focus our attention on C-SRR based metasurfaces, see figure 3.1. In our proposed model, each slit of the C-SRR can be seen as a rectangular waveguide bended with the shape of C. So, the biggest slit is the equivalent to the rectangular waveguide whose length is $l_{ext} = 2\pi(r-c/2)-g$ and the smallest corresponds to another rectangular wavelength whose length is $l_{int} = 2\pi(r - d - 3c/2) - g$ respectively. As a waveguide, the lowest frequency that allows the transmission of the wave is the cut-off frequency of the lowest mode (TE_{10}), when the resonance wavelength λ_0 is twice the length of the waveguide. It is also well known that the wave admittance of the rectangular waveguide varies rapidly around the cut-off frequency, so that we expect that impedance matching is obtained for a frequency very close to it. In order to validate this condition, we performed a set simulations obtaining the two primary resonances for the scattering parameters $|S_{11}|$ and $|S_{21}|$. In figure 3.8 the electrical size $2r = \lambda_0$ is plotted versus the thickness h normalized by λ_0. As the thickness increases, each curve tends to a fixed value equal to r/l, such that $r/[2\pi(r - c/2) - g] = 0.171$ for the biggest slit and $r/[2\pi(r - d - 3c/2) - g] = 0.225$ for the smallest.

Actually, figure 3.8 is very useful for thick C-SRR based metasurface design because it

gives us a good first estimation of λ_0. Nevertheless, it is worth to note that this approximation works accurately for thickness greater than $h = 0.06\lambda_0$ only. The resonance frequency and electrical size should depend also on r, g, d and c also, but simulations demonstrate that the variation with c and g is small, indeed; the cut-off frequency of a rectangular waveguide does not depend on its height. Thus, the problem of filter designing is reduced to estimate the value of r. In addition, given that the first and second resonances operate independently, it is possible to design a tunable C-SRR based metasurface, that resonates at two different frequencies using a single unit cell geometry, varying d only. Therefore, thick C-SRR structures not only have the advantage of small electrical size than thin C-SRRs but also adjustable response to two frequencies working separately.

3.3.3.1 Scattering parameters for CSRR

The transmission curves presented in 3.10 show that the first resonance frequency f_1 tends to a fixed value as h increases with the same bandwidth, so that Q increases, as it had been previously demonstrated in [38]. Likewise, Q increases in the second resonance f_2, but in this case the increment is related with the the fact that the bandwidth becomes narrower in spite of the fact that f_2 decreases. The electric field distribution and the induced surface current induced on the metallic surface only at the resonance frequency, are independent on each slot of the CSRR when it is thick. Thus, within the frequency range between 2.2-2.9 GHz, only the outer slit allows the wave transmission while the internal slot acts as a metallic screen, see figure 3.9(a). Likewise, within the frequency range between 3.8-4.4 GHz, the internal slot fully transmits while the outer reflects almost completely, as shown in figure 3.9(b). When the surface is thin, the coupling between the two slots begins to be important so the resonance cannot be predicted with our model. Another interesting factor is the electric field direction inside each slit because it satisfies the boundary conditions of a bent rectangular waveguide. In fact, this distribution of the electric field is the key factor to describe the geometry of CSRR rectangular widths in an analogous way to rectangular waveguides that transmit at the cut-off of the fundamental mode.

3.4 Metasurface Designer

A user friendly software was created to condense the results obtained in this chapter. Basically, by using the equations 3.21 and 3.19 in conjunction with 3.1, the resonance frequency is calculated for metasurfaces made of SRR, SR2 or SR3. Besides, by means

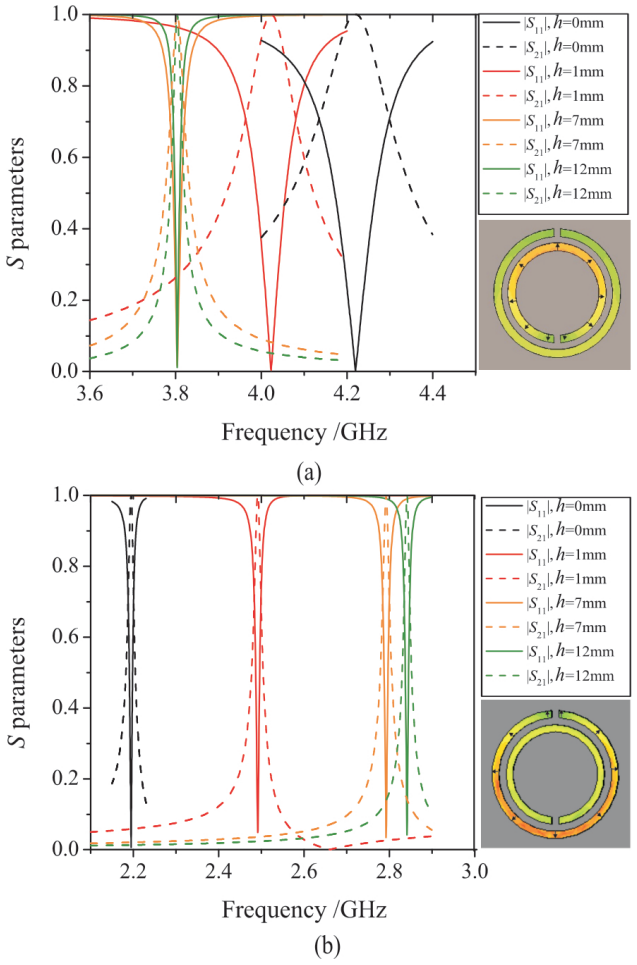

FIGURE 3.9: S-parameters for different values of thickness using full-wave simulation in $CST-Studio$. (a) first resonance, (b) second resonance. Color curves varies for each value of thickness. Reflection S_{11} (solid line)is close to 0 and transmission S_{21} (dashed line) is close to 1 at resonance.

of the waveguide model previously described, the resonance frequency for thick complementary metasurfaces (made of C-SRR, C-SR2 or C-SR3) is calculated in terms of the geometric parameters only. As an application for a dual frequency passband filter by using a C-SRR (see figure 3.9), this software is also useful: given the two expected resonance frequencies, the radius r and the separation of slits d are calculated. The software interface is shown in figure 3.10. It was created by using Labview-2011 programming tool.

The main advantage of this implemented software is that we can to predict the resonance frequency of metasurfaces avoiding full wave numerical simulations. Besides, it give us information about the electric size which is a determining factor for different applications of these resonators. This fact improves the design processes in the sense that the full wave numerical simulation (that yields the S-parameters) can be adjusted within the expected frequency range.

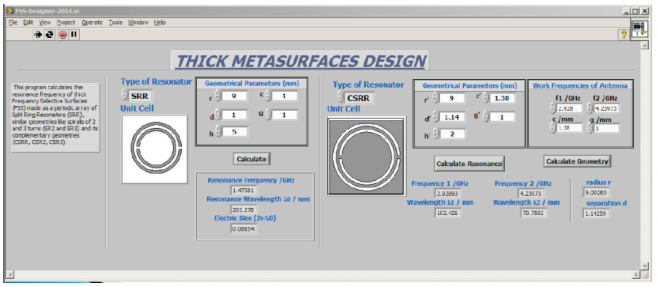

FIGURE 3.10: Software interface of the *Metasurface Designer*. Instructions given inside the program to calculate the resonance frequency of metasurfaces made of SRR based resonators or its complementaries.

Chapter 4

Experimental Development

In this chapter we describe the design, fabrication and experimental validation of three different applications of metasurfaces and SRR based resonators: a short filter for waveguides, a metasurface that acts as a spatial filter, and a microstrp iline based sensor of permittivity. Each one of these experiments have different applications and measuring processes, but very similar results, considering that all of them are based on the same geometries: the SRR, its complementary C-SRR and similar small resonators.

We use of the theoretical models described in chapter 3 to design a short waveguide filter and to analyze its response in terms of its thickness. Basically, the prototypes designed have the advantage that no coupling between the resonator and the waveguide is needed. Furthermore, they are easily tunable. Furthermore, we fabricate metasurface made of Interconnected Split Ring Resonators (I-SRRs) that behave as a spatial filter, whose main advantage is the easily tunable performance and stability. Finally, by means of the equivalent circuit models referred in chapter 2, we also propose a device to measure the permittivity of liquids at the microwave range based on a single C-SRR.

4.1 Experiment 1. Short Waveguide filters based in C-SRRs

A potential use of C-SRRs, C-SR2s, and C-SR3s; is to design very compact waveguide filters. We study the passband response in an experimental and computational form. Furthermore, due to its small electric size, it reaches a higher quality factor Q for thick resonator in comparison with known resonant-cavity waveguide filters, leading to an improvement in the design of miniaturized waveguide filters [39].

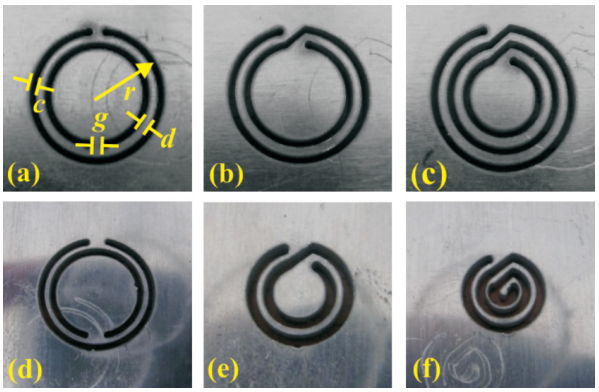

FIGURE 4.1: Prototypes used as waveguide filters. In the first experiment (a,b,c) the resonators have the same geometrical parameters r =9.0mm, $c = d$ =1.0mm, g =2.7mm. In the second experiment each resonator has $c = d$ =1mm but different radius. (d) r =10.1mm, (e) r =6.1mm, (f) r =5.9mm.

Now, we describe the excitation of the C-SRR, C-SR2 and C-SR3 by means of different prototypes: Aluminium sheets with each geometry etched on it and excited by the magnetic field inside a rectangular waveguide. Although these resonators can be excited by different field components, the orientation of the prototypes is such that these are excited by the magnetic field component B_x of the $\mathrm{TE}_{1,0}$ mode of a rectangular waveguide [12]. Two set of experiments were performed: for resonators of the same dimensions and different frequency range of resonance, figure 4.1(a,b,c), and for resonators of different dimensions within the same frequency range, figure 4.1(d,e,f). For the first set of resonators the frequency range varies from [1-3] GHz whereas it varies from [2-3] GHz for the second set.

By using the waveguide model described in Chapter 3, we calculated the expected resonance frequency of the prototypes fabricated. Indeed, we calculated the two primary resonances, when $l = \lambda/2$ and $l = \lambda$. For each prototype, L, f_0, and f_1 predicted of our simplified model are shown in Table 4.1.

Unlike a common rectangular waveguide, in which the transmission is continuous from the cut-off frequency on, what we found in the transmission curves shown below, is that these present a resonance peak at this frequency. This is due to the coupling between the electric field of the incident wave and the electric field that is formed within the slots, the equivalent to the electric field distribution of the TE_{10} mode of a rectangular waveguide. This coupling only occurs at the resonance frequency, so that at this point the transmission is highest. In order to validate the model, a set of numerical simulations is performed for the prototypes of figure 4.1 (a,b,c) for different values of h. As shown in figure 4.2 the resonance frequency increases with h, but in every case it tends to a fixed value. The dark area represents the area out of the experimental frequency range, therefore, we would expect resonance peaks for the prototypes (a) and (c) only.

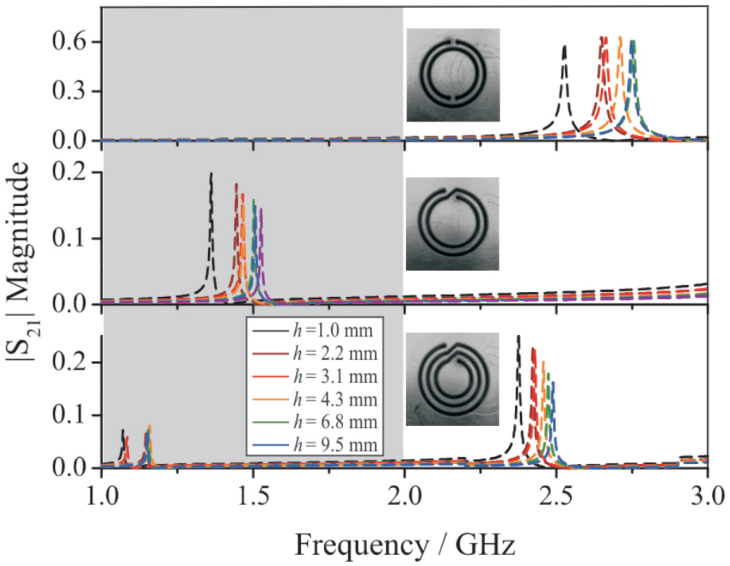

FIGURE 4.2: S_{21} parameter for prototypes (a,b,c) calculated numerically by means of *CST-Microwave Studio*. The dark area represents the area that is not compared with experimental results.

TABLE 4.1: Expected resonance frequencies for each prototype fabricated.These resonances are provided by the equivalent waveguide model for thick resonators.

Prototype	r **/mm**	L **/mm**	f_0 **/GHz**	f_1 **/GHz**
a.	9	54.3	**2.86**	5.72
b.	9	93.7	1.60	3.20
c.	9	123.9	1.21	**2.42**
d.	10.1	57.31	**2.61**	5.23
e.	6.1	59.4	**2.52**	5.05
f.	5.8	62.1	**2.415**	4.83

4.1.1 Experimental Setup

The C-SRR, C-SR2 and C-SR3 were manufactured by etching it into aluminium sheets of thickness 1.0 mm and 2.5 mm by means of a laser drilling machine. As previously mentioned, two sets of resonators were fabricated, one set maintaining the size of the resonator thus changing its resonance frequency, and another set maintaining the same frequency range thus changing its dimensions.

The experimental setup is shown in figure 4.3(a). Each sheet has been introduced between two WR340 rectangular waveguides (figure 4.3(b)). In order to analyze the effect of thickness in the prototype, several layers are placed one behind each other but very close, as shown in figure 4.3(c). The TE_{10} rectangular waveguide mode is launched and the C-SRR is excited by the magnetic field along the $x-$axis. Data has been collected by using a vectorial network analyzer *Agilent E5062* within the frequency range from [2-3]GHz due to the operation range of the WR340 waveguide.

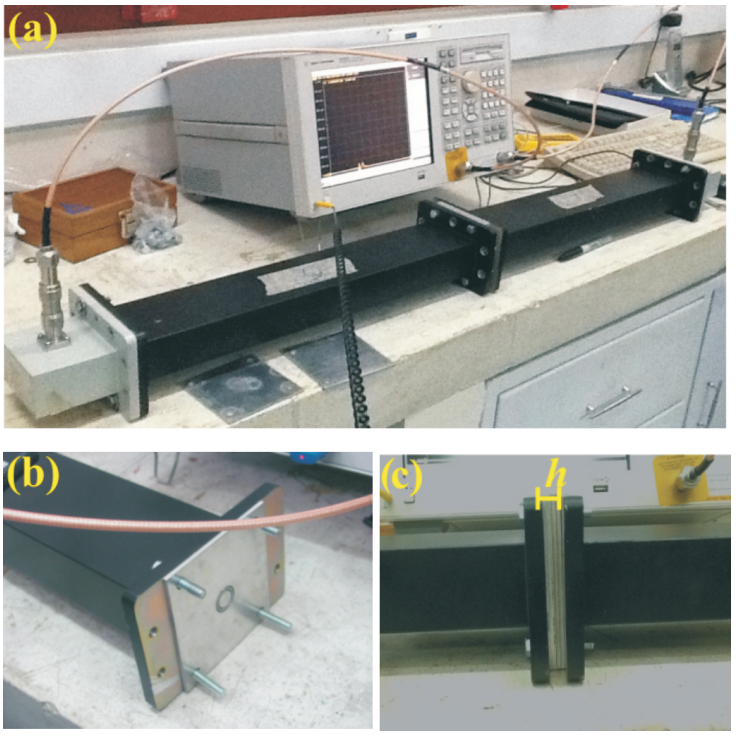

FIGURE 4.3: a.) Experimental Setup: Two rectangular waveguides WR340 with the thick prototype placed between them. b.) Prototype placed in front of the aperture of the waveguide properly oriented. c.) Thickness of the resonator when each metallic sheet is added.

4.1.2 Results

The simulations that reproduce the experimental conditions are carried out by using the frequency domain solver of *CST Microwave Studio* code. It can be seen that the prototype is easily tunable and, specifically, by varying the radius and width of the slits we can determine the length of the *equivalent rectangular waveguide*, its corresponding cut-off frequency and thus, the resonance frequency.

For the first set of prototypes (a,b,c) it is predicted that only the C-SRR and C-SR3 will present peaks of resonance, as shown in figure 4.2. Figure 4.4 shows the transmission coefficient in the experiments and simulations, the amplitude of peaks is only slightly greater in the simulations when compared with the experiments, and this amplitude remains constant as the thickness h increases. The differences in the resonance frequency f_0 are less than 10% for the thinnest filter (h = 1.16mm) and less than 1% when the surface is thick (h =5.08 mm).

On the other hand, f_0 varies only 350 MHz within the range of thickness of the experiment and tends to a constant value of 2.8 GHz, which corresponds to the frequency of the fundamental mode, see Table 4.1. For the C-SR2, it had been previously shown [8] that the C-SRR and C-SR2 of equal dimensions satisfy $f_0^{C-SRR} = 2f_0^{C-SR2}$. Thus,

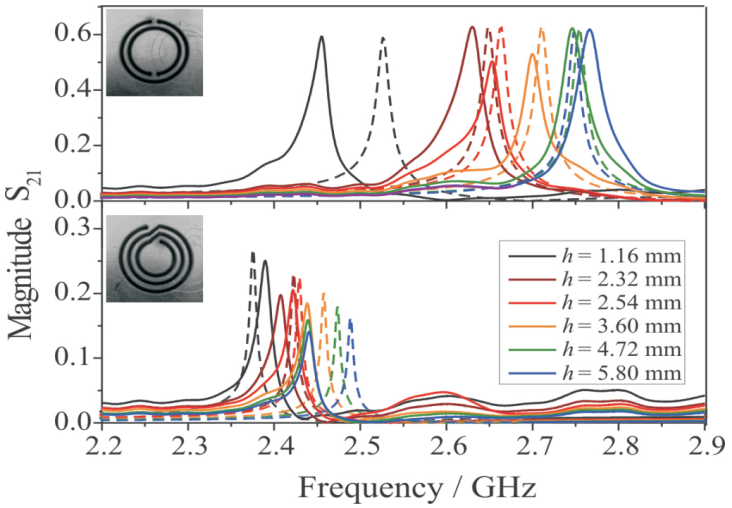

FIGURE 4.4: S_{21} magnitude for C-SRR (a), and C-SR3(b) resonators of the same size. Experimental results (solid line), Simulation results (dashed line).

no resonance was expected within the range of the waveguide [2-3]GHz. Similarly, the C-SR3 resonator satisfies $f_0^{C-SRR} = 2\sqrt{2}f_0^{C-SR3}$, such that f_0 exists out of the range of [2-3]GHz. However, figure 4.3 shows that the resonance above cut-off f_1 exists within this range. Thus, our model not only predicts with good accuracy f_0 but also higher-order resonances as f_1. The differences between the experiments and simulations in the frequency are less than 8%.

If we decrease the size of the C-SRRs, the difficulties in the manufacturing process increase. Considering the limit of the frequency range due to the *WR340* waveguides [40], we designed three resonators whose resonances f_0 appeared within this range, although these resonators do not exactly meet the relations predicted in [38] in which $f_0^{C-SRR} = 2f_0^{C-SR2} = 2\sqrt{2}f_0^{C-SR3}$. Thus, the C-SR2 spiral should have half the electrical size in comparison with the C-SRR.

It is still possible to verify that measuring the the length of the slits, and then computing $f_0 = 2c/L$, the numerical and experimental curves tend to the expected values shown in Table 4.1 when h increases. Thus, we have verified the validity of our equivalent rectangular waveguide model, which significantly simplifies the design process of these resonators.

For both experiments, we found that the Q factor increases with h (although its response is not uniform) and, as shown in figures 4.4 and 4.5, Q increases for each geometry. However, the transmission is reduced significantly: while the C-SRR satisfies $|S_{21}|^{f_0} = 0.7$, C-SR2 and C-SR3 reach only $|S_{21}|^{f_0} = 0.25$ and $|S_{21}|^{f_0} = 0.15$ respectively. Thus, prototypes of best performance, are the prototypes (a) and (d). Although the spirals have smaller electric size, its coupling with the incident wave only occurs at a single frequency, so the dissipation at other frequencies is higher.

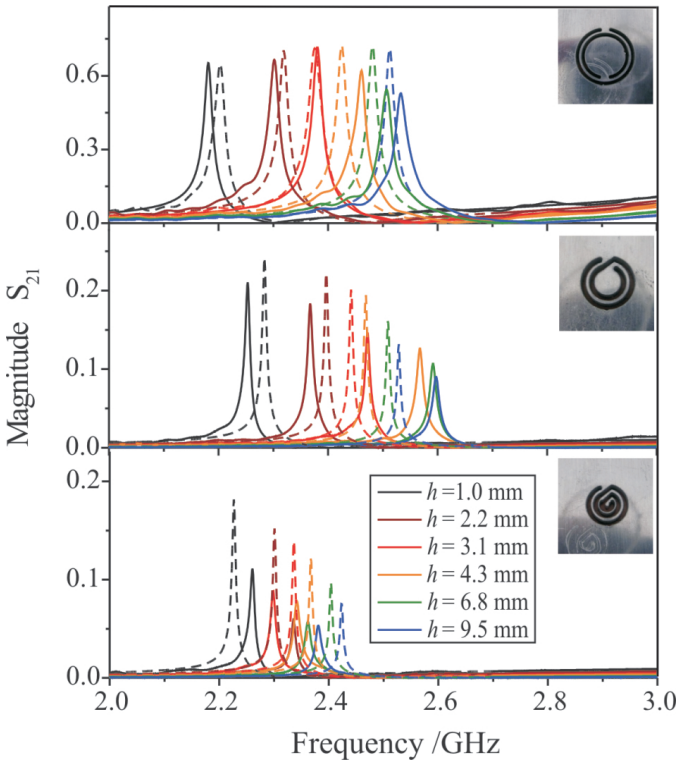

FIGURE 4.5: S_{21} magnitude for C-SRR, C-SR2 and C-SR3 resonators of different sizes. Experimental results (solid line), Simulation results (dashed line).

4.2 Experiment 2. Metasurface for Spatial Filtering

Two metasurfaces made of a finite set of parallel 1D chains of interconnected split ring resonators (I-SRRs) and its complementaries (I-C-SRRs) previously proposed by [41] were studied, fabricated and tested. An interesting fact of this FSS include that the angular filtering of plane waves has been used for decades to increase the directivity of antennas and/or suppress grating lobes. Due to its small electrical size, the structure described in this section is advantageous when compared with previous implementations. Besides, the metasurface that we fabricated is small enough to cover the horn antenna aperture but a filtering response is still obtained.

To establish an electrical connection between ordinary rings in the same row, as shown in figure 4.6 (a), (or its dual complementary on-screen figure 4.6(b)), the chain of rings that is formed gives a peculiar behavior: the stopband response of the new structure, for a particular polarization, becomes tunable, thus, the center frequency can be adjusted simply by varying the angle of incidence. Likewise, due to Babinet's principle, its complementary metasurface is also tunable in a bandpass response. The equivalent circuit for this metasurface has been previously proposed by Ortiz, et al. [41] in which each unit cell can be seen as a loaded transmission line with the proper inductance and capacitance to reproduce the resonant frequency.

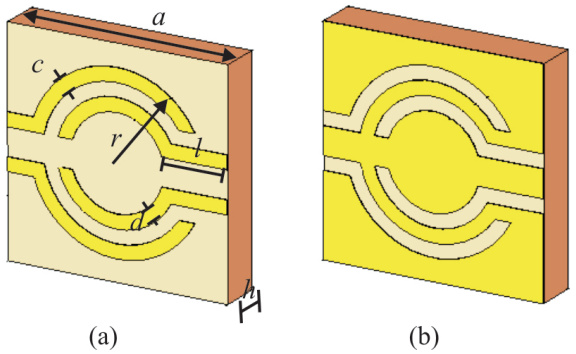

FIGURE 4.6: Unit cells of the metasurfaces made of interconnected SRRs (I-SRRs) (a) and interconnected C-SRRs (b). The geometrical parameters are a = 4mm , c = d =0.5mm, h= 1.52 mm, r = 3.2 mm. The materials used are Copper (yellow) and lossless substrate Rogers RO 3003 with ϵ_r =3 (brown).

4.2.1 Fabrication Techniques

The manufacturing method used was photolitography. It was used a photo-plotter *Film-star* of *Bungard* to fabricate the masks shown in figure 4.7 (a) and (c). These masks are the negative image of the geometry etched on the metallic layer. The drop off of masks is revealed by using an isolator machine *SET Micro - check MG1410* for UV exposure and the revealing process used a sprinkler of acid *Splash Center* of *Bungard*. Limitations in the manufacturing process allowed us to make FSSs up to 13.7× 11.4 cm^2 of area approximately with 14 × 17 unit cells. A photograph of the structures made of copper are shown in Figure 4.7 (b,d) with the dimensions of figure 4.6. The dielectric used was the commercial substrate for microwaves *Rogers 3003*, which has a thickness of 1.70 mm, nominal dielectric constant of ϵ_r =3 and a tangent of losses $tan\delta$ = 0.0018.

Considering that it was the first manufacture with this process of photolitography, there are some defects in the metallic metallic pattern printed on the substrate. These defects are associated to the chemical process of revealing involved in the manufacture of the masks as it was not uniform. Thus, when the mask is exposed with the copper sheet on the UV exposure, the illuminated pattern is not uniform either. In order to improve the uniformity in the fabrication process, it is suggested to use masks whose area fits on the chemical holder, in such a way that its easier to handle. This process must be done inside a dark room, therefore it is also suggested to improve the quality of the illumination (properly filtered) inside the room in order to check that both masks and layers are properly revealed. The process to remove the copper was uniform thanks to the *Splash Center*, but it is still required that all the processes are carried out properly in order to manufacture a FSS of good quality.

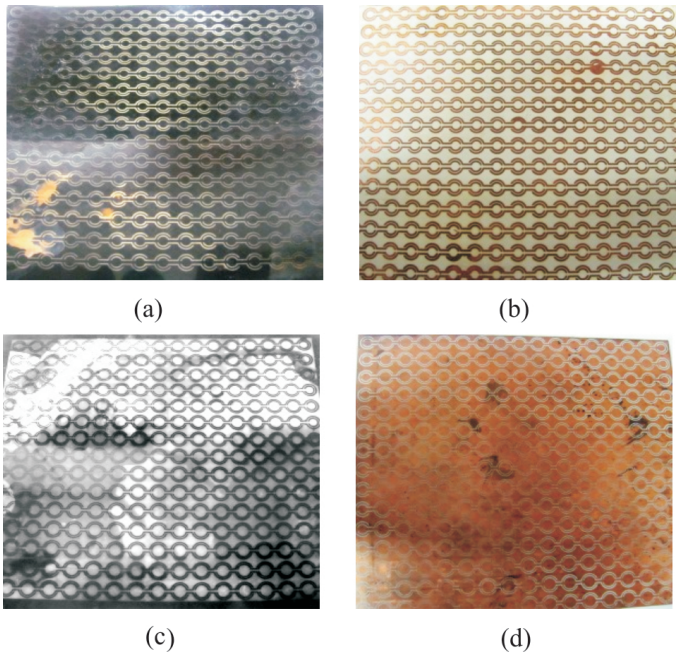

FIGURE 4.7: Fabrication of Metasurfaces. a) Mask used for the I-SRR, b) Metallic layer with the I-SRR etched on it. c) Mask used for the I-C-SRR, d) Metallic layer with the I-C-SRR etched on it.

4.2.2 Measurements on the Anechoic Chamber

Transmission and reflection characteristics of FSS screens can be measured with a few methods. To measure the transmission, the FSS under test is placed between two directive antennas, one as the transmitter of the signal and the other acting as the receiver. While blocking the direct path of propagation, the FSS filters the frequency from the transmitter, thus leaving its particular response on the received power by the receiver.

In order to test the filtering response of the previous fabricated metasurfaces we measured the scattering parameters inside a *RF Anechoic Chamber*. In this setup, the emitter antenna Fig. 4.8(a) and the receiver antenna Fig. 4.8 (b) are fixed and facing one to another, while the FSS is placed between them. Both antennas are standard horn antennas $WR-187$ that work within the frequency range of 3.95-5.85 GHz. These three elements are placed inside the anechoic chamber of 5.2 $\times$ 3.1 $\times$ 3.1 m, a room designed to completely absorb reflections of electromagnetic waves, Figure 4.8(c). The interior surfaces of the chamber are covered with radiation absorbent material, usually consisting of an urethane foam loaded with conductive carbon black and cut into pyramids with dimensions set specific to the wavelengths of interest, in this case, up to 18 GHz. We analysed the filtering response of the spatial filters described above by measuring the scattering parameters with a Vectorial Network Analyzer HP8510 at the anechoic chamber of the **Center of Technology and Communications of Catalunya (CTTC, Barcelona-Spain)**.

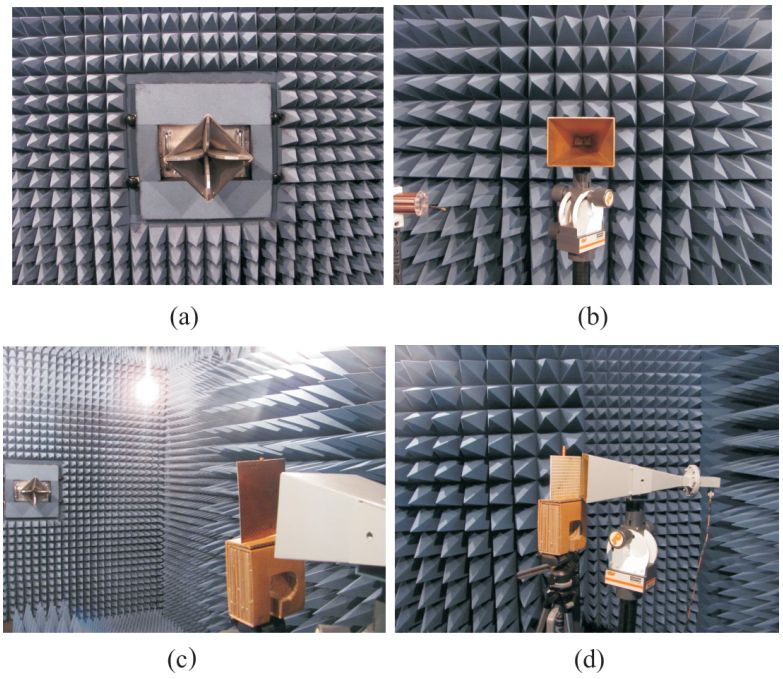

FIGURE 4.8: Experimental setup to study the filtering response a FSS inside an anechoic chamber. (a) Receiver Antenna, (b) Emitter Antenna, (c) Anechoic chamber setup for the complementary screen, (d) Anechoic chamber setup for the original screen.

Prior to the measurements, the antennas and the FSS are aligned inside the chamber with a laser aligner. Due to the finite and small size of the fabricated FSS, its response as filter is only noticeable if it is placed close to one of the antennas, as shown in Figure 4.8 (c) and 4.8 (d) for the original FSS and the complementary respectively. Indeed, no measurable difference was found when the metasurface was placed at a distance of 50 cm from the emitter antenna. Therefore, the FSS is placed close to the antenna aperture, at a distance of 2 cm of one of the antennas and oriented perpendicular to the imaginary line that joins both antenna's apertures. It is expected that its response as a filter is difficult to appreciate since the approximation of normal incidence is not completely fulfilled. Even with these experimental complications, it is interesting to find a spatial filter response as it will be shown below.

4.2.3 Results

To analyse the scattering process obtained from the test of the metasurface response, we carried out a process of normalization. The S_{21} magnitude is measured with and without the sample, then; we calculate the ratio of both measurements and we get the data that is presented as the transmission of the FSS itself. Due to the defects on the metasurface made of C-SRRs, it turned out as a uniform metallic screen and no filtering

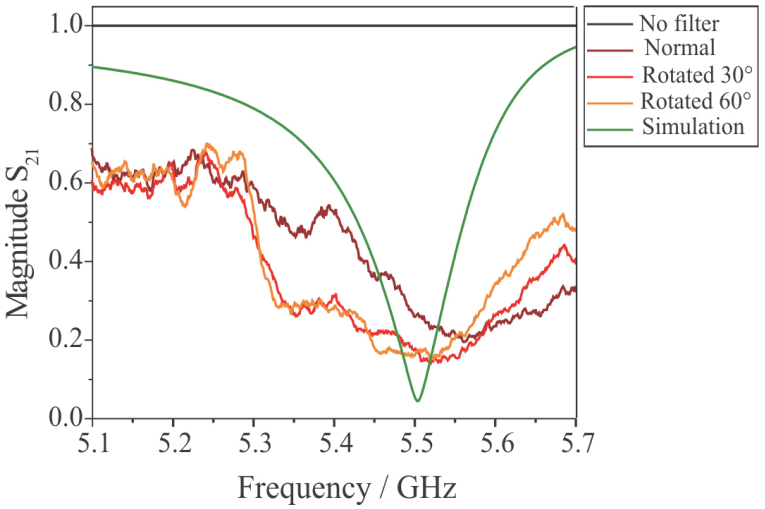

FIGURE 4.9: Experimental and computational transmission of the FSS. Athough the signal is low and noisy, a filtering response is found and match with the expected simulation results (green line).

results were found. However, the metasurface made of SRR had a better quality of fabrication and its filtering response is shown in Figure 4.9.

Among the positive aspects, we got a good match in the resonance frequency and, in lesser extent, the bandwidth between the experiments and the simulation under normal incidence. The limitation on the metasurface size also affects the measurement for large angles of incidence because only one part of the radiation pattern is filtered. For this reason the curve obtained experimentally for 30 and 60 is no longer reliable, since they are muddied by the practical difficulties, distorting the analysis that can be done based on the previously exposed description of them. However, at normal incidence, we have validated the filtering response of the small metasurface fabricated as a stop-band filter (dip on the S_{21} curve). In order to characterize its spatial filtering response it is necessary to fabricate a bigger metasurface, e.g. an array of smaller metasurfaces, like the ones we fabricated.

Another proposal, is to design a filtenna (filter + antenna) [4]. This device has functions of bandpass filter and horn antenna, and it would be very suitable for applications in military platforms where frequency selective surfaces are used for antennas and radar cross section (RCS) reduction. Figure 4.10(a) shows the simulation of this proposal by simulating the emitter horn antenna WR-187 with the metasurface placed in front of it. Figure 4.10(b) shows the reduction of the RCS in comparison with the absence of the filter at the normal direction of incidence only. Although the RCS is higher at different angles, it can be reduced by placing a radome covering the antenna, the radome reduces the RCS out of the normal incidence. Besides, figure 4.10 (c) shows that at certain

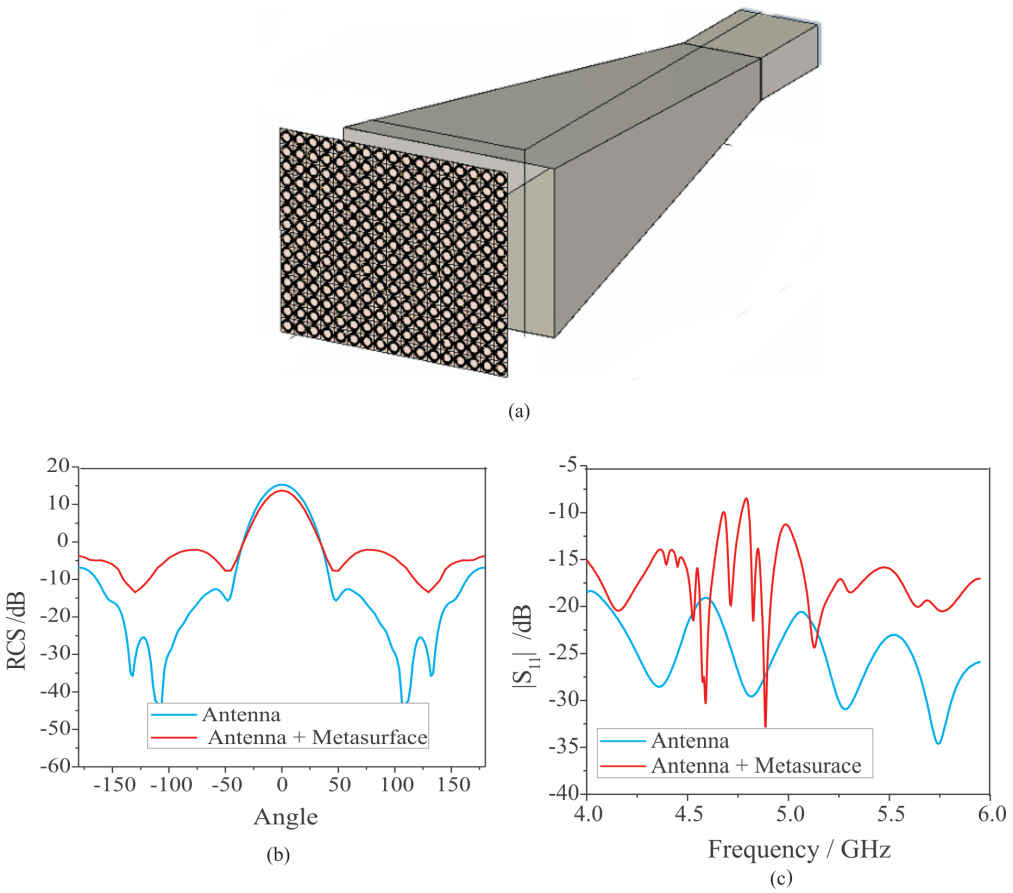

FIGURE 4.10: Proposal to design an antenna integrated with a spatial filter to reduce its RCS. (a) simulation characteristics: Standard horn antenna $WR-187$ that operates within [3.95-5.85] GHz with a metasurface made of I-SRRs placed in front of it at a distance of 2cm in order to simulate the experimental conditions shown in figure 4.8(c). (b)S_{11} parameter. (c) Radar cross section with and without filter.

frequencies, 4.63 GHz and 4.86 GHz the reflection is minimum, so that the transmission is maximum, showing the filtering behavior of the metasurface.

4.3 Experiment 3. Permittivity Measurements using Microstrip Technology and C-SRRs

In this section, the C-SRR is used with a microstrip line to create a device able to measure the electric permittivity of liquids. Simulations and measurements of the S-parameters are performed to correlate the resonance frequency to the known permittivity of five samples, in order to calibrate the device. Once calibrated, we also provide an estimate of the permittivity of a solution of silver nanoparticles. These measurements are attractive given the limited non-invasive techniques available for nanomaterial characterization and the lack of results at the microwave range.

Measurements of the complex permittivity of gases, liquids, and solids at the microwave range, have been developed using devices in which the electromagnetic fields are known,[42]. These microwave techniques employ a cavity resonator which is completely filled in the dielectric region with the solution under test. In the case of 2D materials, many advances in microstrip based sensors and coplanar waveguides are used in order to have compact, lightweight and low-cost devices [43].

For instance, by using a microstrip line, its work frequency can be calculated by means of the phase shift $\phi = \sqrt{\epsilon_e} k_0 L$, where $k_0 = \frac{2\pi f}{c}$, c is the speed of light and ϵ_e is the effective dielectric constant of a homogeneous medium that replaces the air and the substrate of the microstrip. When the phase shift is half wavelength, the frequency is [2]

$$f = \frac{c}{2\sqrt{\epsilon_e} L}, \quad \epsilon_e = \frac{\epsilon_r + 1}{2} + \frac{\epsilon_r - 1}{2} \frac{1}{\sqrt{1 + 12d/w}}. \tag{4.1}$$

Thus, once the work frequency is measured, the effective permittivity can be computed, yielding the permittivity of the solution. However, the volume needs to be big enough because of the approximation 4.1, which requires all the space to be replaced by the solution. A different approach uses resonator techniques [44], in which a microstrip line is drilled with holes and the solution is placed on them. See figure 4.11 (up). In this case, the permittivity is calculated by means of an effective permittivity of the substrate and the solution under test. Instead, when we use small resonators, we can estimate the permittivity of the solution under test only.

Baena et al.[30] analyzed the resonant response of the C-SRR highlighting its small electrical size and good Q. By etching this geometry onto the ground plane of a microstrip line, it is possible to measure the permittivity of the solution under test, placing it into the apertures of the C-SRR.

Until now, no truly measurements of the permittivity of a solution of silver nanoparticles have been reported. Due to the advantages of the C-SRR geometry, it would be possible to measure the electrical response of nanocomposites in terms of it concentration and particle size. It will be shown that this characterization is useful to determine its use for electrical energy storage at the microwave range.

In comparison with a similar device proposed by Castro et. al [44], shown in figure 4.11; the main difference is the way that the resonance is introduced: The microstrip line with circles behaves as a Fabry-Perot resonator such that the resonance appears when the length of the microstrip is half wavelength. On the other hand, the resonance of the C-SRR appears because of the induced electric and magnetic dipoles described in Chapter 2.

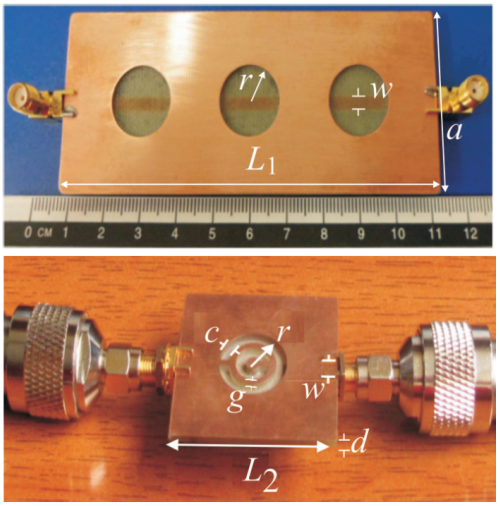

FIGURE 4.11: a.) Proposal of [44] for permittivity measurements based in circular cavities. b.) Proposal based in C-SRR geometry. The geometric parameters are $L_1 =$ 10cm, $a = 36$ mm, $L_2 = 33$ mm , $w = 3$ mm, $r = 8$ mm, $c = 2$ mm, $g = 2$mm, $d =$ 1.57 mm. The depth of the circular cavities and the slots is $h = 1$ mm.

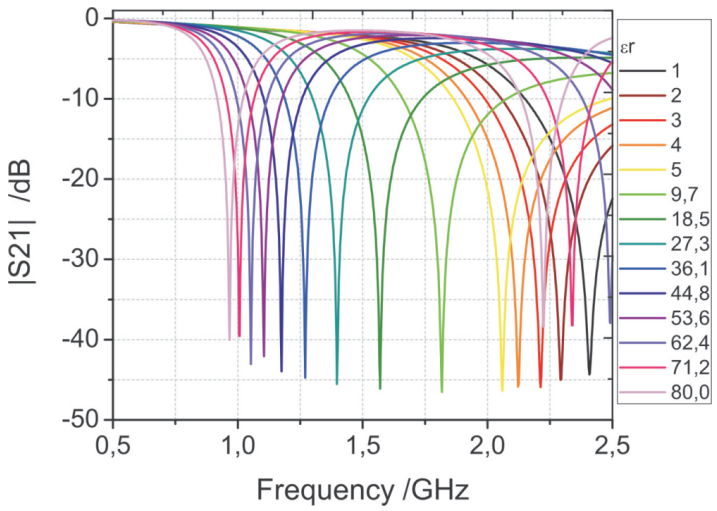

FIGURE 4.12: $|S_{21}|$ coefficient varying ϵ_r of the filling solution. The geometrical parameters of the device are described in Fig. 4.11.

4.3.1 Numerical Simulation

In order to test the response of the device before the experiment, the $S-$parameters were calculated by full-wave simulation within the frequency range [0.5-2.5]GHz. We got a relation between the resonance frequency and ϵ_r shown in figure 4.12 by varying the relative permittivity of the filler and calculating the minimum in the $|S_{21}|$ parameter.

The simulation shows that the minimum frequency shifts from 2.4-0.8 GHz when the relative permittivity changes from 1-80. We are interested in simplifying the simulation process considering that the C-SRR resonates because of its geometry only and that the electric field lines are more intense in the slits rather than the rest of the structure.

Material	ϵ_r	C-SRR Model (GHz)	CST Simulation (GHz)
Air	1	3.84	3.26
Immersion Oil	3.2	3.05	2.54
FR4	4.3	2.84	2.34
Acetone	20.7	1.62	1.29
Ethyl Alcohol	24.3	1.51	1.20
Water	80.4	0.87	0.68

TABLE 4.2: Permittivity of solvents to be tested experimentally and its resonance frequency calculated by means of LC-circuit model of the C-SRR geometry and *CST-Studio* numerical simulation. The relative permittivity of the commercial solvents is known. [44]

To validate this approximation, we used a program that calculates the resonance of the C-SRR by means of the circuit model and we compared it with a *CST-Studio* simulation in which the substrate was replaced by the solvent under test. We performed the simulations for the five commercial solvents tested experimentally. The results shown in Table 4.2, stablish that when $\epsilon_{solution} \approx \epsilon_{substrate}$, the resonance is higher than the resonance achieved when the microstrip is introduced, thus the approximation is no longer valid.

4.3.2 Results

The response of the device for permittivity measurements was analyzed with five different solutions. For the fabrication process, we designed the geometrical parameters by using Eagle software. The device was manufactured using basic processes of photolithography and etching on a FR4 substrate covered with a thin layer of copper. The slits were manufactured with a Bungard CCD/2 (Germany) computer-controlled milling machine using a 1 mm drill bit, drilling up to 1mm of depth. Filling the slits with 200 μL of the solvents in Table 4.2, we verified the matching between the experimental and simulated curves,(figure 4.13). The experimental curves present a ripple that prevent us from obtaining information about the dielectric losses, (figure 4.14). It is associated to the calibration process because the cables of the Vectorial Network Analyzer mismatch the entrance impedance of the microstrip. In order to avoid this ripple for further analysis of the quality factor, we propose the TRL Calibration Method, presented in [2].

The decreasing form of the curve in figure 4.13 establishes two regions of interest, the response of the technique for solvents with low and high permittivity. Below ϵ_r =20 approximately, small variations in ϵ_r yield high variation of the frequency, so different oils could be accurately measured, for instance. Likewise at high ϵ_r like the silver nanoparticles solution, even the smaller variation of frequency represent an important change in the permittivity. Therefore, the possibility of measuring this small differences

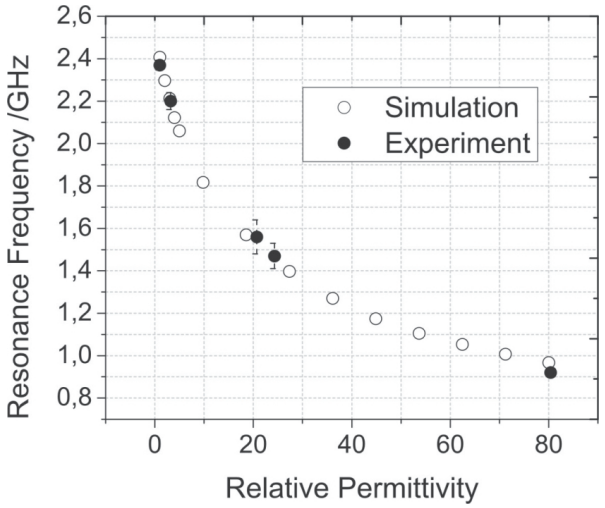

FIGURE 4.13: Resonance Frequency vs. Relative Permittivity. (white) Results from simulations using *CST-Microwave Studio* (black) experimental results with the liquids shown in 4.2.

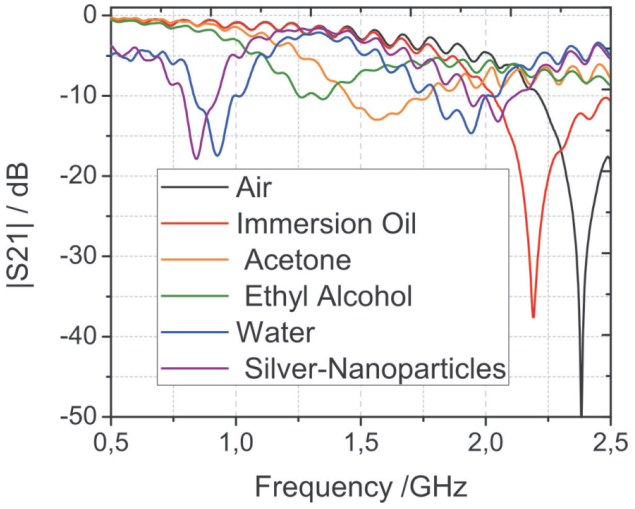

FIGURE 4.14: Experimental measurements. (Up)The structure manufactured has the same geometrical parameters described in Fig. 4.14 (Down) S_{21} parameter when different solutions are placed in the sensor. The ripple is associated to the calibration process.

would allow us to characterize the nanocomposites in terms of any intrinsic characteristic, like the concentration of nanoparticles or the particle size.

Equation 4.2 allows us to estimate the permittivity of a solution of silver nanoparticles ϵ_r^{Ag-NPs} =101.46 $\pm$ 19.53. Higher than the permittivity of water, this result is interesting because it means that these nanocomposites possess strong response to electric field in the microwave range. Improvements of resonator techniques could be performed to analyze the response of the electromagnetic fields for solvents with a response that depends on the concentration of its components. Both improvements in design and fabrication could be performed by cutting the ground plane with other C-SRR's related

geometries, like spirals (CSR2) whose resonator response has been previously described in [**?**].

$$\begin{gathered} \epsilon_r = A \exp^{-f/B} + C \\ A = 916.37 \pm 78.54 \quad B = 0.393 \pm 0.013, \quad C = -0.121 \pm 0.74 \\ r^2 = 0.998 \end{gathered} \tag{4.2}$$

Chapter 5

Conclusions

The conclusions that were obtained from the research carried out for this masters thesis are the following:

On the theoretical description of the $S-$parameters We found that the transmission and reflection coefficients must move along circumferences on the complex plane when varying the frequency close to one single resonant frequency. Besides, the circumferences are also correlated one each other between the original screen and its complementary screen by means of the Babinet's Principle. Good agreement between the theory and numerical simulations was shown. The constraints found between the reflection coefficient and the cross polarization terms may be useful for limiting the types of realistic responses desired for new metasurfaces. It is verified that under symmetries the cross polarization terms dissapear.

On the other hand, even under non ideal conditions, the loci of circumferences remains but its radius is limited by the absorption. In addition, by means of the Babinet's principle, the relation between the coefficients of the original and complementary screens remains valid. However, these curves are not equal because each one varies with frequency, and the resonance frequencies are different on each case.

On the parametric study of thick metasurfaces First, it was found that the cell size strongly affects the quality factor Q and the resonance frequency f_0, such that as a increases f_0 tend to a constant value: the characteristic frequency of the resonator. Likewise, under ideal conditions the Q factor may increase significantly as the bandwidth is reduced to a single resonance frequency. Secondly, it was found that Q and f_0 of SRR based metasurfaces strongly depend on the thickness. In the opposite way, maximum at resonance (S_{11} for SRR based metasurfaces and

S_{21} for C-SRR based metasurfaces) remains constant and it mainly depends on the geometry used. The SRR(C-SRR) can achieve a maximum around 0.75 in magnitude while the spirals SR2 and SR3 (C-SR2- C-SR3) achieve 0.5 and 0.3 respectively. This maximum is related with the excitation of the resonator: due to the charge distribution along the rings, the induced magnetic (electric) moment is stronger for the SRR than the SR2 and SR3, thus, not fully excitation is obtained under the same polarization. For further applications as thick stop/pass band filters, it is necessary to find an equilibrium between the Q and the maximum obtained at resonance, being the SRR and the C-SRR the most suitable geometry.

On the LC-circuit model for thick SRR metasurfaces A circuit model for calculating the resonance frequency of thick SRR and SR2 has been proposed and checked by means of numerical simulations. Besides, it was shown that the ratio between the resonance frequency of the SRR and the SR2 is independent of the thickness and approximately equal to 2, similarly to the case of thin particles. This analytical model can be useful for designing thick FSS with higher Q than that of thin particles. The inductance is calculated as the inductance of a cylinder of average radius r_0 and the capacitance was calculated as a sum of the capacitance of a coaxial cylinder and the capacitance of the borders $C_{border} = 2\pi r C_{\text{p.u.l}}$, with $C_{\text{p.u.l}}$ the capacitance between two coplanar strips. Good agreement between f_0 calculated by full-wave numerical simulations and by the proposed model is found.

On the waveguide model for thick C-SRR metasurfaces We proposed a waveguide model in which the slits of complementary SRR based metasurfaces were seen as bent rectangular waveguides. In comparison with a common rectangular waveguide whose first frequency that allows full transmission is the cut-off frequency ($f_c = 2c/L$) with L the length of the waveguide, in our model the transmission is obtained at this frequency only; due to the mismatch between the incident wave and the surface. This model is very useful to find the geometric parameters necessary for to design a passband filter made of C-SRR geometry that completely transmits at a fixed frequency. The most important parameters are the ratio and the thickness; and thus, this equivalent rectangular waveguide model turns out to be more precise and easier than the equivalent LC-circuit models. Besides, for thick structures the resonances work independently for each slit of the C-SRR, which allow us to design tunable filters with high Q for two different frequencies within the same unit cell. The results of these models were summarized in a "user friendly" software for the design of thick metasurfaces.

On the Short Waveguide filter experiment The usefulness of short resonators of small electric size for the design of short bandpass filters in a rectangular waveguide

has been analyzed for three different geometries, designed with the models stated above in conjunction with numerical simulations. It is believed that the proposed prototypes can be of practical interest for the fabrication of very compact filters, since their length is simply given by the thickness of the metallic sheet, which is on the millimetre scale. Besides, from the different geometries that satisfy the small electric size, we have proven the one of best performance, the CSRR.

On the Spatial Filter small metasurface experiment It has been demonstrated that a small metasurface made of interconnected resonators has the capability of providing spatial angular filtering even when it is placed very close to the antenna. We started from the design of [41] using interconnected split ring resonators (I-SRR) and its complementary structure (IC-SRR) as unit cells. I-SRRs and I-CSRRs provide a stopband and a passband, respectively, whose central frequencies can be tuned by changing the angle of incidence without affecting too much the bandwidth. Besides, as its filtering response was found very close to the antenna (the metasurface area was comparable with the aperture of the horn antenna) we propose the design of a filtenna (filter + antenna). Improvements in the fabrication and characterization process are also proposed, considering that it was the first metasurface made at the National University of Colombia. In fact, part of the usefulness of this metasurface is the analysis of the fabrication process and the management of an anechoic chamber for characterization procedures.

On the Device for permittivity measurements of liquids experiment We developed a resonant device based on the C-SRR for measuring the permittivity of different solutions within the microwave range (0.5-2.5 GHz). In addition to the frequency selectivity, the ability of this device to provide an accurate measurement and the advantage of size reduction in comparison with previous resonators has been shown. An analytical model has been used to simplify the computational simulation and it is demonstrated that these models are valid for solutions of high permittivity. The computational results compared with experimental results provide a good qualitative agreement, as well as a very good quantitative prediction of the permittivity of the solvent under test: a solution of silver nanoparticles diluted in water with an estimated permittivity $\epsilon_r = 101.46 \pm 19.53$. The experimental results for the bandwidth are inaccurate due to a mismatch between the ports and the microstrip line, although they can be improved by performing a TRC calibration process.

Appendix A

Publications sent to Journals and International Conferences

Journals

- **Revista Momento** L. M. Pulido-Mancera, J. C. González, A. Ávila, J. D. Baena. "Permittivity Measurements Based in Microstrip Technology". **Accepted**
- **Journal of Applied Physics** L. M. Pulido-Mancera, J. D. Baena, "Theoretical Constraints on the Transmission and Reflection through Frequency Selective Surfaces". **To be submitted**
- **IEEE and Microwave Wireless Components Letters** L. M. Pulido-Mancera, J. D. Baena. "Short Waveguide Filters based on Complementary Split Ring Resonator and Related Geometries". **To be submitted**

International Conferences

- L. M. Pulido-Mancera, J. D. Baena, J. L. Araque Quijano. "Thickness Effects in the Resonance of Metasurfaces made of SRRs and C-SRRs". *2013 IEEE International Symposium on Antennas and Propagation ans USNC/URSI National Radio Science Meeting.* Orlando, Florida, EE.UU. 7-13 July, 2013. **Published**
- L. M. Pulido-Mancera, J. D. Baena. "Waveguide Bandpass Filters of Thick Complementary Small Resonators". *2014 IEEE International Symposium on Antennas and Propagation ans USNC/URSI National Radio Science Meeting.* Memphis, Tennessee July 6-12, 2014. `arxiv.org/abs/1043.5167` **Accepted**

- L. M. Pulido-Mancera, J. D. Baena. "Equivalent Circuit Model for Thick Split Ring Resonators and Thick Spiral Resonators". *2014 IEEE International Symposium on Antennas and Propagation ans USNC/URSI National Radio Science Meeting.* Memphis, Tennessee July 6-12, 2014. `arxiv.org/abs/1403.5144` **Accepted**

- L. M. Pulido-Mancera, J. D. Baena, "Small Metasurface for angular filtering at the microwave range." *Metamaterials, Metadevices, and Metasystems 2014*, San Diego California, EE.UU. August 17-21 2014. **Accepted**

- L. M. Pulido-Mancera, J. D. Baena, "Theoretical Constraints on the Transmission and Reflection through Metasurfaces". *Metamaterials'2014.* Copenhagen, August 25-30, 2014. **Submitted**

- L. M. Pulido-Mancera, J. D. Baena. "Waveguide Bandpass Filters made of Thick Complementary Small Resonators". *Metamaterials'2014.* Copenhagen, August 25-30, 2014. **Submitted**

Bibliography

[1] J. S. Miranda, J. L. Sebastian, M. Sierra, and J. Margineda. *Ingeniería de Microondas. Tecnicas Experimentales.* Prentice Hall, 2002.

[2] D. M. Pozard. *Microwave Engineering, 3rd 3d.* John Wiley and Sons, 2005.

[3] F. Bayatpur. *Metamaterial-Inspired Frequency-Selective Surfaces.* PhD thesis, University of Michigan, 2009. URL `http://deepblue.lib.umich.edu/handle/2027.42/64588`.

[4] J. L. Durbin and M. Saed. Tunable filtenna using varactor tuned rings with an ultrawideband antenna. *IEEE Microwave and Wireless Components Letters*, 23(9): 477–479, 2013.

[5] D. R. Smith, J. B. Pendry, and M. C. K. Wiltshire. Metamaterials and negative refractive index. *Science*, 305(5685):788–792, 2004. URL `DOI:10.1126/science.1096796`.

[6] J. B. Pendry, A. J. Holden, D. J. Robins, and W. J. Stewart. magnetism from conductors and enhanced nonlinear phenomena. *IEEE Transactions of Microwave Theory and Technology*, 47:2075–2084, 1999.

[7] N. Engheta and R. W. Ziolkowski. *Metamaterials: Physics and Engineering Explorations.* Wiley-IEEE Press, 2006.

[8] R. Marqués, F. Mesa, J. Martel, and F. Medina. Comparative analysis of edge- and broadside- coupled split ring resonators for metamaterial design theory and experiments. *IEEE Trans. Antennas and propagation*, 51(10):2572–2581, 2003. URL `http://dx.doi.org/10.1109/TAP.2003.817562`.

[9] S. M. Rao, D. R. Wilton, and A. W. Gibson. Electromagnetic scattering by surfaces of arbitrary shape. *IEEE TRANSACTIONS ON ANTENNAS AND PROPAGATION*, 30(3):409 – 418, 1982. URL `http://dx.doi.org/10.1109/TAP.1982.1142818`.

[10] J. D. Jackson. *Classical Electrodynamics.* John Wiley and Sons, 1962.

[11] R. Yang, R. Rodríguez-Berral, F. Medina, and Y. Hao. Analytical model for the transmission of electromagnetic waves through arrays of slits in perfect conductors and lossy metal screens. *Journal of Applied Physics*, 109(103107), December 2011. URL `http://dx.doi.org/10.1063/1.3583561`.

[12] R. Marqués, M. Sorolla, and F. Martín. *Metamaterials with Negative Parameters.* Wiley Series in Microwave and Optical Engineering, 2007.

[13] T.K. Wu. *Frequency Selective Surfaces and Grid Arrays.* John Wiley and Sons, 2005.

[14] B. A. Munk. *Frequency Selective Surfaces: Theory and Design.* New York Wiley, 2000.

[15] B. Hobberman. Everything you ever wanted to know about frequency-selective surface filters but were afraid to ask. 2005. URL `http://cosmology.phys.columbia.edu/group_web/about_us/memos/hooberman_filters_memo.pdf`.

[16] C. A. Balanis. *Antenna Theory Analysis And Design, 3rd. ed.* Johm Wiley and Sons, 2005.

[17] R. Marqués, J. D. Baena, M. Beruete, F. Falcone, T. Lopetegi, M. Sorolla, F. Martín, and J. Garcia. Ab-initio analysis of frequency selective surfaces based on conventional and complementary split ring resonators. *J. Opt.A: Pure Appl. Opt.*, 7:S38–S43, 2005. URL `http://dx.doi.org/10.1088/1464-4258/7/2/005`.

[18] W. C. Gibson. *The Method of Moments in Electromagnetics.* Chapman and Hall/CRC, 2008.

[19] S. Tetryakov. *Analytical Modelling in Applied Electromagnetics.* Artech House, 2003.

[20] CST-Computer Simulation Technology AG. *CST-Microwave Studio. Workflow and Solver Overview.* 1998-2010.

[21] G. V. Eleftheriades, O. Siddiqui, and A. K. Iyer. Transmission line models for negative refractive index media and associated implementations without excess resonators. *IEEE MICROWAVE AND WIRELESS COMPONENTS LETTERS*, 13 (2):51 – 53, 2003. URL `http://dx.doi.org/10.1109/LMWC.2003.808719`.

[22] M. Durán-Sindreu, J. Naqui, F. Paredes, J. Bonache, and F. Martín. Electrically small resonators for planar metamaterial, microwave circuit and antenna design: A comparative analysis. *Appl. Sci.*, 2:375–395, 2012. URL `http://dx.doi.org/10.3390/app2020375`.

[23] C L. Holloway, E. F. Kuester, J. A. Gordon, J. OHara, J. Booth, and D. R. Smith. An overview of the theory and applications of metasurfaces: The two-dimensional equivalents of metamaterials. *IEEE Antennas and Propagation Magazine*, 54(2), 2012.

[24] Alon S. Barlevy and Y. Rahmat-Samii. Analysis of arbitrary frequency selective surfaces: Analytic consraints. volume 2, pages 1440–1442, Loughborough, UK, 1996.

[25] R. Harrington. *Time-Harmonic Electromagnetic Fields*. The IEEE Press Series on Electromagnetic Wave Theory, 2001.

[26] D. J. Griffiths. *Introduction to Electrodynamics*. Pearson Addison Wesley, third edition, 1999.

[27] C. L. Holloway, A. Dienstfrey, E. F. Kuester, J. F. OHara, A. K. Azad, , and A. J. Taylor. A discussion on the interpretation and characterization of metafilms/metasurfaces: The two-dimensional equivalent of metamaterials. *Metamaterials*, 3:100–112, 2009.

[28] M. Beruete, M. Sorolla, R. Marqués, J. D. Baena, and M. Freire. Resonance and cross-polarization effects in conventional and complementary split ring resonator periodic screens. *Electromagnetics*, 26:247–260, 2006.

[29] V. Dmitriev. Symmetry properties of electromagnetic planar arrays: long-wave approximation and normal incidence. *Metamaterials*, 5:141–148, 2011.

[30] F. Falcone, T. Lopetegi, M. A. G. Laso, J. D. Baena, J. Bonache, R. Marqués M. Beruete, F. Martín, and M. Sorolla. Babinet principle applied to the design of metasurfaces and metamaterials. *Physical Review Letters*, 93(197401), 2005. URL `http://link.aps.org/doi/10.1103/PhysRevLett.93.197401`.

[31] J. D. Ortiz, J. D. Baena, R. Marqués, and F. Medina. A band-pass/stop filter made of srrs and c-srrs. In *2011 IEEE International Symposium on Antennas and Propagation (APSURSI)*, pages 2669–2672, Spokane, WA, 2011. URL `http://dx.doi.org/10.1109/APS.2011.5997074`.

[32] J. D. Baena, R. Marqués, and F. Medina. Artificial magnetic metamaterial design by using spiral resonators. *Physical Review B*, 69(014402), 2004. URL `http://link.aps.org/doi/10.1103/PhysRevB.69.014402`.

[33] J. D. Baena, L. Jelinek, R. Marqués, and J. Zehentner. Analysis of 2d- and 3d-isotropic split ring resonators. In *18th International Conference on Applied Electromagnetics and Communications (ICECom)*, Dubrovnik, Croatia, 2005.

[34] J. García-García, F. Martín, J. D. Baena, R. Marqués, and L. Jelinek. On the resonances and polarizabilities of split ring resonators. *Journal of Applied Physics*, 98(033103), 2005. URL `http://dx.doi.org/10.1063/1.2006224`.

[35] J. B. Pendry, A. J. Holden, D. J. Robbins, and W. J. Stewart. Magnetism from conductors and enhanced nonlinear phenomena. *IEEE Trans. Microwave Theory Tech.*, 47(10), December 1999. URL `http://dx.doi.org/10.1109/22.798002`.

[36] J. García-García, F. Martín, J. D. Baena, R. Marqués, and L. Jelinek. On the resonances and polarizabilities of split ring resonators. *Journal of Applied Physics*, 98(033103), 2005.

[37] I. Bahland and P. Bhartia. *Microwave Solid State Circuit Design*. Wiley, New York, 1988.

[38] L. M. Pulido-Mancera, J. D. Baena, and J. L. Araque Quijano. Thickness effects in the resonance of metasurfaces made of srrs and c-srrs. *2013 IEEE AP-S/USNC-URSI Symposium*, July 7-13 2013. URL `http://arxiv.org/abs/1310.2936v1`.

[39] N. Ortiz, J. D. Baena, M. Beruete, F. Falcone, M. A. G. Laso, T. Lopetegi, R. Marqués, F. Martín, J. García-García, and M. Sorolla. Complementary split ring resonator for compact waveguide filter design. *MICROWAVE AND OPTICAL TECHNOLOGY LETTERS*, 46(1), 2005.

[40] URL `http://www.microwaves101.com/encyclopedia/waveguidedimensions.cfm`.

[41] J. D. Ortiz, J. D. Baena, V. Losada, F. Medina, and J. L. Araque. Spatial angular filtering by fsss made of chains of interconnected srrs and csrrs. *IEEE Microwave and Wireless Components Letters*, 23(9):477–479, 2013.

[42] E. Fratticcioli, M. Dionigi, and R. Sorrentino. A planar resonant sensor for the complex permittivity characterization of materials. *Microwave Symposium Digest*, 2(647), 2002.

[43] A. Abdel-Rahman, M. S. Kheir, A. K. Verma, and A. Omar. A planar resonant sensor for the complex permittivity characterization of materials. *Progress in Electromagnetic Research C*, 13(67), 2010.

[44] J. R. Castro and A. Avila. *Efecto de las características geométricas de estructuras PBG y sus potenciales aplicaciones*. PhD thesis, Universidad de los Andes, 2005.

Theoretical Constraints on Reflection and Transmission through Metasurfaces

Laura Pulido-Mancera, and Juan Domingo Baena,

***Abstract*—We have established a set of useful constraints that should be verified by thin metasurfaces made of perfect electric conductor. Mainly, we found that loci of transmission and reflection coefficients on the complex plane are circumferences. The properties shown in this paper may be useful for limiting the types of realistic responses desired for metasurfaces. On the other hand, under non ideal conditions, similar circumferences are obtained.**

***Index Terms*—Cross polarization effects, metasurfaces.**

I. Introduction

METASURFACES may help to create new types of frequency selective surfaces, polarizers, polarization converters, shields, etc. Surface impedance models for characterizing metasurfaces have been proposed earlier [1], [2]. Sometimes, metasurfaces can show cross polarization effects as demonstrated by Beruete for metasurfaces made of Split Ring Resonators (SRRs) [3]. Besides, the Babinet's principle has been used to propose complementary metasurfaces made of Complementary SRRs (C-SRRs) [4]. Now, from basic fundamentals and an hypothesis on the surface currents on the metasurface, we have established a set of useful constraints that relate the direct reflection coefficients with the cross polarization coefficients. Indeed, under non ideal metasurfaces, the transmission and reflection coefficients also move along circumferences whose radius is determined by the absorption. The properties shown in this paper may be useful for limiting the types of possible responses expected for new metasurfaces as well as the response of its complementaries.

II. Theory

Let us assume normal incidence on a metasurface etched on a sheet of perfect electric conductor, so that conservation of energy and reciprocity are guaranteed. Figure 1(a) shows the waves impinging from the left side E^+_{1x}, E^+_{1y} on a metasurface, and the waves moving away from it $E^-_{1x}, E^-_{1y}, E^-_{2x}, E^-_{2y}$. The scattering matrix $\mathbf{S}$ connects them by the linear relation $\left[E^-_{x1}, E^-_{y1}, E^-_{x2}, E^-_{y2}\right]^t = \mathbf{S} \cdot \left[E^+_{x1}, E^+_{y1}, E^+_{x2}, E^+_{y2}\right]^t$ with

$$\mathbf{S} = \begin{pmatrix} r_{xx} & r_{xy} & | & t_{xx} & t_{xy} \\ r_{yx} & r_{yy} & | & t_{yx} & t_{yy} \\ - & - & - & - & - \\ t_{xx} & t_{xy} & | & r_{xx} & r_{xy} \\ t_{yx} & t_{yy} & | & r_{yx} & r_{yy} \end{pmatrix} \tag{1}$$

L. M. Pulido-Mancera and J. D. Baena are with the Department of Physics, Universidad Nacional de Colombia, Bogotá, Colombia, e-mail: lmpulidom@unal.edu.co.

Manuscript sent April 21, 2014

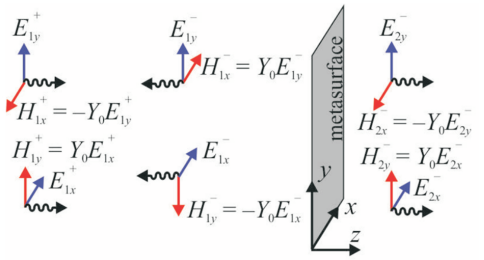

Fig. 1. Incident and scattered waves through a metasurface. Notation of the electric and magnetic fields corresponds to each side of the metasurface (subscript 1, 2) and incoming of outgoing waves (superscript + or − respectively).

With r_{xx} for instance, the reflection coefficient along the x axis due to an incident electric field along the x axis too. Likewise, the cross polarization effects,r_{xy} the reflection on the x axis produced by an incident wave polarized along the y axis. Rewriting $r_x \equiv r_{xx}$ and $r_y \equiv r_{yy}$ the *direct* reflection coefficients, $t_x \equiv t_{xx}$ and $t_y \equiv t_{yy}$ the *direct* transmission coefficients, and $c \equiv r_{xy} = r_{yx} = t_{xy} = t_{yx}$; it is worth to note that, due to the reflection symmetry along the $z-$axis, the coefficients for one direction of propagation equal those of the opposite direction. From the reciprocity theorem $r_{xy} = r_{yx}$ and $t_{xy} = t_{yx}$, besides, from the continuity of the electric field on the screen ($z = 0$) we have $r_{yx} = t_{yx}, r_{xy} = t_{xy}$ and

$$1 + r_{xx} = t_{xx}. \tag{2}$$

Thus, the $\mathbf{S}$ matrix can be written as

$$\mathbf{S} = \begin{pmatrix} r_x & c & 1+r_x & c \\ c & r_y & c & 1+r_y \\ 1+r_x & c & r_x & c \\ c & 1+r_y & c & r_y \end{pmatrix} = \begin{pmatrix} \mathbf{R} & \mathbf{R} \\ \mathbf{R} & \mathbf{R} \end{pmatrix} + \begin{pmatrix} \mathbf{0} & \mathbf{1} \\ \mathbf{1} & \mathbf{0} \end{pmatrix}, \tag{3}$$

with $\mathbf{R}$ the 2×2 reflection matrix. It is well known that for reciprocal and lossless structures $\mathbf{S} \cdot \mathbf{S}^* = \mathbf{1}$. Imposing this property onto 3 we rapidly get the relation

$$\left[\begin{pmatrix} \mathbf{R} & \mathbf{R} \\ \mathbf{R} & \mathbf{R} \end{pmatrix} + \begin{pmatrix} \mathbf{0} & \mathbf{1} \\ \mathbf{1} & \mathbf{0} \end{pmatrix}\right] \cdot \left[\begin{pmatrix} \mathbf{R} & \mathbf{R} \\ \mathbf{R} & \mathbf{R} \end{pmatrix} + \begin{pmatrix} \mathbf{0} & \mathbf{1} \\ \mathbf{1} & \mathbf{0} \end{pmatrix}\right]^* = \begin{pmatrix} \mathbf{1} & \mathbf{0} \\ \mathbf{0} & \mathbf{1} \end{pmatrix}$$

such that each component satisfies $\mathbf{R} \cdot \mathbf{R}^* + Re[\mathbf{R}] = 0$, or more precisely

$$\begin{pmatrix} |r_x|^2 + |c|^2 + r_{xr} & r_x c^* + r_y^* c + c_r \\ r_y c^* + r_x^* c + c_r & |r_y|^2 + |c|^2 + r_{yr} \end{pmatrix} = \begin{pmatrix} 0 & 0 \\ 0 & 0 \end{pmatrix}. \tag{4}$$

On the other hand, boundary conditions for tangential components of the magnetic field can be written as: $H_{2x} - H_{1x} = J_y$ and $H_{2y} - H_{1y} = -J_x$, where J_x and J_y are components of

the macroscopic surface electric current on the structure. Now, if we assume that the pattern of currents on the resonator is not depending on frequency neither on the incident electric wave polarization, (for frequencies close to the resonance) it is possible to introduce the hypothesis

$$J_y = kJ_x. \tag{5}$$

This condition is particularly valid when the pattern of currents is determined by the geometry of the resonator only, as it usually happens if it is electrically small. Applying this hypothesis 5 and properly traducing magnetic fields into electric fields, we can achieve the relation

$$-E_{2y}^{-} + E_{1y}^{+} - E_{1y}^{-} = -k(E_{2x}^{-} - E_{1x}^{+} + E_{1x}^{-}). \tag{6}$$

Assuming either $x-$ or $y-$polarized normal incident waves and normalizing by the incident field, we get

$$r_x = c/k \quad r_y = kc \quad r_x r_y = c^2. \tag{7}$$

Considering this new relation 7 between the direct reflection coefficients and the cross coefficients into the first term of equation 4, which in fact is associated to energy conservation, we can show that all the coefficients r_x, t_x, and c describe circumference paths on the complex plane as

$$\left(r_{xr} + \frac{1}{2(1+|k|^2)}\right)^2 + r_{xi}^2 = \left(\frac{1}{2(1+|k|^2)}\right)^2 \tag{8}$$

$$\left(t_{xr} - 1 + \frac{1}{2\,(1+|k|^2)}\right)^2 + t_{xi}^2 = \left(\frac{1}{2(1+|k|^2)}\right)^2 \tag{9}$$

These equations remain valid for r_x and r_y. Basically, while the reflection moves along a circumference within a frequency range of a single resonance, the transmission moves along the same circumference but displaced by the unity. A smaller trajectory is followed by the cross coefficients, which lie on the same side of the reflection loci. The second term of equation 4 allows us to demonstrate that k is complex but $\left(\frac{r_x - r_y}{c}\right)$ is real, stated below

(10)

Now, for thin and lossless plates the Babinet's principle must hold [4]. This principle states that the total field transmitted by a metallic screen with an arbitrary aperture, added to the total field transmitted by its complementary screen (illuminated by the complementary incident wave) gives the incident wave over this last structure ($E_x - cB_x^c = E_x^0$). This principle expressed in terms of the transmission coefficients can be simply stated as

$$t_{xx}E_x^0 + t_{xy}E_y^0 + t_{yx}^c E_x^{0c} + t_{yy}^c E_y^{0c} = E_x^0 \tag{11}$$

We can divide the equation 11 into two separated problems: under $x-$polarization incidence ($E_x^0 \neq 0$, $E_y^0 = 0$), or $y-$polarization incidence ($E_x^0 = 0$, $E_y^0 \neq 0$) which yields the simplified equations

$$\begin{aligned} t_x + t_y^c &= 1 \\ t_{xy} - t_{yx}^c &= 0 \end{aligned} \tag{12}$$

and

$$\begin{aligned} r_x + r_y^c &= -1 \\ r_{xy} - r_{yx}^c &= 0 \end{aligned} \tag{13}$$

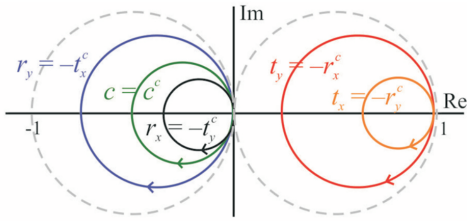

Fig. 2. Theoretical sketch of reflection coefficients r_x and r_y, transmission coefficients t_x and t_y, the cross polarization coefficient c, and its equivalence with the coefficients of the complementary metasurface: r_x^c,r_y^c,t_x^c,t_y^c,c^c.

for the reflection coefficients. Figure 2 summarizes the loci of all coefficients (given by eqs. 8, 9 and **??**) and its equivalence on the complementary metasurface.

Special attention is required on the hypothesis 5. This equation is properly working for resonators were the current is forced to lie on specific metal paths. For complementary resonators, the electric current is, in some way, more free to flow on bigger metal regions, so that the hypothesis is no longer true. A way to fix this problem would be to change the hypothesis to another similar relation with effective surface magnetic currents on the slots. Alternatively, we can also use the Babinet's principle joint to boundary conditions, in order to obtain the relations shown in figure 2.

III. Numerical Validation

To check the theory, a set of numerical simulations were carried out by using *CST Microwave Studio*. Figure 3 shows the scattering parameters for two surfaces presenting mirror symmetry [5]. One made of Split Ring Resonators, that satisfy the small electric size and thin metal strips needed to use the hypothesis of $J_y = kJ_x$ and another one made of its complementary (C-SRR), both made of perfect electric conductor. The geometrical parameters (a), were set as $a =$ 15 mm, $r = 9$ mm, and $c = d = g =$1mm. The reflection and transmission coefficients of the **S** matrix are depicted on the complex plane for the SRR (c) and the CSRR (d), where the relations that the Babinet's principle yield $r_x^c = -t_y$ (red), $r_y^c = -t_x$ (orange), $t_x^c = -r_y$ (blue) and $t_y^c = -r_x$ (black) are verified and no cross polarization effects are observed. Considering its resonant response, these coefficients vary in frequency presenting a dip or peak according to the surface and the $S-$parameter under study, as shown in figure 3(e) and (f).

In the case of unsymmetrical geometries, like spirals, a metallic strip forming an *Achimedes' Spiral* was designed as well as its complementary with the same geometrical parameters of the SRR. The spirals designed had two loops, so named *Archimedes Spiral Resonator 2* (ASR2) and its complementary (C-ASR2), as shown in Figure 4(a, b) respectively. In the $S-$parameters plotted in the complex plane (c, d) it is possible to see the loci associated to **??**. Moreover $c = c^c$ is satisfied as well as the other relations presented in figure 2.

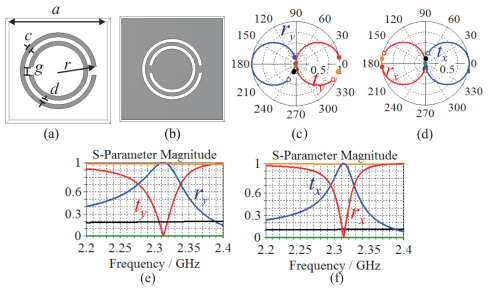

Fig. 3. Scattering parameters for metasurfaces presenting mirror symmetry. a) SRR, b) C-SRR.

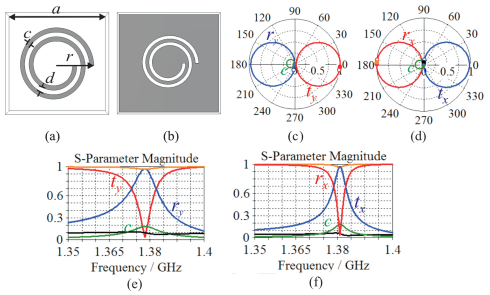

Fig. 4. Scattering parameters for asymmetrical metasurfaces. a) ASR2, b) C-ASR2.

IV. Resonator Design

Under no ideal conditions, it is necessary to add the *Absorbency* $|a|^2$ to the energy conservation such that $|r|^2 + |t|^2 + |a|^2 = 1$. The effect of this term on the circumferences described by the reflection and transmission coefficients is a change of its radius by subtracting the term $\frac{|a|^2}{2(1+|k|^2)}$ on the right side of equation 8, 9 and **??**. We performed the same set of numerical simulations for the metasurfaces made of SRR, C-SRR, ASR2 and C-ASR2, but in this case we used a substrate Rogers RT5880LZ of relative permittivity $\epsilon_r = 1.96$, thickness h =0.5 mm, and loss tangent of 0.0019. The metallic paths were simulated with copper, as shown in figures 5 and 6. Under these conditions the resonance frequency between the SRR and C-SRR, is not the same due to the substrate as shown in figure 5(e,f). Figure (c,d) shows that these circumferences are smaller. Another interesting fact of these curves, is that the initial and final points of the circumferences do not lie on the real axis as it do under ideal conditions because of a phase shift introduced by the thickness of the substrate. Besides, the latter case, the cross polarization effects are reduced, and more energy is absorbed than radiated in the crossed polarization.

In the case of metasurfaces made of ASR2 (C-ASR2), figure 6(a,b), the cross polarization appear and the relations of Babinet's principle are still satisfied.

V. Conclusions

We found that the transmission and reflection coefficients must move along circumferences on the complex plane when varying the frequency close to one single resonant frequency. Besides, the circumferences are also correlated one each other between the original screen (made of SRRs for instance) and the complementary screen (made of CSRRs). Good agreement between the theory and numerical simulations is shown. The constraints shown in this paper may be useful for limiting the types of realistic responses desired for new metasurfaces. Besides, with the circumferences found in the complex plane it is possible to find a real constant of proportionality between the induced currents J_x and J_y of a small resonator without symmetries. Under realistic conditions, we verify that the loci of these coefficients remain as circumferences whose radius is smaller by means of the absorption.

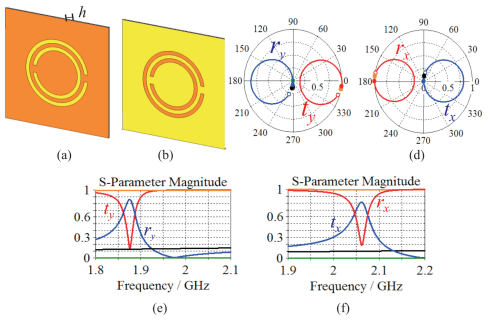

Fig. 5. Scattering parameters for metasurfaces presenting mirror symmetry under realistic conditions. a) SRR, b) C-SRR.

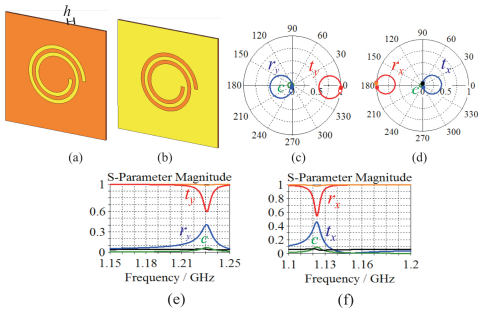

Fig. 6. Scattering parameters for asymmetrical metasurfaces under realistic conditions. a) ASR2, b) C-ASR2.

References

[1] R. Marqués, J. D. Baena, M. Beruete, F. Falcone, T. Lopotegi, M. Sorolla, F. Martín, and J. García, "Ab-initio analysis of frequency selective surfaces based on conventional and complementary Split Ring Resonators", *J. Opt. A: Pure Appl. Opt., vol. 7, pp. S38-S43, 2005.*

[2] C. L. Holloway, A. Dienstfrey, E. F. Kuester, J. F. O'Hara, A. K. Azad, and A. J. Taylor, " A discussion on the interpretation and characterization of metafilms/metasurfaces: The two-dimensional equivalent of metamaterials," *Metamaterials, vole. 3, pp. 100-112,2009.*

[3] M. Beruete, M. Sorolla, R. Marqués, J. D. Baena, and M. Freire, "Resonance and cross.polarization effects in conventional and complementary split ring resonator periodic screens," *Electromagnetics, vol. 26, pp. 247-260, 2006.*

[4] F. Falcone, T. Lopotegi, M. A. G. Laso, J. D. Baena, J. Bonache, M. Beruete, R. Marqués, F. Martín, and M. Sorolla," Babinet Principle Applied to the Design of Metasurfaces and Metamaterials", *Phys. Rev.. Lett* , vol. **93**, no 19, p.197401, 2005.

[5] V. Dimitriev, "Symmetry properties of electromagnetic planar arrays: long-wave approximation and normal incidence," *Metamaterials, vol. 5, pp. 141-148, 2011.*

Short Waveguide Filters based on Complementary Split Ring Resonator and Related Geometries

L. M. Pulido-Mancera. J. D. Baena. Physics Department
Universidad Nacional de Colombia
Bogotá, Colombia
lmpulidom@unal.edu.co, jdbaenad@unal.edu.co

***Abstract*—We explore the potential use of complementary split ring resonators (CSRRs) and complementary spirals of two and three turns (CSR2 and CSR3) to design very compact waveguide filters. We demonstrate its passband response in an experimental and computational form. In addition to its small electric size in comparison with known resonant-cavity waveguide filters, a higher quality factor (Q) for thick resonators is found. Actually, it is shown that the design process can be highly simplified by means of a new waveguide model that may avoids full wave numerical simulations. Thus, it is possible to design waveguide filters with lengths equal to the thickness of a metallic sheet and whose Q can be increased using thicker metallic sheets rather than cascade arrays, leading to an improvement in the design of miniaturized waveguide filters.**

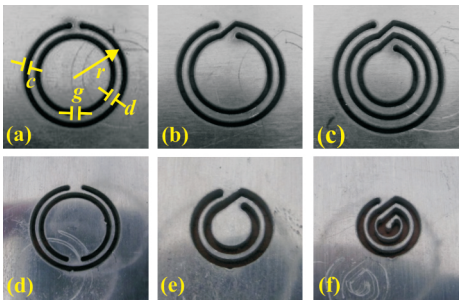

Fig. 1. Prototypes used as waveguide filters. In the first experiment (a,b,c) the resonators have the same geometrical parameters r =9.0mm, $c = d$ =1.0mm, g =2.7mm. In the second experiment each resonator has different radius but $c = d$ =1mm. (d) r =10.1mm, (e) r =6.1mm, (f) r =5.9mm.

I. Introduction

The Split ring resonator (SRR) was first introduced by Pendry et al. (1999) in order to produce artificial media with a strong magnetic response at microwaves and radio frequencies [1]. Its complementary structure, the CSRR recently reported by [2], have been inspired on the Babinets principle and, similar to the SRRs, it is an electrically small particle that exhibits a quasi-static resonance. A 2D array of CSRRs behaves as a passband filter whose resonance frequency depends on its geometrical parameters only. Similarly, for waveguide applications it allows us to replace the well-known resonant cavities coupled by circular irises in waveguide filters, resulting in a compact design [3].

The design process of infinitely thin CSRRs and similar geometries like spirals, has been developed by means of equivalent LC-Circuit Models in order to predict the resonance frequency: The intrinsic circuit model for the CSRR (dual of the SRR model) has a parallel combination of two inductances connecting the inner disk to the ground and the capacitance of a disk of radius r surrounded by a ground plane at a distance of its edge. Likewise, equivalent circuit models for planar CSR2 and CSR3 can be found in [4]. However, when the thickness increases, duality given by Babinet's principle is no longer valid and different approaches to predict the resonance in terms of the thickness are needed [5].

In the following, we will describe the excitation of the CSRR, CSR2 and CSR3 by means of different prototypes: Aluminium sheets with each geometry etched on it and excited by the magnetic field inside a rectangular waveguide. Besides, a new approach to predict the resonance frequency of thick resonators will be described to facilitate the design process and the passband response will be verified by means of numerical simulations and waveguide experiments.

Although the CSRR, CSR2 and CSR3 can be excited by different field components, the orientation of the prototypes fabricated is such that these are excited by the magnetic field component B_x of the $TE_{1,0}$ mode of a rectangular waveguide [7]. Two set of experiments were performed: for resonators of the same dimensions and different frequency range of resonance, Fig. 1(a,b,c), and for resonators of different dimensions within the same frequency range, Fig. 1(d,e,f). The geometrical parameters correspond to h the thickness of the metal plate, c the slit width, d the separation between slits, g the gap and r the external radius of the CSRR. Due to the fact that this behaviour is quasi-static, the CSRR dimensions are actually much smaller than the wavelength of incident radiation, for the first set of resonators the frequency range varies from [1-3]GHz and varies from [2-3]GHz for the second set of resonators.

II. Rectangular Waveguide Model for Thick CSRRs

When the prototype is thick, each slit of the CSRR (CSR2 or CSR3) can be seen as a rectangular waveguide bended with the shape of C or spiral respectively. Hence, as a waveguide, the lowest frequency that allows maximum transmission is the cutoff frequency f_0 of the mode TE_{10}, when $\lambda_0 = 2L$ with λ_0 the resonance wavelength and L the length of the slit. The second resonance f_1 (associated to λ_1) appears when $\lambda_1 = L$ is satisfied. For each prototype, L, f_0, and f_1 predicted of our simplified model are shown in Table I.

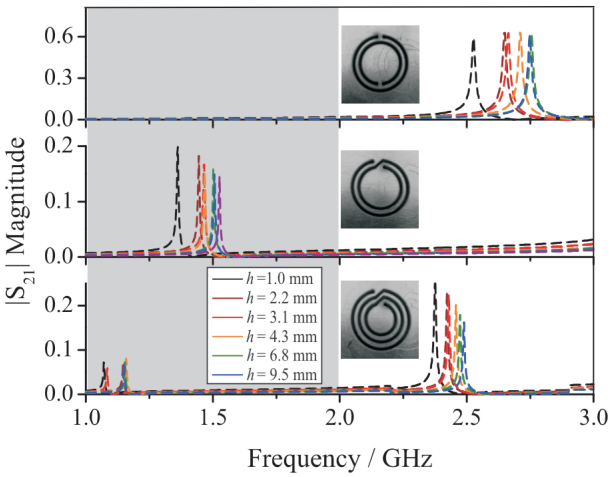

Fig. 2. S_{21} parameter for prototypes (a,b,c) calculated numerically by means of *CST-Microwave Studio*. The dark area represents the area that is not compared with experimental results.

TABLE I
EXPECTED RESONANCE FREQUENCIES FOR EACH PROTOTYPE FABRICATED.THESE RESONANCES ARE PROVIDED BY THE EQUIVALENT WAVEGUIDE MODEL FOR THICK RESONATORS.

Prototype	r **/mm**	L **/mm**	f_0 **/GHz**	f_1 **/GHz**
a.	9	54.3	**2.86**	5.72
b.	9	93.7	1.60	3.20
c.	9	123.9	1.21	**2.42**
d.	10.1	57.31	**2.61**	5.23
e.	6.1	59.4	**2.52**	5.05
f.	5.8	62.1	**2.415**	4.83

Unlike a common rectangular waveguide, in which the transmission is continuous from the cut-off frequency, what we found in the transmission curves shown below, is that these present a resonance peak at this frequency. This is due to the coupling between the electric field of the incident wave and the electric field that is formed within the slots, the equivalent to the electric field distribution of the TE_{10} mode of a rectangular waveguide. This coupling only occurs at the resonance frequency, so that at this point the transmission is highest.

In order to validate this model, a set of numerical simulations was performed for the prototypes of Fig. 1 (a,b,c) for different values of h. As shown in Fig. 2 the resonance frequency increases with h but in every case, it tends to a fixed value. The dark area represents the area out of the experimental frequency range, therefore, we would expect resonance peaks for the prototypes (a,c) only.

III. Experimental Setup

The CSRR, CSR2 and CSR3 were manufactured by etching it into aluminium sheets of thickness 1.0 mm and 2.5 mm by means of a laser drilling machine. As previously mentioned, two sets of resonators were fabricated, one set maintaining the size of the resonator thus changing its resonance frequency, and another set maintaining the same frequency range thus changing its dimensions.

The experimental setup is shown in Fig. 3a. Each sheet has been introduced between two WR340 rectangular waveguides,

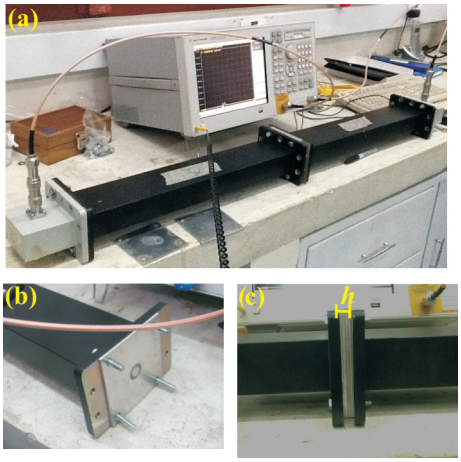

Fig. 3. a.) Experimental Setup: Two rectangular waveguides WR340 with the thick prototype placed between them. b.) Prototype placed in front of the aperture of the waveguide properly oriented. c.) Thickness of the resonator when each metallic sheet is added.

Fig. 3b. In order to analyze the effect of thickness in the prototype, several layers were placed one behind each other but very close, Fig. 3c. The TE_{10} rectangular waveguide mode is launched and the CSRR is excited by the magnetic field along the $x-$axis. Data has been collected by using a vectorial network analyzer Agilent E5062 within the frequency range from [2-3]GHz due to the operation range of the WR340.

IV. Results

The simulations related to the experiment were carried out by using the frequency domain solver of *CST Microwave Studio* code. It can be seen in the geometry of each prototype that the structure is very easy to tune and, specifically, by varying its radius and width of the slits we can determine the length of the *equivalent rectangular waveguide*, its corresponding cutoff frequency, thus, the resonance frequency.

For the first set of prototypes (a,b,c) it is predicted (Fig 2) that only the CSRR and CSR3 will present peaks of resonance. As shown in Fig. 4, the transmission coefficient in the experiments and simulations are compared. It may be observed in this Figure that the amplitude of peaks is only slightly greater in simulations than in experiments, and this amplitude remains constant as the thickness h increases. The differences in the resonance frequency f_0 are less than 10% for the thinnest filter ($h = 1.16$mm) and less than 1% when the surface is thick (h =5.08 mm). On the other hand, f_0 varies only 350 MHz within the thickness range of the experiment and tends to a constant value of 2.8 GHz, which corresponds to the frequency of the fundamental mode, see Table I. For the CSR2, it had been previously shown [4] that the CSRR and CSR2 of equal dimensions satisfy $f_0^{CSRR} = f_0^{CSR2}$. Thus, no resonance was expected within the range of the waveguide [2-3]GHz. Similarly, the CSR3 resonator satisfies $f_0^{CSRR} = 2\sqrt{2} f_0^{CSR3}$, such that f_0 exists out of the range of [2-3]GHz. However, it can be seen in Fig. 2c. that the first high order resonance f_1 exist within this range. Thus, our model not only predicts with good accuracy f_0 but also higher-order

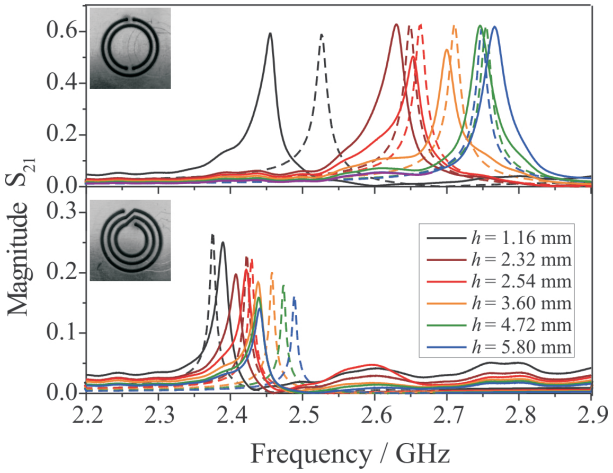

Fig. 4. a.) S_{21} magnitude for CSRR, CSR2 and CSR3 resonators of the same size. Experimental results (solid line), Simulation results (dashed line).

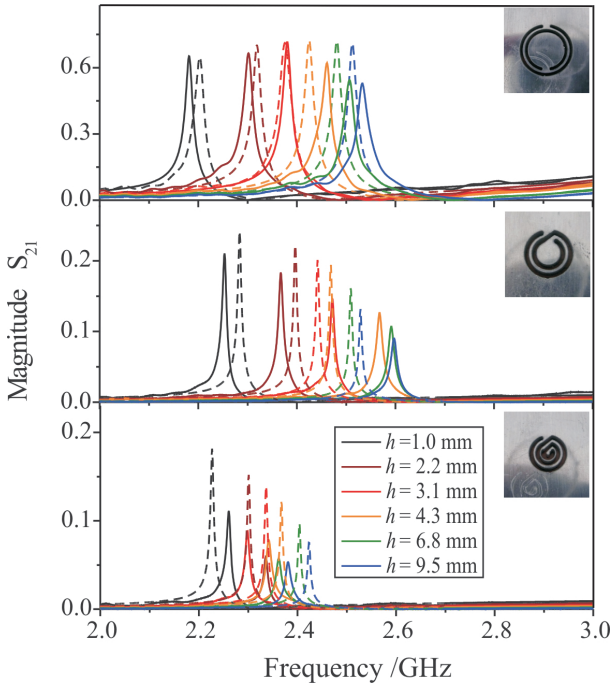

Fig. 5. S_{21} magnitude for CSRR, CSR2 and CSR3 resonators of different sizes. Experimental results (solid line), Simulation results (dashed line).

resonances as f_1. The differences between the experiments and simulations in the frequency are less than 8%.

For the second experiment, in the same way that every resonator becomes smaller, also it is more difficult to manufacture. Considering the limit of the frequency range due to the WR340 waveguides, we designed three resonators whose resonances f_0 appeared within this range, although these resonators do not exactly meet the relations predicted in [6] in which $f_0^{CSRR} = 2f_0^{CSR2} = 2\sqrt{2}f_0^{CSR3}$. Thus, the CSR2 spiral should have half the electrical size in comparison with the CSRR.

Although in the manufacturing process this condition is not fulfilled exactly, yet it is possible to verify that if we measure the length of the slits, and then calculate $f_0 = 2c/L$, numerical and experimental curves tend to the expected values shown in Table I when h increases. Thus, we have verified the validity of our equivalent rectangular waveguide model, which significantly simplifies the design process of these short resonators.

For both experiments, it was found that the Q factor increases with h (although its response is not uniform) and, as shown in Figs. 4, 5, Q also increases for each geometry. The CSRR presents an average $Q =$ and CSR3 $Q =$. However, the transmission is reduced significantly: while the CSRR satisfies $|S_{21}|^{f_0} = 0.7$, CSR2 and CSR3 reach only $|S_{21}|^{f_0} = 0.25$ and $|S_{21}|^{f_0} = 0.15$ respectively. Thus, prototypes of best performance as short bandpass filters, are the prototypes (a, d). Although the spirals have smaller electric size, its coupling with the incident wave only occurs at a single frequency, so the dissipation at any other frequencies is higher.

V. Conclusions

In this paper, the usefulness of short resonators of small electric size for the design of short bandpass filters in a rectangular waveguide has been analyzed for three different geometries. The design of the filter is very simple; it has a very small length and exhibits a high tunability, easily predicted by an *equivalent rectangular waveguide model* which has tourned out to be more precise and easier than the equivalent LC-circuit models. This can be made by changing the dimensions of the CSRR and increasing the thickness of the metal sheet. It is believed that the proposed prototypes can be of practical interest for the fabrication of very compact filters, since their length is simply given by the thickness of the metallic sheet, which is on the millimetre scale. Besides, from the different geometries that satisfy the small electric size, we have proven the one of best performance, the CSRR.

References

[1] J. B. Pendry, A. J. Holden, D. J. Robins, J. W. Stewart,"Magnetism from conductors and enhanced nonlinear phenomena".*IEEE Trans. Microwave Theory Tech*, vol. **47** pp.2075-2084, 1999.

[2] F. Falcone, T. Lopetegi, M. A. G. Laso, J. D. Baena, J. Bonache, M. Beruete, R. Marqués, F. Martín and M. Sorolla, Babinet Principle Applied to the Design of Metasurfaces and Metamaterials", *Physical Review Letters* , vol. **93**, no 19, p.197401, 2005.

[3] N. Ortiz, J. D. Baena, M. Beruete, F. Falcone, M. A. G. Laso, T. Lopetegi, R. Marqués, F. Martín, J. García-García, M. Sorolla, " Complementary split-ring resonator for compact waveguide filter design". *Microwave and Optical Technology Letters*, vol. **46** pp.88-92, 2005.

[4] J. D. Baena, J. Bonache, F. Martín, R. Marqués, F. Falcone, T. Lopetegi, M. A. G. Laso, J. GarcíaGarcía, I. Gil, M. Flores, M. Sorolla, Equivalent-Circuit Models for Split-Ring Resonators and Complementary Split-Ring Resonators Coupled to Planar Transmission Lines *IEEE Transactions on Microwave Theory and Techniques*, vol. **53**, no 4, p.1451-1460, 2005.

[5] R. Yang, R. Rodríguez-Berral, F. Medina and Y. Hao, "Analytical Model for the Transmission of Electromagnetic Waves Through Arrays of Slits in Perfect Conductors and Lossy Metal Screens", *Journal of Applied Physics* , vol. **109**, p. 103107, 2011.

[6] L.M. Pulido-Mancera, J.D. Baena, J.L. Araque Quijano, "Thickness Effects on the Resonance of Metasurfaces made of SRRs and CSRRs", *2013 IEEE AP-S/USNC-URSI Symposium*, July 7-13, 2013.

[7] R. Marqués, M. Sorolla and F. Martín, *Metamaterials with Negative Parameters*. Wiley Series in Microwave and Optical Engineering, 2007.

Permittivity Measurements Based in Microstrip Technology.

Medidas de Permitividad Basadas en Tecnología de Microstrip

L.M. Pulido-Mancera[1], J.C. González [2], A. Ávila [2], J.D. Baena [1]

[1] Departamento de Física
Universidad Nacional de Colombia
[2] Departamento de Ingeniería Eléctrica y Electrónica
Universidad de los Andes

Abstract

The Complementary Split Ring Resonator (CSRR) is used with a microstrip line to create a device able to measure the electric permittivity of liquids. Simulations and measurements of the S-parameters are performed to correlate the resonance frequency to the known permittivity of five samples and calibrate the device. Once calibrated, we also provide an estimate of the permittivity of a solution of silver nanoparticles. These measurements are attractive given the limited the noninvasive techniques available for nanomaterial characterization and the lack of results at the microwave range. The results estimate the relative permittivity of the silver nanoparticles ϵ_r^{Ag-NPS} =101.46 $\pm$ 19.53.

Keywords: Microstrip Line, SRR, Nanocomposite

Resumen

El anillo resonador cortado complementario se utilizó en conjunto con una línea de microcinta para crear un dispositivo capaz de medir la permitividad de líquidos. La simulación y medida de los parámetros de dispersión fueron

lmpulidom@unal.edu.co

obtenidos para correlacionar la frecuencia de resonancia con la permitividad conocida de cinco muestras y así calibrar el dispositivo. Una vez calibrado, fue posible obtener un valor estimado de la permitividad de una solución con nanopartículas de plata. Estas medidas son interesantes dadas las limitadas técnicas no invasivas disponibles para la caracterización de nanomateriales y la falta de medidas en el rango de microondas. Los resultados estiman la permitividad de la solución de nanopartículas ϵ_r^{Ag-NPS} =101.46 ± 19.53.

Palabras clave: Línea de Microcinta, SRR, Nanocompuestos

1. Introduction

Measurements of the complex permittivity of gases, liquids, and solids at the microwave range, have been developed by using devices in which electromagnetic fields are known,[1]. These microwave techniques employ a cavity resonator or a length of waveguide which are completely filled in the dielectric region with the solution under test. In the case of 2D materials, many advances in microstrip based sensors and coplanar waveguides have been developed in order to have compact, lightweight and low-cost devices [2].

For instance, by using a microstrip line, its work frequency can be calculated by means of the phase shift $\phi = \sqrt{\epsilon_e} k_0 L$, where $k_0 = \frac{2\pi f}{c}$, c is the speed of light and ϵ_e is the effective dielectric constant of a homogeneous medium that replaces the air and the substrate of the microstrip. When the phase shift is half wavelength, the frequency is [3]

$$f = \frac{c}{2\sqrt{\epsilon_e} L}, \quad \epsilon_e = \frac{\epsilon_r + 1}{2} + \frac{\epsilon_r - 1}{2} \frac{1}{\sqrt{1 + 12d/w}}. \tag{1}$$

Thus, once the work frequency is measured, the effective permittivity can be computed thus, the permittivity of the solution. However, the volume needed should be big enough because the approximation of 1 requires that all the space must be replaced by the solution. A different approach uses resonator techniques [4] in

which the microstrip line is drilled with holes and the solution is placed on them. See Fig 1. (up). In this case, the measurement is calculated by means of an effective permittivity. In order to avoid the calculation of an effective permittivity, the use of resonators can be developed to estimate the permittivoty of the solution under test only.

Baena et al.[5] analyzed the resonant response of the Complementary Split Ring Resonator highlighting its small electrical size and good quality factor. A microstrip line with holes having this shape could perform a good response for permittivity measurements with less volume of solution under test and higher precision. Moreover, until now, no truly measurement of the permittivity of a solution of silver nanoparticles has been introduced. Due to the advantages of the CSRR geometry, it would be possible to measure the electrical response of nanocomposites in terms of it concentration and particle size. It will be shown that this characterization is useful to determine its use for electrical energy storage at the microwave range.

2. Theory

A metallic layer with shape of the CSRR drilled on it can be used as a frequency filter. Its resonance frequency depends on the geometrical parameters and the permittivity of the substrate placed behind the metallic layer. Basically, when a electromagnetic signal excites the CSRR, the induced currents in the metallic layer can be modelled by means of an inductance and a capacitance. The inductance is calculated as $L_0 = 2\pi r_0 L_{\text{pul}}$ with L_{pul} the inductance formed in the circular metallic strip between the rings. The capacitance is calculated as the one formed in a planar ring of average radius r_0, width c and relative permittivity of the solution. [6], [5]. In comparison with a similar approach developed by [4], in which the geometry used was the circle instead of the CSRR, as shown in Fig. 1. The main difference is the way as the resonance is introduced: The microstrip line with circles behave as a Fabry-Perot resonator such that the resonance appears when the length of the microstrip is half wavelength. On the other hand, the resonance

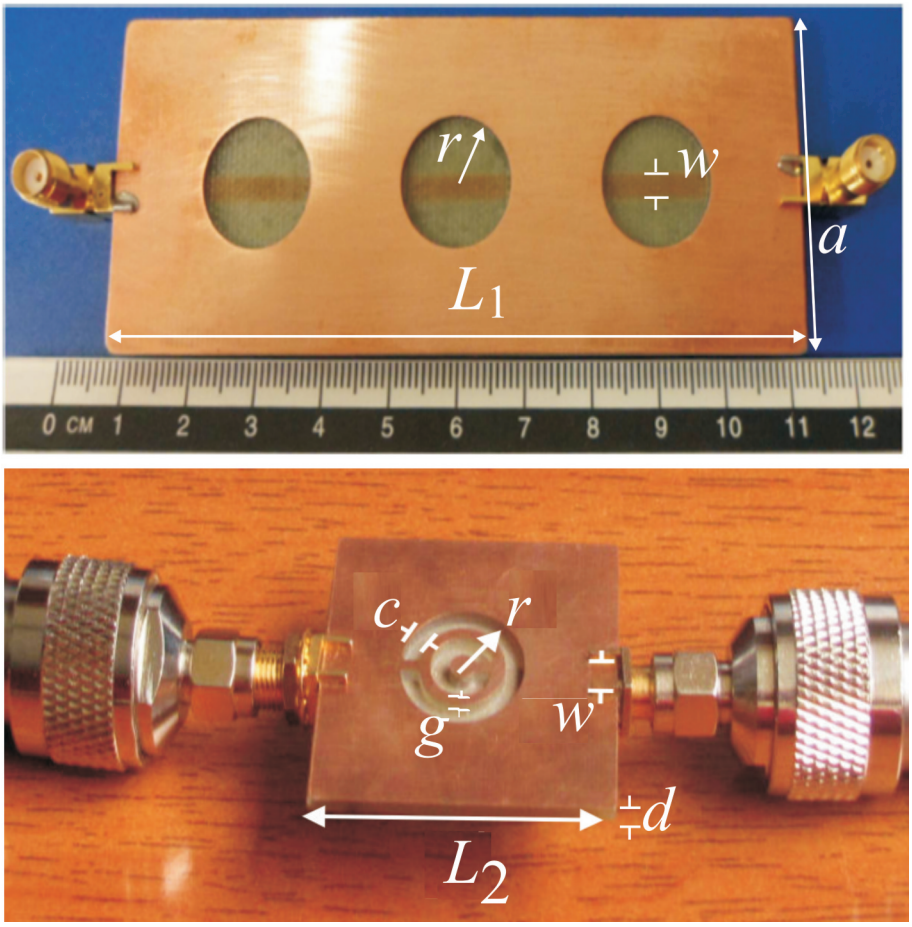

FIGURA 1. *a.) Proposal of [4] for permittivity measurements based in circular cavities. b.) Proposal based in CSRR geometry. The geometric parameters are* $L_1 = 10cm$, $a = 36$ *mm*, $L_2 = 33$ *mm* , $w = 3$ *mm*, $r = 8$ *mm*, $c = 2$ *mm*, $g = 2mm$, $d = 1.57$ *mm. The depth of the circular cavities and the slots is* $h = 1$ *mm.*

of the CSRR appears because of the magnetic field perpendicular to the metallic surface [6] that induces some currents forming the equivalent LC-circuit described above.

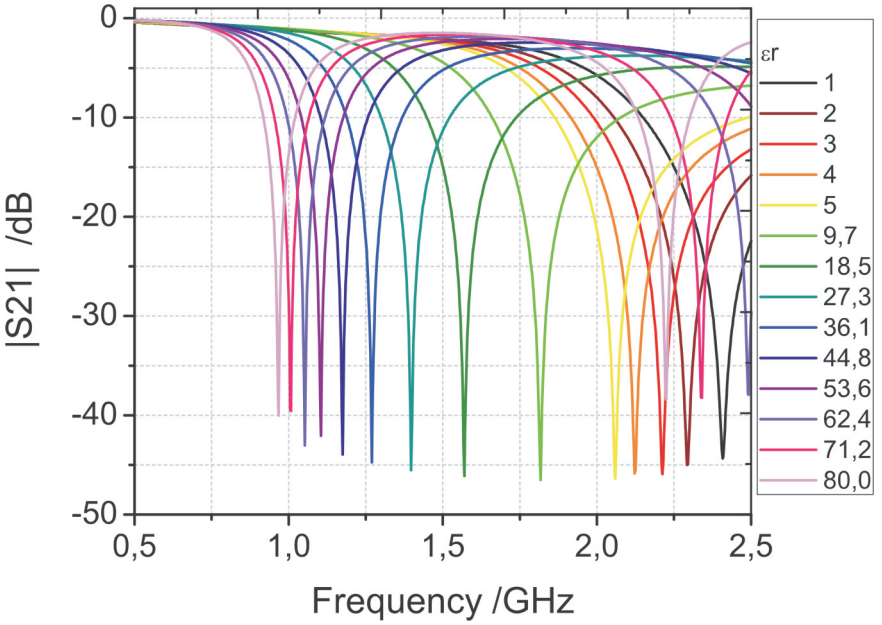

FIGURA 2. $|S_{21}|$ *coefficient varying* ϵ_r *of the fill solution. The geometrical parameters of the device are described in Fig. 1.*

3. Numerical Simulation

In order to test the response of the device before the experiment, the $S-$parameters within the frequency range [0.5-2.5] were calculated by full-wave simulation, using the commercial software *CST-Microwave Studio*. We got a relation between the resonance frequency and ϵ_r shown in Fig. 2 by varying the relative permittivity of the filler and calculating the minimum in the $|S_{21}|$ parameter.

The simulation shows that the minimum frequency shifts from 2.4-0.8 GHz when the relative permittivity changes from 1-80. We are interested into simplify the simulation process considering that the CSRR resonates by its geometry only and that the electric field lines are more intense in the slits rather than the rest of the structure. To validate this approximation, we used a program that calculates the resonance of the CSRR by means of the circuit model and we compared it with a *CST-Studio* simulation in which the substrate was replaced by the solvent under test. We performed this simu-

Material	ϵ_r	CSRR Model (GHz)	CST Simulation (GHz)
Air	1	3.84	3.26
Immersion Oil	3.2	3.05	2.54
FR4	4.3	2.84	2.34
Acetone	20.7	1.62	1.29
Ethyl Alcohol	24.3	1.51	1.20
Water	80.4	0.87	0.68

FIGURA 3. Permittivity of solvents to be tested experimentally and its resonance frequency calculated by means of LC-circuit model of the CSRR geometry and *CST-Studio* numerical simulation. The relative permittivity of the commercial solvents is known. [7]

lations for the five commercial solvents tested experimentally. The results shown in Table 3, stablish that when $\epsilon_{solution} \approx \epsilon_{substrate}$, the resonance is higher than the resonance achieved when the microstrip is introduced, such that the approximation is no longer valid. This difference caused the change in the electric field distribution when the microstrip line is added.

4. Experimental Development

The device for permittivity measurements was fabricated and analyzed with five different solutions. For the fabrication process, we designed the geometrical parameters by using Eagle software. The device was manufactured using basic processes of photolithography and etching on a substrate FR4 covered with a thin layer of copper. The slits were manufactured with a Bungard CCD/2 (Germany) computer-controlled milling machine using a 1 mm drill bit, drilling up to 1mm of depth. Filling the slits with 200 μL of the solvents in Table 3, we verified the matching between the experimental and simulated curves, see Fig.5. The experimental curves present a ripple that prevent us from information about the dielectric losses. It is associated to a calibration process because the cables of the VNA mismatch the impedance of the microstrip. In order to avoid this ripple for further analysis of the quality factor, we propose the TRL Calibration Method, presented in [3].

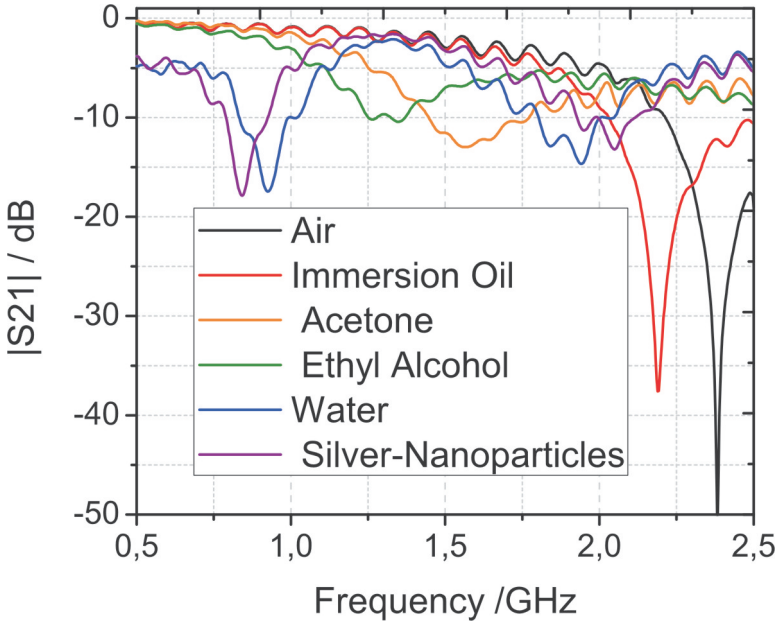

FIGURA 4. *Experimental measurements. (Up)The structure manufactured has the same geometrical parameters described in Fig. 2 (Down)* S_{21} *parameter when different solutions are placed in the sensor. The ripple is associated to the calibration process.*

The decreasing form of the curve in Fig. 5 stablish two regions of interest, the response of the technique for solvents with low and high permittivity. Below ϵ_r =20 approximately, small variations in ϵ_r yields high variation of the frequency, so different oils could be accurately measured, for instance. On the other hand, at high ϵ_r as the silver nanoparticles solution, even the smaller variation of frequency represent an important change in the permittivity. Therefore, the possibility of measuring this small differences allows us to characterize the nanocomposites in terms of any intrinsic characteristic, like the concentration or the particle size. Equation 4 allows us to estimate the permittivity of a solution of silver nanoparticles ϵ_r^{Ag-NPS} =101.46 $\pm$ 19.53. Higher than the permittivity of water, this result is interesting because it means that these nanocomposites possesses strong response to electric field in the microwave range. Improvements of resonator techniques could be performed the

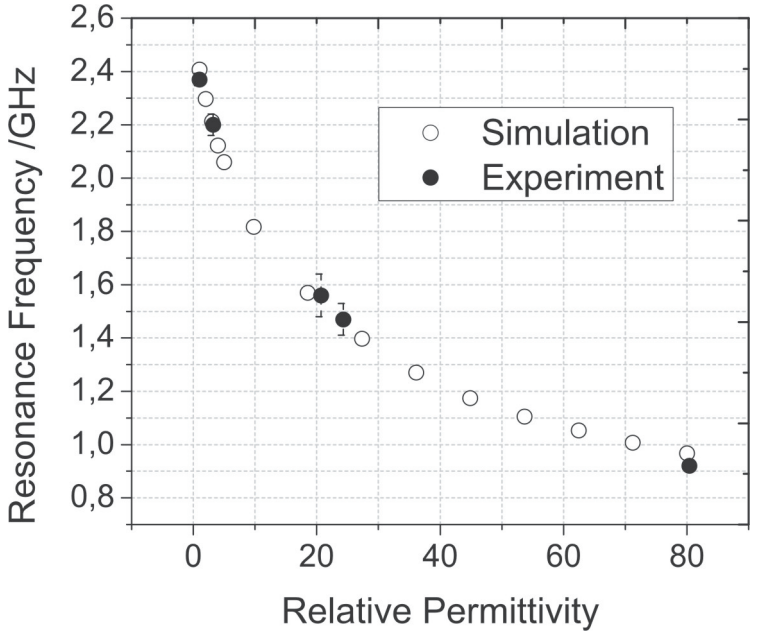

FIGURA 5. *Resonance Frequency vs. Relative Permittivity for the sensor in the experimental and computational form.*

analyze the response of the electromagnetic fields for solvents with a response that depends on the concentration of its components. Both improvements in design and fabrication could be performed by cutting the ground plane with other CSRR's related geometries, like spirals (CSR2) whose resonator response has been previously described in [6].

$$\epsilon_r = A\exp^{-f/B} + C$$
$$A = 916{,}37 \pm 78{,}54 \quad B = 0{,}393 \pm 0{,}013, \quad C = -0{,}121 \pm 0{,}74$$
$$r^2 = 0{,}998$$

5. Conclusions

The resonant device based on the CSRR had been developed for measuring the permittivity of different solutions within the microwave range (0.5-2.5 GHz). In addition to the frequency selectivity, the ability of this device to provide an accurate measure and the

advantage of size reduction in comparison with previous resonators has been shown. An analytical model has been used to simplify the computational simulation and it is demonstrated that these models are valid at high permittivities. The computational results compared with experimental results provide a good qualitative agreement, as well as a very good quantitative prediction of the permittivity of the solvent under test (i.e. for a solution of silver nanoparticles diluted in water with an estimated permittivity ϵ_r^{Ag-NPS} =101.46 $\pm$ 19.53). The experimental results for the bandwidth are inaccurate due to a mismatch between the ports and the microstrip line, although they can be improved by performing a calibration process. Two regions in the curve of frequency and permittivity have been discussed, and the most relevant qualitative predictions rely at high permittivity, in which the nanocomposites respond. Improvements in design and fabrication, have been proposed.

Referencias

[1] E. Fratticcioli, M. Dionigi, and R. Sorrentino, Microwave Symposium Digest **2**, 647 (2002).

[2] A. Abdel-Rahman, M. S. Kheir, A. K. Verma, and A. Omar, Progress in Electromagnetic Research C **13**, 67 (2010).

[3] D. M. Pozard, *Microwave Engineering, 3rd 3d* (John Wiley and Sons, 2005).

[4] J. R. Castro and A. Avila, "Efecto de las características geométricas de estructuras pbg y sus potenciales aplicaciones," .

[5] J. Baena, J. Bonache, F. Martín, R. Marqués, F. Falcone, T. Lopetegi, G. Laso, J. García, I. Gil, M. F. Portillo, and M. Sorolla, IEEE Transaction and Microwave Theory and Techniques **53** (2005).

[6] R. Marqués, F. Mesa, J. Martel, and F. Medina, IEEE TRANSACTIONS ON ANTENNAS AND PROPAGATION **51**.

[7] "www.instrumaics.co.nz/site/instrumatics/files/documents/dielectric-constant-values.pdf," .

Thickness Effects in the Resonance of Metasurfaces made of SRRs ans C-SRRs

L.M. Pulido-Mancera[1], J.D. Baena[1], J.L. Araque[1]
1 Group of Applied Physics, Physics Department, Universidad Nacional de Colombia
2 Electrical Engineering Department, Universidad Nacional de Colombia
lmpulidom@unal.edu.co

***Abstract*—Different periodical Frequency Selective Surfaces(FSS) whose unit cell are the Split Ring Resonators (SRR) or related geometries and their corresponding complementary screens were studied. This kind of FSS, sometimes called metasurfaces, have the advantage of avoiding secondary grating lobes because of the small electrical size of the unit cell. The main aim of this paper is to investigate the effects of the metal thickness for these FSSs. It was found that the quality factor decrease for unconnected elements (strips) and increase for connected elements (slots). Besides, as the thickness increases, the resonance frequency decrease for the case of unconnected elements while increases for connected elements.**

***Index Terms*—SRRs, FSS, metasurfaces.**

I. Introduction

The topic of Frequency Selective Surfaces has a long life and can be considered as classic. For instance, a comprehensive revision of the topic can be found in [1]. Roughly speaking, FSSs are filters for electromagnetic waves in free space, which often are considered plane waves. Last years, FSS have received fresh ideas coming from metamaterials. FSS made as periodical array of the Split Ring Resonator (SRR) or related geometries has attracted much attention because of the advantage of a small unit cell compared to the wavelength. It means that secondary grating lobes are avoided. It was demonstrated by Falcone and co-workers [4], [2] that a periodical 2D array of SRRs behaves as a band stop filter and, according to the Babinets principle, its complementary screen behaves as a band pass filter. Both the stopband and the passband are typically narrow, so that the quality factor(Q) is relatively big.

In order to improve the quality factor of the band pass filters, there are two typical routes: cascading several layers or making one single thick layer. For the former case, and for negligible coupling between neighboring layers, the transfer function of a single layer is multiplied by itself as many times as the number of layers. It clearly means an increment of Q for passbands, but a decrement for stopbands. If, instead of the cascade, the structure consist of only one thick layer, then it can be roughly thought as a continuous set of infinite layers and, analogously to the previous case, a thicker FSS will provide higher Q for passbands, but lower for stopbands. However, the Babinets principle does not apply for the case of thick metal layers, so that the behavior of the complementary screen cannot be derived directly from the behavior of the original screen. In this work, parametric studies for the thick

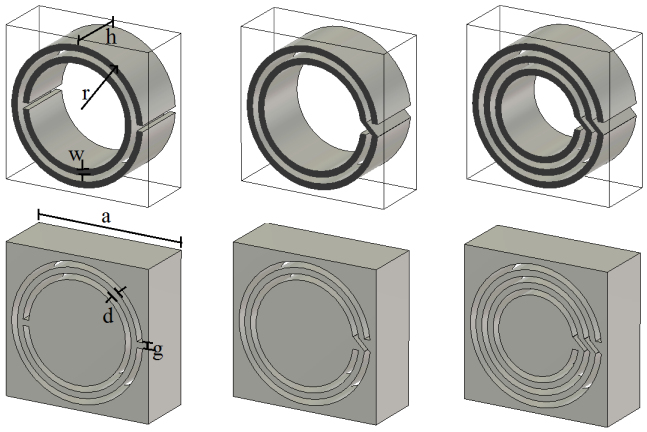

Fig. 1. Unit cells of the simulated FSSs.First row: the Split Ring Resonator (SRR) and the Spiral Resonators of two and three turns (SR2 and SR3). Second row: complementary unit cell which will be termed as C-SRR, C-SR2, and C-SR3 respectively. The geometric parameters are (all in mm): a = 5,c = d = g =0.2, r = 2.3. The thickness h is varied within the interval 0 to 7 mm.

FSSs shown in 1 were carried out. Transmission and reflection coefficients under normal incidence were obtained for many different metal thickness. Special attention was dedicated to understand the effect of the thickness on their Q factors and resonance frequencies.

II. Preliminary Theoretical Considerations

For very thin samples and good conductors (ideally infinitesimal thickness and perfect conductors), the basic theory of this metasurfaces is already well explained in [2], and references therein. Basically, they firstly analyzed the behavior of the screen made with SRR and after the Babinets principle was applied in order to obtain the behavior of the complementary screen. This idea can be easily extended to other related topologies as the Spiral Resonators of 2 and 3 turns (SR2 and SR3). Equivalent circuit models for thin SRR, SR2, SR3, and their complementary counterpart can be found in [3]. However, as the thickness becomes non negligible, then Babinets principle starts to fail. Neither the equivalent circuit models works properly. Thus, we have started to envisaged a theory in order to predict the variations due to the thickness. At the moment of writing this paper, it was to early to show any result of this theories.

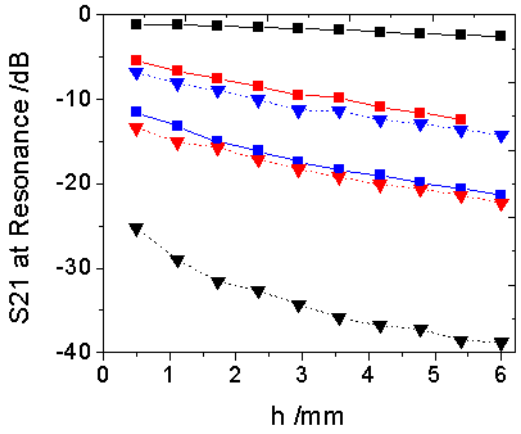

Fig. 2. Transmission coefficient at the resonance frequency vs thickness of the sample.

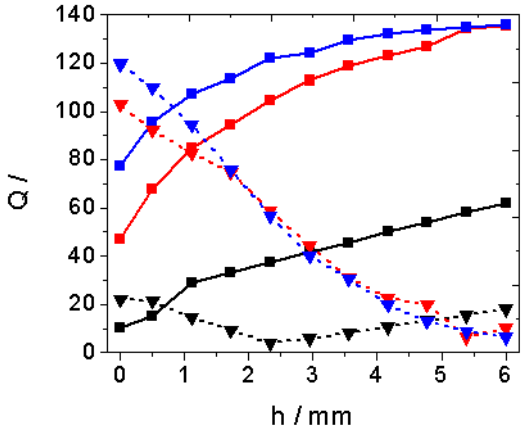

Fig. 3. Quality factor (Q) vs thickness of the sample.

III. Numerical Results

In order to get some previous insights about the problem, a set of many numerical simulations were run over the commercial software CST Microwave Studio Software. All the FSSs described in Fig. 1 were simulated for different types of metal: Perfect Electric Conductor (PEC), copper, and aluminum. Due to lack of space, just results for aluminum samples are shown here. Although it is not shown here, narrow stopband were observed for SRR, SR2, and SR3 while narrow passbands for C-SRR, C-SR2, and C-SR3, even for the thickest sample. Figure 2 shows the transmission coefficients at the resonance frequency versus the thickness of the samples. It is worth to note that the best performance is found for the FSSs made of SRR and C-SRR, because they are the nearest to values 0 and 1, respectively. On the other hand, FSSs made of SR2, C-SR2, SR3, and C-SR3 showed very poor performance.

Figure 3 shows the Q factor. As the thickness of the samples are increased, the Q factor drops down for FSSs presenting a stopband (SRR, SR2, and SR3) while it grows for FSSs presenting a passband (C-SRR, C-SR2, and C-SR3). The resonance frequency f_0 respect to h is depicted in Fig. 4. It is worth to note that, according to the Babinets principle, the resonance frequencies for FSSs made of strips and slots elements coincide when the thickness h tends to zero. Interestingly, the resonance frequency of FSSs made of original particles (SRR, SR2, and SR3) shift to lower frequencies while for complementary screens (C-SRR, C-SR2, C-SR3) it shift to higher frequencies.

IV. Conclusions

The effects of the metal thickness has been studied for the FSSs shown in Fig. 1. It was found that the quality factor and the resonance frequency strongly depends on the thickness. As the thickness is increased, original screens (first row of Fig. 1) suffer a decrement in both the quality factor and the resonance frequency. Oppositely, complementary screens (second row of Fig. 1) suffer an increment in both magnitudes. Therefore, for further applications, complementary screens might be more promising because of its higher quality factor. For instance, applications such as passband radomes to hide directive antennas need very high Q factor which could be obtained by using thick complementary screens. It makes this study interesting from a practical standpoint.

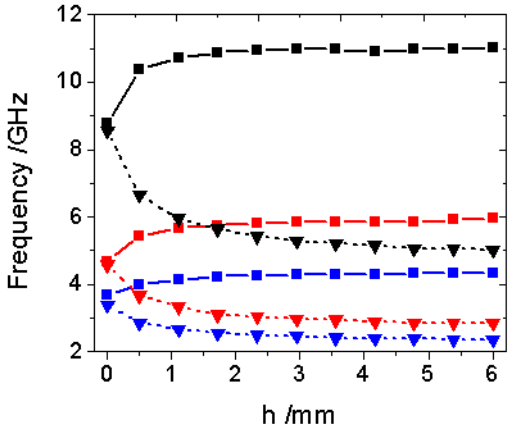

Fig. 4. Resonance frequency vs thickness of the sample h.

References

[1] T.K. Wu. *Frequency Selective Surface and Grid Array*. John Wiley and Sons, Inc. 1995.

[2] R. Marqués, J.D. Baena, M. Beruete,F. Falcone,T. Lopetegi, M. Sorolla, F. Martín and J. Garcia. *AB-initio analysis of frequency selective surfaces based on conventional and complementary split ring resonators*. J. Opt. A: Pure Appl. Opt. **7** (2005) S38S43.

[3] R. Marqués, F. Mesa, J. Martel, F. Medina. *Comparative Analysis of Edge- and Broadside- Coupled Split Ring Resonators for Metamaterial DesignTheory and Experiments*. IEEE Transactions on Antennas and propagation, Vol **51**, No 10, 2003.

[4] F. Falcone, T. Lopetegi, M. A. G. Laso, J. D. Baena, J. Bonache, M. Beruete, R. Marqués, F. Martín, M. Sorolla. *Babinet Principle Applied to the Design of Metasurfaces and Metamaterials*. Physical Review Letters , Vol **93**, No 19,2005.

Waveguide Model for Thick Complementary Split Ring Resonators

L. M. Pulido-Mancera, J. D. Baena
Group of Applied Physics, Physics Department, Universidad Nacional de Colombia
lmpulidom@unal.edu.co

***Abstract*—This paper presents a very simple analytical model for the design of Frequency Selective Surfaces based on Complementary Split Ring Resonators (CSRR) within the microwave range. Simple expressions are provided for the most important geometrical parameters of the model, yielding an accurate description of the CSRR resonance frequency and avoiding full-wave numerical simulations. Besides, a qualitative description of the band-pass filter behavior of these structures is described, considering its high quality factor Q.**

***Index Terms*—CSRRs, FSS, metasurfaces.**

I. Introduction

Frequency Selective Surfaces (FSSs) are filters for electromagnetic waves in free space, which often are considered plane waves. Last years, metamaterial based FSSs have received much attention because of the advantage of a small unit cell compared to the wavelength, which means that secondary grating lobes are avoided.[1] It was demonstrated by Falcone and co-workers [4] that a periodical 2D array of Split Ring Resonator (SRR) behaves as a stop band filter and, according to the Babinets principle, its complementary screen (CSRR) behaves as a band pass filter. Both the bandstop and the passband are typically narrow, so that the quality factor (Q) is relatively big.

For the 2D case, the resonance frequency of the SRR and CSRR can be described by using an equivalent LC-circuit model [3]. However, numerical simulations have shown that when the thickness of the SRR increases, the resonance frequency is not the same as the complementary CSRR, the Babinet's principle is no longer satisfied. [5]. LC-circuit models can still be applied for thick SRR resonators, but to thick CSRR resonators a different perspective is needed.

Transmission line models describe the response of thick periodic metallic structures, and reduce the problem to the computation of the scattering parameters of a height-step discontinuity in a parallel plate waveguide [6]. The incoming electromagnetic plane wave, described as a transmission line, must match the admittance in the surface of the FSS to be propagated along rectangular slits, considered a transmission line too. The S-parameters depends on the equivalent admittances of the incident wave, the surface and the slits and the admittance-matching occurs only at certain frequencies, such that the S-parameters presents different peaks and dips.

In this paper, we propose a simple explanation to the first two resonances found in the S_{11} and S_{21} parameters, when the thickness of the CSRR increases. This brief explanation will simplify the calculation of the geometrical parameters to design FSSs, avoiding numerical simulations.

II. Analytical model

Let us consider a periodic array of identical slits with the CSRR geometry, made in a thick conducting plate. Figure 1 represents a frontal view of the system under study, with a being the period of the structure, h the thickness of the metal plate, c the slit width, d the separation between slits, g the gap and r the external radius of the CSRR. An electromagnetic plane wave (TEM) impinges normally on the structure with its magnetic field oriented in the $x-$direction.

In our proposed model, each slit of the CSRR can be seen as a rectangular waveguide bended with the shape of C. In this sense, the length L of each waveguide is $2\pi(r-c/2)-g$ and $2\pi(r-d-3c/2)-g$ respectively. As a waveguide, the first frequency that allows the transmission of the wave is the cut-off frequency of the lowest mode (TE_{10}), when the resonance wavelength λ_0 is twice the length of the waveguide.

In order to validate this condition, we performed several simulations using *CST-Microwave Studio Software* and we obtained the two primary resonances of the $|S_{11}|$ and $|S_{21}|$ parameters. As shown in Fig. 1, the x axis is the thickness h divided by λ_0, and the y axis is the resonance frequency $f_0 = c/\lambda_0$, rewritten in terms of the electrical size $2r/\lambda_0$. As the thickness increases, each curve tends to a fixed value that corresponds to the ratio between the diameter and the length of each waveguide, such that $2r/(2\pi r - c/2) - g$ =0.171 and $2r/2\pi(r-d-3c/2)-g = 0.225$.

Figure 1 is very useful for the FSS design because it gives us information in order to estimate accurately λ_0: it is necessary to choose a thickness greater than $h = 0.006\lambda_0$ and $L = \lambda_0/2$, with L being dependent on r, g, d and c. Other simulations that are not presented in this paper show that the variance of c and g is small, indeed the cut-off frequency in a waveguide does not depend on its height. Thus, the problem of filter design is reduced to estimate the value of r. In addition, given that the first and second resonances operate independently, it is possible to design a CSRR adjustable to two different frequencies using a single unit cell geometry and just varying d. In this sense, thick CSRR structures not only has the advantage of small electrical size but also adjustable response to two frequencies working separately.

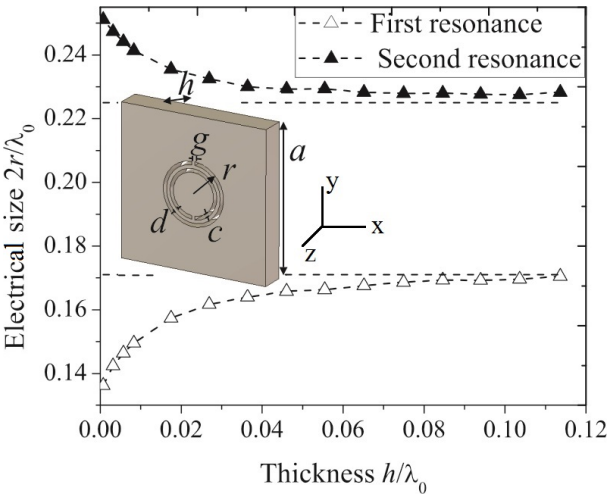

Fig. 1. Electric size vs. Thickness h normalized by resonance wavelength. The normalization shows that the CSRR converges to the cut-off frequency when the thickness increases. The geometrical parameters used in this simulation are a =43mm, r =9mm, $c = d = g$ =1mm. h vary within the range of 0-12mm.

III. S-PARAMETERS FOR CSRR

The transmission curves show how the first resonance frequency f_1 tends to a fixed value as the thickness h increases. Figure 2a. shows the S parameters corresponding to the first resonance. As shown, f_1 increases but its bandwidth remains constant, thus; the quality factor $Q = f/\Delta f$ increases, as it had been previously demonstrated in [5]. Likewise, Q increases in the second resonance f_2, but in this case the increment is related with the bandwidth becomes narrower in spite of the fact that f_2 decreases.

By analyzing the electric field distribution and the surface current induced on the metallic surface only at the resonance frequency, it is possible to observe how each slot of the CSRR resonates independently when the structure is thick. Thus, within the frequency range between 2.2-2.9 GHz, only the outer slit allows the wave transmission while the internal slot acts as a metallic screen, Fig. 2a. Likewise, within the frequency range between 3.8 - 4.4 GHz, the internal slot fully transmits while the outer reflects almost completely, Fig.2b. When the surface is thin, the coupling between the two slots begins to be important so the resonance cannot be predicted with our proposed model.

Another interesting factor is the electric field direction inside each slit because it satisfies the boundary conditions of a bent rectangular waveguide. In fact, this distribution of the electric field was the key factor that allowed us to describe the geometry of CSRR rectangular widths in an analogous way to rectangular waveguides that transmit at the cut-off of the fundamental mode.

IV. CONCLUSIONS

This model is very useful to find the geometric parameters necessary for to design a structure made of CSRR geometry that completely transmits at a fixed frequency. The most important parameters are the ratio, $r = c/4\pi f_{res}$, and the thickness $h = 0.06\lambda_{res}$. Besides, for thick structures the resonances work independently for each slit of the CSRR, which allow us to design tunable filters with high Q for two different frequencies within the same unit cell.

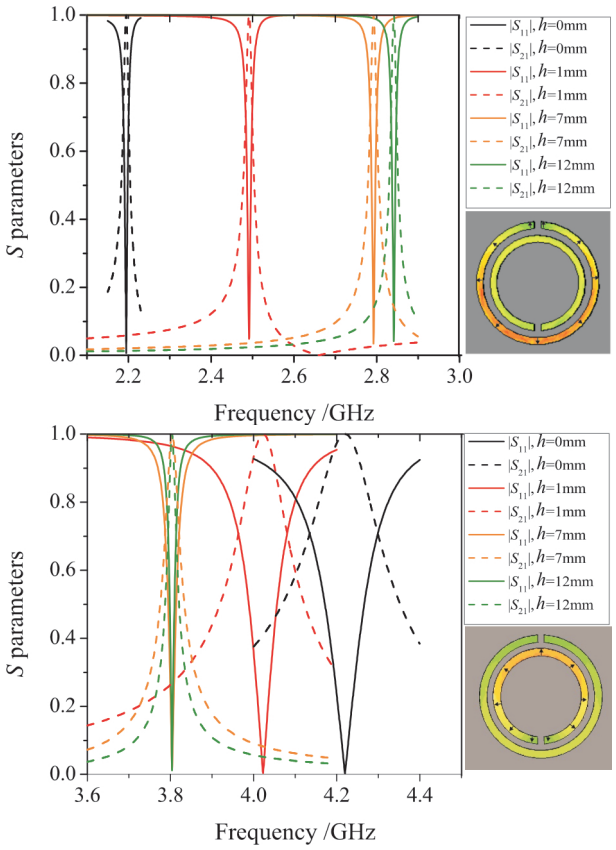

Fig. 2. S-parameters for different values of thickness using full-wave simulation in CST-Studio. a.) first resonance, b.) second resonance. Color curves varies for each value of thickness. Reflection S11 (solid line)is close to 0 and transmission S21 (dashed line) is close to 1 at resonance.

REFERENCES

[1] R. Marqués, M. Sorolla and F. Martín, *Metamaterials with Negative Parameters*. Wiley Series in Microwave and Optical Engineering, 2007.

[2] F. Falcone, T. Lopetegi, M. A. G. Laso, J. D. Baena, J. Bonache, M. Beruete, R. Marqués, F. Martín and M. Sorolla, "Babinet Principle Applied to the Design of Metasurfaces and Metamaterials", *Physical Review Letters* , vol. **93**, no 19, p.197401, 2005.

[3] R. Marqués, F. Mesa, J. Martel and F. Medina, "Comparative Analysis of Edge- and Broadside- Coupled Split Ring Resonators for Metamaterial Design Theory and Experiments", *IEEE Trans. Antennas and propagation*, vol. **51**, no. 10, pp. 2572-2581, 2003.

[4] F. Falcone, T. Lopetegi, M. A. G. Laso, J. D. Baena, J. Bonache, M. Beruete, R. Marqués, F. Martín and M. Sorolla, "Babinet Principle Applied to the Design of Metasurfaces and Metamaterials", *Physical Review Letters* , vol. **93**, no 19, p.197401, 2005.

[5] L. M. Pulido-Mancera, J. D. Baena, J. L. Araque Quijano, "Thickness Effects in the Resonance of Metasurfaces Made of SRRs and C-SRRs", *2013 IEEE AP-S/USNC-URSI Symposium*, July 7-13, 2013.

[6] R. Yang, R. Rodríguez-Berral, F. Medina and Y. Hao, "Analytical Model for the Transmission of Electromagnetic Waves Through Arrays of Slits in Perfect Conductors and Lossy Metal Screens", *Journal of Applied Physics* , vol. **109**, p. 103107, 2011.

Equivalent Circuit Model for Thick Split Ring Resonators and Thick Spiral Resonators

L. M. Pulido-Mancera, J. D. Baena
Physics Department
Universidad Nacional de Colombia, Bogotá, Colombia
lmpulidom@unal.edu.co

***Abstract*—A simple theoretical model which provides circuit parameters and resonance frequency of metallic thick resonators is presented. Two different topologies were studied: the original Pendry's SRR and spiral resonators of two and three turns. Theoretical computations of resonant frequencies are in good agreement with values obtained with a commercial electromagnetic solver. The model could be helpful for designing thick frequency selective surfaces (FSS) based on this types of resonators, so called metasurfaces.**

I. Introduction

The Split Ring Resonator (SRR) initially proposed by Pendry in 1999 [1] has been widely analyzed because of its small electrical size and strong magnetic polarizability at resonance which makes it a proper unit cell of metamaterial. For instance, the SRR joint to a metallic wire was used as the unit cell of the first experimental demonstration of a left-handed metamaterial by David Smith and co-workers in 2000 [2]. After, particles showing similar behavior, like spiral resonators of two turns (SR2) [3], have been also considered in order to reduce the electrical size of the unit cell. Main properties of these type of resonators can be approached by relatively easy LC-circuit models where the circuit parameters may be fully obtained from geometrical dimensions and material properties. In the case of infinitely thin resonators, readers could find some designer formulas in [4] for several different topologies. However, this calculations were only done for extremely thin resonator but some times it is interesting to manufacture thick structures in order to make the Q-factor higher.

In this paper a generalization of the LC-circuit model for thick resonators is presented. For instance, this model may be helpful for designing thick Frequency Selective Surfaces (FSS) with high quality factor based on these types of resonators, also known as metasurfaces. Namely, along this paper, we focus our attention on thick particles with transverse shape of SRR and SR2 (see Fig. 1).

II. LC-circuit model for thick resonators

A. Calculation of L

As the thickness h is increased, although the induced current is spread along the z direction, numerical simulations indicate that its profile on plane xy approximately remains. Simulations also shows that near the borders of the metal strips the surface current diverges, so that it could be properly approximated by a Maxwellian distribution (see Fig. 2). The inductance

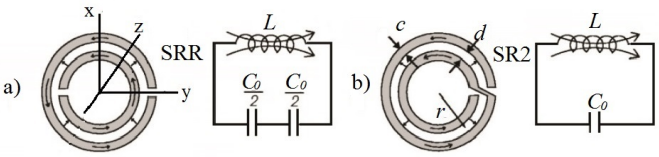

Fig. 1. Resonant particles and its equivalent circuits: SRR (a) and SR2 (b). The arrows on the strips represent the current direction and the arrows within the gaps represent the displacement current. Both particles have the same average radius r =7.5mm and $c = d$ =1mm.

can be approached to that of a thin hollow metal cylinder of average radius r. The inductance of this ideal cylinder can be approximated by using the variational expression $L = 2U_m/I^2$, where U_m is the magnetic energy. Assuming a Maxwellian distribution of the surface current density along the z direction, we can get the following expression

$$\vec{J}(\rho, z) = J_{s\varphi}(z)\delta(\rho - r)\hat{\varphi} = \frac{J_{s0}}{\sqrt{1-(2z/h)^2}}\delta(\rho - r)\hat{\varphi} \quad (1)$$

where J_{s0} is the surface current density at $z = 0$. The integration of (1) gives the current

$$I = \int_{-h/2}^{h/2} \frac{J_{s0}dz}{\sqrt{1-(\frac{2z}{h})^2}} = J_{s0}\frac{h\pi}{2} \quad (2)$$

On the other hand, the magnetic energy is

$$U_m = \frac{1}{2}\int_V \vec{A}\cdot\vec{J}dV = \frac{1}{2}(2\pi r J_{s0})\int_{-\infty}^{\infty}\frac{A_\varphi(r,z)dz}{\sqrt{1-(2z/h)^2}} \quad (3)$$

where the potential vector $\vec{A}$ can be calculated from the Laplace equation in cylindrical coordinates and corresponding boundary conditions:

$$\frac{\partial^2 A_\varphi}{\partial z^2} + \frac{\partial}{\partial\rho}(\frac{1}{\rho}\frac{\partial}{\partial\rho}(\rho A_\varphi)) = 0 \quad (4)$$

$$A_\varphi(r_+, z) = A_\varphi(r_-, z) \quad (5)$$

$$\frac{\partial(\rho A_\varphi)}{\partial\rho}|_{r_+} - \frac{\partial(\rho A_\varphi)}{\partial\rho}|_{r_-} = r\mu_0 J_{s\varphi}(r) \quad (6)$$

Using Fourier transforms for the surface current density and vector potential, equation (4) turns into the Bessel equation

$$\frac{\partial^2\tilde{A}_\varphi}{\partial x^2} + \frac{1}{x}\frac{\partial\tilde{A}_\varphi}{\partial x} - (1+\frac{1}{x^2})\tilde{A}_\varphi = 0, \quad (7)$$

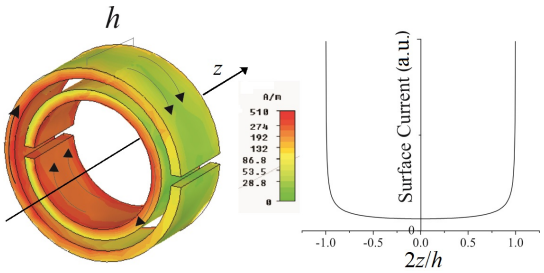

Fig. 2. Maxwellian distribution of the current along the surface of the cylinder vs. thickness.

where $x = k_z\rho$. The solution of this equation is

$$\tilde{A_\varphi}(r,k_z) = \frac{J_{s0}\mu_0 h}{i\sqrt{2\pi}} \frac{J_0(\frac{xh}{2r})I_1(x)K_1(x)}{k_z(K_1(x)I_0(x)+K_0(x)I_1(x))} \quad (8)$$

where $I_n(x)$ and $K_n(x)$ are the modified Bessel functions. Once the potential vector and the surface current are known, the variational expression $L = 2U_m/I^2$ can be used to get

$$L = 2r\mu_0 \int_0^\infty \frac{(J_0(xh/2r))^2 dx}{x(I_0(x)I_1^{-1}(x)+K_0(x)K_1^{-1}(x))} \quad (9)$$

B. Calculation of C

In a first order approximation, the capacitance could be calculated by using the well known formula for the capacitance of a long cylindrical capacitor:

$$C_h = \frac{2\pi h\epsilon}{\ln(r/(r-d))}; \quad (10)$$

where h is the height or thickness, d distance between the two coaxial cylinders, and ϵ the permittivity filling the space between the cylinders. However, for relatively small h the fringing effect should not be neglected. We assume that the fringing electric field is similar to the field created by two coplanar extremely thin rings with the same shape of the transversal section of the cylindrical capacitor. The fringing capacitance may be approximated by $C_0 = 2\pi r C_{pul}$, where C_{pul} represents the capacitance per unit of length of two parallel coplanar strips [5].

C. The resonance frequency of SRR and SR2

Considering that the two halves of the SRR are connected in series, the resonance frequency of its equivalent circuit is $\omega_0^{\mathrm{SRR}} = (L(C_h + C_0)/4)^{-1/2}$. On the other hand, the capacitance of the thick SR2 must be 4 times bigger, since the two halves are connected in parallel, i.e. $\omega_0^{\mathrm{SR2}} = (L(C_h + C_0))^{-1/2}$. Therefore, the resonance frequency of SR2 is half the value for SRR, which means that the electrical size of the former is smaller than that of the last.

III. Numerical validation

In order to check the validity of the model, many numerical simulations were carried out by using the frequency domain solver of *CST Microwave Studio*. All particles were made of perfect electric conductor in free space. The geometrical

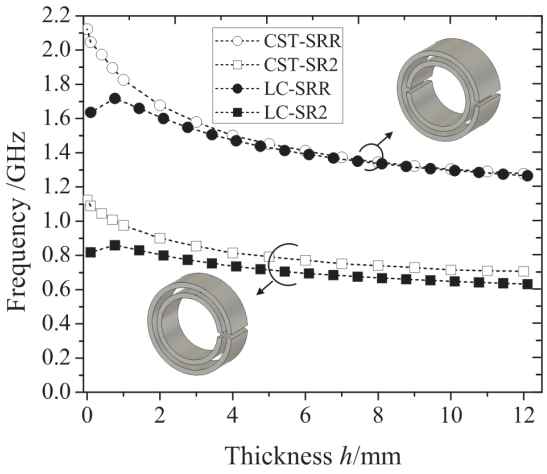

Fig. 3. Resonance frequency vs. thickness h calculated by means of the LC-circuit model and full-wave simulations by using *CST Microwave Studio*.

parameters on the transverse xy-plane were held constant and equal to the values indicated in caption of Fig. 1. In Fig. 3 the resonance frequency has been plotted against the thickness h varying within the range 0-12mm. This figure is also showing the values coming from the LC equivalent circuit model. For most part, the agreement between model is good. The disagreement observed for thin particles can be attributed to the fact that the approximation of L for a cylinder of infinitely thin metal is not longer valid, since h start to be comparable to c or d.

Besides, it is remarkable that the ratio of 2 between the resonance frequencies of thin SRR and SR2, which was previously reported [3], is still obtained for thick particles.

IV. Conclusions

A circuit model for calculating the resonance frequency of thick SRR and SR2 has been proposed and checked by means of numerical simulations. Besides, it was shown that the ratio between the resonance frequency of the SRR and the SR2 is independent of the thickness and approximately equal to 2, similarly to the case of thin particles [3]. This analytical model can be useful for designing thick FSS with higher Q-factor than that of thin particles.

References

[1] J. B. Pendry, A. J. Holden, D. J. Robbins, W. J. Stewart, "Magnetism from Conductors and Enhanced Nonlinear Phenomena", *IEEE Trans. Microwave Theory Tech.*, vol. **47** , no. 10, pp. 2075-2084, 1999.

[2] D.R. Smith, W.J. Padilla, D.C. Vier, S.C. Nemat-Nasser, S. Schultz, "Composite Medium with Simultaneously Negative Permeability and Permittivity", *Phys. Rev. Lett.* **84**, p. 4184, 2000.

[3] J. D. Baena, R. Marqués, F. Medina, "Artificial Magnetic Metamaterial Design by Using Spiral Resonators", *Physical Review B*, vol. **69**, p. 014402, 2004.

[4] J. D. Baena, J. Bonache, F. Martín, R. Marqués, F. Falcone, T. Lopetegi, M. A. G. Laso, J. GarcíaGarcía, I. Gil, M. Flores, M. Sorolla,"Equivalent-Circuit Models for Split-Ring Resonators and Complementary Split-Ring Resonators Coupled to Planar Transmission Lines", *IEEE Trans. Microwave Theory Tech.*, vol. **53** , no. 4, pp. 1451-1461, 2005.

[5] I. Bahl and P. Bhartia, *Microwave Solid State Circuit Design*. Willey, 1988.

8th International Congress on Advanced Electromagnetic Materials in Microwaves and Optics - Metamaterials 2014
Copenhagen, Denmark, 25-30 August 2014

Waveguide Bandpass Filters made of Thick Complementary Small Resonators

L. M. Pulido-Mancera and J. D. Baena

Universidad Nacional de Colombia, Physics Department, Bogotá, Colombia
lmpulidom@unal.edu.co

We explore the potential use of complementary split ring resonators (csrr's) and complementary spirals of two and three turns (csr2 and csr3) to design very compact waveguide filters. We demonstrate its passband response in an experimental and computational form. Besides, it is shown that the design process can be highly simplified by means of a new waveguide model that reduce full wave numerical simulations. Thus, it is possible to design waveguide filters with lengths equal to the thickness of a metallic sheets, leading to an improvement in the design of miniaturized waveguide filters.

I. Introduction

The split ring resonator (srr) was first introduced by Pendry et al. (1999) in order to produce artificial media with a strong magnetic response at microwaves and radio frequencies [1]. Its complementary structure, the csrr recently reported by [2], have been inspired on the Babinet's principle and, similar to the SRRs, it is an electrically small particle that exhibits a quasi-static resonance. A 2D array of csrrs behaves as a passband filter whose resonance frequency depends on its geometrical parameters only. Similarly, for waveguide applications it allows us to replace the well-known resonant cavities coupled by circular irises in waveguide filters, resulting in a compact design [3].

The design process of infinitely thin csrrs and similar geometries like spirals, has been developed by means of equivalent LC-Circuit Models in order to predict the resonance frequency: The intrinsic circuit model for the csrr (dual of the SRR model) has a parallel combination of two inductances connecting the inner disk to the ground and the capacitance of a disk of radius r surrounded by a ground plane at a distance of its edge. Likewise, equivalent circuit models for planar csr2 and csr3 can be found in [4]. However, when the thickness increases, duality given by Babinet's principle is no longer valid and different approaches to predict the resonance in terms of the thickness are needed [5].

II. Waveguide model for thick csrr

Let us consider metallic plate with the csrr geometry etched on it. A frontal view of the resonator with its geometrical parameters are shown in Figure 1a). The same geometrical parameters were used for the csr2 (Fig. 1b) and the csr3 (Fig. 1c). The resonator is excited by a harmonic magnetic field towards the x direction, corresponding to the TE_{10} mode of the rectangular waveguide. In our model, when the surface is thick, each slit of the csrr (csr2 or csr3) can be seen as a rectangular waveguide bended with the shape of C or spiral respectively. Hence, as a waveguide, the lowest frequency that allows maximum transmission is the cutoff frequency f_0 of the mode TE_{10}, when $\lambda_0 = 2L$ with λ_0 the resonance wavelength and L the length of the slit. The second resonance f_1 (associated to λ_1) appears when $\lambda_1 = L$ is satisfied. For each prototype, L, f_0, and f_1 predicted of our simplified model are shown in Table 1.

Table 1: Resonances expected with the waveguide model for thick resonators.

Properties	csrr	csr2	csr3
Length /mm	52.40	94.34	125.61
f_0 / GHz	2.86	1.58	1.19
f_1 / GHz	5.72	3.16	2.38

Fig. 1: Resonators used for metasurfaces design. a) csrr, b)csr2, c) csr3. The geometric parameters for all the geometries are $r = 9.0mm$, $c = d = 1.0mm$, $g = 2.9mm$ and h varies from 1.2 mm to 5.8 mm. The thinnest layer is $h = 1.2$mm and the thicker layer is $h = 2.6$mm

III. Experimental Setup

Experiments were carried out by placing the metallic resonator layers shown in Fig. 1 between two waveguides connected through the flange. For each geometry, a set of metallic layers were placed one behind each other between two standard WR340 waveguide of 86 $\times$ 43 mm^2 cross sectional area and cutoff frequency at 1.736 GHz. This area is 16 times bigger than the resonator's area which allow us to find the resonance frequency of a single resonator rather than the resonance of its images produced by the electric walls of the WR340 waveguide.

Full two port calibration up to the coaxial port was performed before the measurements. Each WR340 is connected at the and to coaxial adapters, which are used to excite and detect the signal as shown in Fig. 2a). The vector network analyzer Agilent E5062 is used to measure the $|S_{21}|$ and $|S_{11}|$ parameters every time that a new layer is inserted between the waveguides: Fig. 2b) shows how to create a thicker resonator, Fig. 2c). Considering that we are focused in the passband response of these structures, in this paper we will present the results for the S_{21} parameter of the geometries whose resonance associated to λ_0 or λ_1 appears.

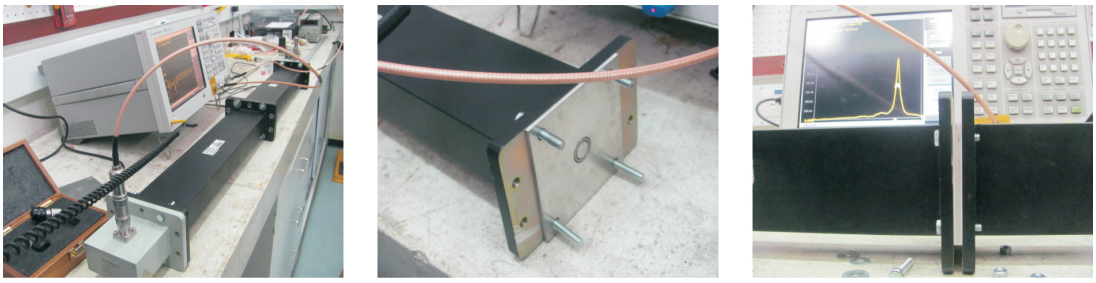

(a) (b) (c)

Fig. 2: Experimental Setup. a)Setup to measure the transmission band when the resonator is placed between two waveguides WR340. b) Orientation of the re resonator in front of the aperture to get the proper excitaion mode. c) Equivalent thick resonator

IV. Results

The results for the experimental setup of Fig 2 relating to csrr, csr2, and csr3 are shown in Fig 3. In all cases, the $|S_{21}|$ and $|S_{11}|$ parameters were measured and compared with full wave numerical simulation using *CST-Microwave Studio* software within the frequency range [2 - 3 GHz]. It may be observed that the amplitude of peaks found in the $S-$parameters is only slightly greater in simulations than in the experiment, and this amplitude remains approximately constant despite the resonator becomes thicker and higher losses are expected. The differences in resonance frequency f_0 are less than 10% for the thinnest layer ($h = 1.16$) and less than 1% when the surface is thick. See Fig 3. On the other hand, it can be seen that when the thickness of the filter increases, f_0 varies only 350 MHz, approaching constant value of 2.82 GHz, which corresponds to the frequency of the fundamental mode shown in Table 1. Thus, we have verified experimentally our previously waveguide model for thick csrrs based resonators. In the case of the spiral of two turns, csr2, it had been previously shown that the

relation between the resonance of the csrr and csr2 of equal dimensions satisfies $f_0^{csrr} = 2f_0^{csr2}$ [6]. Thus, it is expected no resonance within the range of frequencies of the WR340. Similarly, for the spiral of three turns (csr3), $f_0^{csrr} = 2\sqrt{2}f_0^{csr3}$ is satisfied. Again, f_0 does not appear within the range of frequencies of the WR340. Instead, it can be seen (See Fig 3) the first high order resonance f_1 of Table 1. Therefore, our model not only predicts the first resonance as the cutoff frequency of the equivalent waveguide, but also predicts higher-order resonances. However, in this last case the losses are greater, so that the filter csr3 is not suitable as a good passband filter within this frequency range.

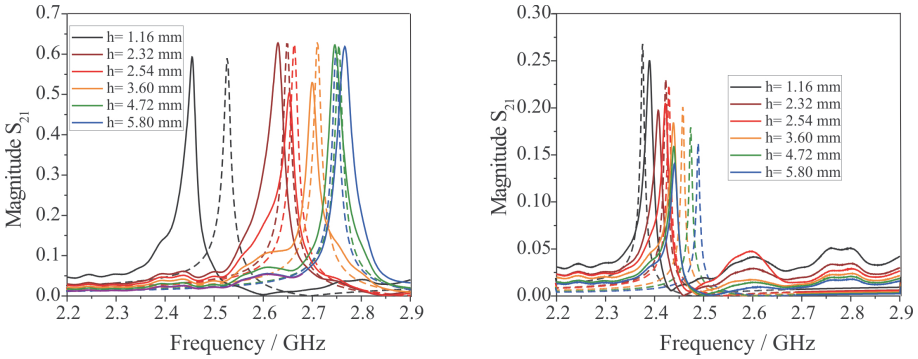

Fig. 3: Results from experiments and simulations varying the thickness of the filter. a) S_{21} for csrr (first resonance f_0), b) S_{21} for csr2 (no resonance), C) S_{21} for csr3 (second resonance f_1).

V. Conclusions

This model is very useful to find the geometric parameters necessary to design a metasurface made of csrr resonators that completely transmits at a fixed frequency within the microwave range. Besides, it was demonstrated by full wave simulation and waveguide experiments the accuracy in the prediction of the resonance frequency of thick resonators. For instance, for the thick csrr we found that $f_0^{sim} = 2.82$ GHz, f_0^{exp} =2.82 GHz which tends to f_0^{model} =2.86 GHz. Besides, it can be verified that the model remains valid for higher order resonances, as shown with the csr3 and its resonance at f_1 within the same frequency range. In the future, it would be necessary to vary the size of each resonator in order to find the resonance peaks for all the geometries proposed.

References

[1] J. B. Pendry, A. J. Holden, D. J. Robins, J. W. Stewart,"Magnetism from conductors and enhanced nonlinear phenomena".*IEEE Trans. Microwave Theory Tech*, vol. **47** pp.2075-2084, 1999.

[2] F. Falcone, T. Lopetegi, M. A. G. Laso, J. D. Baena, J. Bonache, M. Beruete, R. Marqués, F. Martín and M. Sorolla, Babinet Principle Applied to the Design of Metasurfaces and Metamaterials", *Physical Review Letters* , vol. **93**, no 19, p.197401, 2005.

[3] N. Ortiz, J. D. Baena, M. Beruete, F. Falcone, M. A. G. Laso, T. Lopetegi, R. Marqués, F. Martín, J. García-García, M. Sorolla, " Complementary split-ring resonator for compact waveguide filter design". *Microwave and Optical Technology Letters*, vol. **46** pp.88-92, 2005.

[4] J. D. Baena, J. Bonache, F. Martín, R. Marqués, F. Falcone, T. Lopetegi, M. A. G. Laso, J. GarcíaGarcía, I. Gil, M. Flores, M. Sorolla, Equivalent-Circuit Models for Split-Ring Resonators and Complementary Split-Ring Resonators Coupled to Planar Transmission Lines *IEEE Transactions on Microwave Theory and Techniques*, vol. **53**, no 4, p.1451-1460, 2005.

[5] R. Yang, R. Rodríguez-Berral, F. Medina and Y. Hao, "Analytical Model for the Transmission of Electromagnetic Waves Through Arrays of Slits in Perfect Conductors and Lossy Metal Screens", *Journal of Applied Physics* , vol. **109**, p. 103107, 2011.

[6] L.M. Pulido-Mancera, J.D. Baena, J.L. Araque Quijano, "Thickness Effects on the Resonance of Metasurfaces made of SRRs and CSRRs", *2013 IEEE AP-S/USNC-URSI Symposium*, July 7-13, 2013.

8th International Congress on Advanced Electromagnetic Materials in Microwaves and Optics – Metamaterials 2014
Copenhagen, Denmark, 25-30 August 2014

Theoretical Constraints on Reflection and Transmission through Metasurfaces

L. M. Pulido-Mancera, J. D. Baena

National University of Colombia, Department of Physics, Bogotá, Colombia
jdbaenad@unal.edu.co

***Abstract* – We have established a set of useful constraints that should be verified by thin metasurfaces made of perfect electric conductor. Mainly, we found that loci of transmission and reflection coefficients on the complex plane are circumferences. The properties shown in this paper may be useful for limiting the types of realistic responses desired for new metasurfaces.**

I. INTRODUCTION

Metasurfaces may help to create new types of frequency selective surfaces, polarizers, polarization convertors, shields, etc. Surface impedance models for characterizing metasurfaces have been proposed earlier [1, 2]. Sometimes metasurfaces can show cross polarization effects as demonstrated by Beruete for metasurfaces made of Split Ring Resonators (SRRs) [3]. Besides, the Babinet's principle has been used to propose complementary metasurfaces made of Complementary SRRs (C-SRRs) [4]. Now, from basic fundamentals we have established a set of useful constraints that should be verified by thin metasurfaces made of perfect electric conductor. We found that transmission and reflection coefficients must move along circumferences on the complex plane when varying the frequency close to one single resonant frequency. These circumferences are also correlated one each other. The properties shown in this paper may be useful for limiting the types of possible responses expected for lossless metasurfaces.

II. THEORY

Let us assume normal incidence on a metasurface graved on a sheet of perfect electric conductor, so that conservation of energy and reciprocity are guaranteed. Figure 1(a) is showing waves impinging onto the left side of the metasurface and waves moving away from it. The scattering matrix **S** connects them by the linear relation $[E_{x1}^-, E_{y1}^-, E_{x2}^-, E_{y2}^-]^t = \mathbf{S} \cdot [E_{x1}^+, E_{y1}^+, E_{x2}^+, E_{y2}^+]^t$, where the superscript t means matrix transposition. The scattering matrix can be written down as follows:

$$\mathbf{S} = \left(\begin{array}{cc|cc} r_x & c & t_x & c \\ c & r_y & c & t_y \\ \hline t_x & c & r_x & c \\ c & t_y & c & r_y \end{array}\right) = \left(\begin{array}{cc|cc} r_x & c & 1+r_x & c \\ c & r_y & c & 1+r_y \\ \hline 1+r_x & c & r_x & c \\ c & 1+r_y & c & r_y \end{array}\right) = \begin{pmatrix} \mathbf{R} & \mathbf{R} \\ \mathbf{R} & \mathbf{R} \end{pmatrix} + \begin{pmatrix} \mathbf{0} & \mathbf{1} \\ \mathbf{1} & \mathbf{0} \end{pmatrix} \tag{1}$$

where $r_x \equiv r_{xx}$ and $r_y \equiv r_{yy}$ are reflection coefficients, $t_x \equiv t_{xx}$ and $t_y \equiv t_{yy}$ are transmission coefficients, and $c \equiv r_{xy} = r_{yx} = t_{xy} = t_{yx}$ represents any cross polarization effect. It is worth to note that, due to the reflection symmetry along the z-axis, coefficients for one direction of propagation equal those of the opposite direction. From reciprocity: $r_{xy} = r_{yx}$ and $t_{xy} = t_{yx}$. From continuity of **E** tangential at $z = 0$: $r_{xy} = t_{xy}$, $r_{xy} = t_{xy}$, $1 + r_{xx} = t_{xx}$, $1 + r_{yy} = t_{yy}$. It is well known that for reciprocal and lossless structures $\mathbf{S} \cdot \mathbf{S} = \mathbf{1}$. Imposing this property onto (1) we rapidly get the relation $\mathbf{R} \cdot \mathbf{R}^* + \mathrm{Re}[\mathbf{R}] = 0$, or more precisely

$$\begin{pmatrix} |r_x|^2 + |c|^2 + r_{xr} & r_x c^* + r_y^* c + c_r \\ r_x^* c + r_y c^* + c_r & |r_y|^2 + |c|^2 + r_{yr} \end{pmatrix} = \begin{pmatrix} 0 & 0 \\ 0 & 0 \end{pmatrix} \tag{2}$$

Boundary conditions for tangential components of the magnetic field can be written as $H_{2x} - H_{1x} = J_y$ and $H_{2y} - H_{1y} = -J_x$, where J_x and J_y are components of the macroscopic surface electric current on the metasurface. Assuming that the pattern of currents on the resonator for frequencies close to the resonance is not depending on frequency neither on the polarization state of the incident wave, we can introduce the hypothesis $J_y = k\,J_x$, being k a real constant. This condition is particularly valid when the pattern of currents is just determined by the geometry of the resonator, as it usually happens for electrically small resonators used in metamaterials. Applying this hypothesis on the boundary condition for the tangential component of **H** and properly traducing magnetic fields into electric fields, by using usual relations for plane waves, we achieve the next relation (see notation in Fig. 1(a)): $-E_{2y}^{-} + E_{1y}^{+} - E_{1y}^{-} = -k\,(E_{2x}^{-} - E_{1x}^{+} + E_{1x}^{-})$. Now, assuming either x- or y-polarized incident waves and normalizing by the incident field, we get the next relations: $r_x = k^{-1}c$ and $r_y = kc$ (interestingly $r_x\, r_y = c^2$). Finally, combining these relations with the two equations coming from the diagonal components of (2), we can demonstrate that both reflection coefficients, r_x and r_y, move on circumferences on the complex plane described by the following formulas

$$\left(r_{xr} + \frac{1}{2}\frac{1}{1+|k|^2}\right)^2 + r_{xi}^2 = \left(\frac{1}{2}\frac{1}{1+|k|^2}\right)^2, \quad \left(r_{yr} + \frac{1}{2}\frac{1}{1+|k|^{-2}}\right)^2 + r_{yi}^2 = \left(\frac{1}{2}\frac{1}{1+|k|^{-2}}\right)^2 \tag{6}$$

where subscripts r and i means real and imaginary parts. Transmission coefficients describe also circumferences, since $1 + r_x = t_x$, $1 + r_y = t_y$. Besides, since the cross polarization coefficient c is proportional to reflection coefficients, it must also lie along a circumference. Figure 1(b) summarizes the loci of all coefficients.

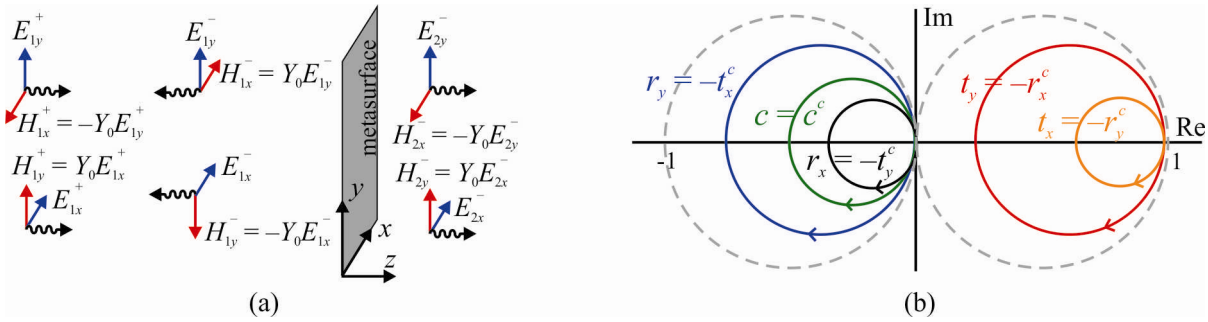

Fig. 1. (a) Diagram of fields for the case of an incident wave travelling from left to right. (b) Theoretical sketch of reflection coefficients r_x and r_y, transmission coefficients t_x and t_y, and the cross polarization coefficient c.

Special attention is required on the previous hypothesis of $J_y = k\,J_x$. This hypothesis is properly working for resonators made of thin metal strips because the current is forced to lie on specific metal paths. However, for their complementary resonators the electric current is, in some way, more free to flow on bigger metal regions, so that the hypothesis is not longer true. A way to fix this problem would be to change the hypothesis to another similar relation with effective surface magnetic currents on slots. Alternatively, we can also use the Babinet's principle joint to boundary conditions. It is easy to demonstrate that coefficients of the complementary structure are related to those of the original structure as follows: $r_x^c = -t_y$, $r_y^c = -t_x$, $t_x^c = -r_y$, $t_y^c = -r_x$, and $c^c = c$.

III. Numerical Validation

To check the theory, a set of numerical simulations were carried out by using *CST Microwave Studio*. Figure 2 shows the scattering parameters for two metasurfaces presenting mirror symmetry: one made of SRRs (a) and the other made of the C-SRRs (d). Geometrical parameters were set as a = 15mm, r = 9mm, and $c = d$ = 1mm. Reflection, transmission and cross polarization coefficients are depicted on the complex plane for the SRR-metasurface (b) and the C-SRR-metasurface (e). Magnitudes of coefficients are plotted versus the

frequency for the SRR-metasurface (c) and the CSRR-metasurface (f). The polar plots in Fig. 2(b) and (e) agree with the theoretical polar plot of Fig. 1(b). It is worth to note that the mirror symmetry cancels the cross polarization effect, $c = 0$, according to one of the properties shown in [5].

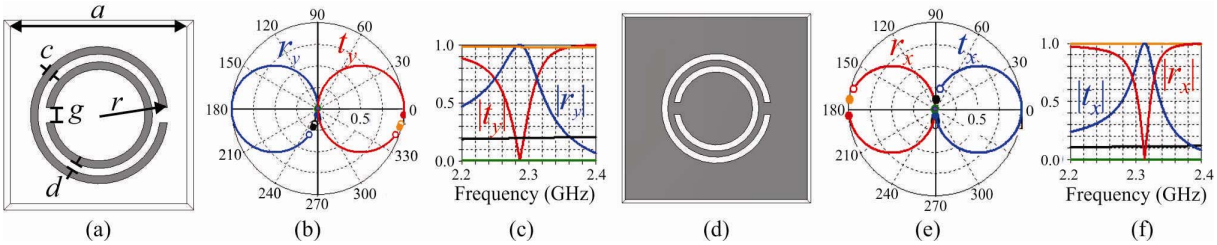

Fig. 2. Scattering parameters for metasurfaces made of SRR and C-SRR.

Similarly, Fig. 3 shows scattering parameters for unsymmetrical metasurfaces made of Arquimides' spirals. The metasurface made of Arquimides' Spiral Resonator of two turns (SR2) (a) and its complementary counterpart (C-SR2) (d) were simulated for geometrical parameters a = 15mm, r = 9mm, and $c = d$ = 1mm. Reflection, transmission and cross polarization coefficients are depicted on the complex plane for the SR2-metasurface (b) and the C-SR2-metasurface (e). Magnitudes of coefficients are plotted versus the frequency for the SR2-metasurface (c) and the C-SR2-metasurface (f). Once again, the polar plots in Fig. 3(b) and (c) agree with the theoretical polar plot of Fig. 1(b). In this case, the cross polarization effect appears.

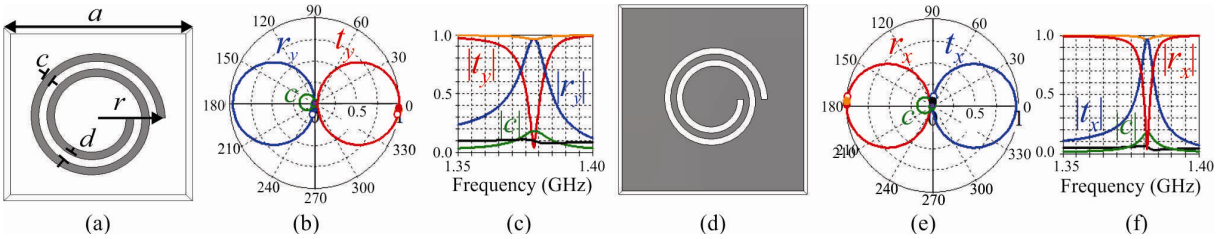

Fig. 3. Scattering parameters for metasurfaces made of SR2 and C-SR2.

IV. Conclusion

A set of useful constraints for the scattering parameters of lossless thin metasurfaces have been presented. It was theoretically demonstrated that transmission, reflection, and cross polarization coefficients describe certain correlated circumferences on the complex plane. Good agreement between the theory and numerical simulations is shown. These properties paper may be useful for limiting the types of responses of new metasurfaces.

References

[1] R. Marqués, J. D. Baena, M. Beruete, F. Falcone, T. Lopetegi, M. Sorolla, F. Martín, and J. Garcia, "Ab initio analysis of frequency selective surfaces based on conventional and complementary split ring resonators," *J. Opt. A: Pure Appl. Opt.*, vol. 7, pp. S38-S43, 2005.

[2] C. L. Holloway, A. Dienstfrey, E. F. Kuester, J. F. O'Hara, A. K. Azad, and A. J. Taylor, "A discussion on the interpretation and characterization of metafilms/metasurfaces: The two-dimensional equivalent of metamaterials," *Metamaterials*, vol. 3, pp. 100-112, 2009.

[3] M. Beruete, M. Sorolla, R. Marqués, J. D. Baena, and M. Freire, "Resonance and cross-polarization effects in conventional and complementary split ring resonator periodic screens," *Electromagnetics*, vol. 26, pp. 247-260, 2006.

[4] F. Falcone, T. Lopetegi, M. A. G. Laso, J. D. Baena, J. Bonache, M. Beruete, R. Marqués, F. Martín, and M. Sorolla, "Babinet principle applied to the design of metasurfaces and metamaterials," *Phys. Rev. Lett.*, vol. 93, p. 197401, 2004.

[5] V. Dmitriev, "Symmetry properties of electromagnetic planar arrays: long-wave approximation and normal incidence," *Metamaterials*, vol. 5, pp. 141-148, 2011.